



FACULTY OF SCIENCE AND TECHNOLOGY

MASTER THESIS

Study programme / specialisation:
Mechanical and Structural Engineering
and Materials Science / Civil Engineering
Structures

The spring semester, 2022

Author: Einar Mesloe

Open / Confidential
Einar Mesloe
.....
(signature author)

Course coordinator:
Sudath Chaminda Siriwardane Siriwardane Arachchilage

Supervisor(s): Yanyan Sha

Thesis title: Impact response of fibre reinforced concrete

Credits (ECTS): 30

Keywords:
Basalt fibre concrete
Pendulum test
LS-dyna

Pages: 74
+ appendix: 43

Stavanger, 29.06.2022
date/year

Impact response of fibre reinforced concrete

Einar Mesloe
University of Stavanger
Department of mechanical and structural engineering

Acknowledgement

This thesis marks the end of a five-year road to obtain a Master of Science in Engineering Structures and Materials at the University of Strangety.

I would like to express sincere gratitude to my supervisor, Yanyan Sha, for the guidance I have received during the writing of this thesis. The help has been crucial, both in the experimental work and the numerical simulation. To overcome the laboratory challenges, a special thanks are owed to senior engineer Samdar Kakay.

Lastly, I would like to thank my fellow students for taking part in relevant discussions, and making these last few years as memorable as possible.



Einar Mesloe

Reading guide

To optimize the readers experience, all tables, figures, and equations are tagged with a given ID of two numbers, where the first number indicates the chapter and the second number is a reference to the given table, figure or equation.

All references are made with the IEEE method showcasing the author and the year of publishing, with a link to the bibliography at the end of the report. The appendix are included at the end of the report where the first appendix are denoted in a capital letter.

Abstract

Fiber reinforced concrete have for long been researched to better find its possibilities withing concrete structures. Today fibre reinforced concrete is mainly used for slabs resting on the ground, or as thin shotcrete. In some cases the fibre replaces the traditional reinforcement completely, and can reduce costs on project considerably. With further investigation fibre reinforced concrete could possible replace traditional reinforcement partial, while improve its mechanical behavior and durability. Bridge piers are exposed to many different accidental loads, such as vehicle impacts, explosions, and barge collision. The bridge structure must be designed to handle this types of load, and its impact response is an essential part of understating the forces acting on the pier.

In order to determine the piers response, scaled down laboratory experiment are performed, as building a full scale is inefficient. Pendulum test were performed on three 100x100x1500mm concrete column, with a fiber dosage of 0.0%, 0.5% and 1.0%. The results from the impact test together with the mechanical properties of the basalt fibre reinforced concrete were used to develop a numerical model, to simulate the laboratory test. The accuracy of the model is determined by comparing the experimental results with the numerical results.

Sammen drag

Fiberarmert betong har lenget vært i fokus for å forbedre mulighetene til å bli brukt innenfor betongkonstruksjoner. I dag brukes fiberarmert betong hovedsakelig til plater som hviler på bakken, eller som tynn sprøytebetong. I noen tilfeller erstatter fiberen den tradisjonelle armeringen fullstendig, og kan redusere kostnadene på prosjektet betraktelig. Med ytterligere undersøkelser kan fiberarmert betong erstatte tradisjonell armering delvis, samtidig som dens mekaniske egenskaper og slitestyrke forbedres. Støttesøyler til broer er meget utsatt for mange forskjellige ulykkes laster, som kjøretøykollisjoner, eksplosjoner, og lekterkollisjon. Brokonstruksjonen må utformes slik at denne typen belastning blir håndtert uten å kollapse, og en vesentlig del av design prosessen handler om strukturens vibrasjon og kraftfordeling.

For å bestemme søylens respons etter slike ulykkes laster, blir mindre skalerte laboratoriet eksperimenter utført, da full-skala testen er ikke spesielt kostnadseffektivt. Pendeltester ble utført på tre 100x100x1500mm betongsøyler, med en fiberdosering på 0.0%, 0.5%, og 1.0%. Resultatene fra pendeltesten sammen med de mekaniske egenskapene til fiberbetongen, ble en numerisk modell utviklet, for å simulere laboratoriet testen. Ble sjekket ved å sammenligne de eksperimentelle dataene med de numeriske resultatene.

Contents

| | |
|--|-------------|
| List of Figures | xiii |
| 1 Introduction | 3 |
| 1.1 Background | 3 |
| 1.2 Scope | 4 |
| 1.3 Thesis structure | 4 |
| 2 Literature Review | 7 |
| 2.1 Fiber reinforced Concrete | 7 |
| 2.2 Impact test on concrete | 10 |
| 3 Impact energy and Dynamic response | 13 |
| 3.1 Impact energy | 13 |
| 3.2 Dynamic response | 15 |
| 4 Properties of fibre concrete | 19 |
| 4.1 Mix design | 19 |
| 4.2 Mechanical properties of hardened concrete | 20 |
| 5 Impact test setup | 29 |
| 5.1 Column design | 29 |
| 5.2 Pendulum setup for impact test | 30 |
| 6 Impact test results | 35 |
| 6.1 Data processing | 36 |
| 6.2 Results | 37 |
| 6.3 Influence of fibres on the results | 54 |
| 6.4 Source of errors | 54 |
| 7 Numerical Analysis | 57 |
| 7.1 Model development | 57 |
| 7.2 Numerical results | 59 |
| 7.3 Sources of inaccuracies | 63 |
| 8 Discussion and Conclusion | 65 |

| | |
|-----------------------------|------------|
| 8.1 Discussion | 65 |
| 8.2 Conclusion | 67 |
| Bibliography | 69 |
| I Appendix | 73 |
| A Concrete Matrix | 74 |
| B Data sheets | 78 |
| C Test protocols | 93 |
| D Accelerometer Data | 98 |
| E Raw Data | 103 |

List of Figures

| | | |
|------|---|----|
| 1.1 | Main difference between regular concrete and FRC. | 4 |
| 2.1 | Different types of fiber shapes | 8 |
| 2.2 | Compression and tension strength of PC versus SFRC | 8 |
| 3.1 | Example of a simplification from a tall structure to a spring mass system | 16 |
| 4.1 | Result from the compression test [MPa]. | 21 |
| 4.2 | Jig for performing the tensile split test | 22 |
| 4.3 | Specimen for flexural tensile strength test | 23 |
| 4.4 | Applied force - Strain diagram | 24 |
| 4.5 | Setup for the residual test | 25 |
| 4.6 | Example of Force-CMOD diagram | 26 |
| 4.7 | Load-CMOD diagram with F_L | 27 |
| 4.8 | Applied force - CMOD diagram | 28 |
| 4.9 | LOP and residual strength | 28 |
| 5.1 | Dimensions of designed specimen | 30 |
| 5.2 | Setup for impact experiment [mm] | 31 |
| 5.3 | Accelerometer fastened with double sided tape | 32 |
| 5.4 | Laser displacement equipment used | 33 |
| 5.5 | 500 kN Load Cell mounted with a steel tip on the end of the pendulum . | 34 |
| 6.1 | Removal of unusable data from Specimen05 run3 | 36 |
| 6.2 | displacement response of Specimen05 run1 | 38 |
| 6.3 | Period calculation of Specimen05 run1 | 39 |
| 6.4 | Displacement response of Specimen00 run1 | 40 |
| 6.5 | Displacement response of Specimen10 run1 | 40 |
| 6.6 | Period calculation of Specimen00 run1 | 41 |
| 6.7 | Period calculation of Specimen10 run1 | 41 |
| 6.8 | Laser Specimen00 run1 | 42 |
| 6.9 | Laser Specimen00 run3 | 42 |
| 6.10 | Laser Specimen05 run1 | 43 |
| 6.11 | Laser Specimen05 run2 | 43 |

| | | |
|------|--|----|
| 6.12 | Laser Specimen05 run3 | 44 |
| 6.13 | Laser Specimen10 run1 | 44 |
| 6.14 | Laser Specimen10 run2 | 45 |
| 6.15 | Laser Specimen10 run3 | 45 |
| 6.16 | Force-time series for Specimen00 | 46 |
| 6.17 | Force-time series for Specimen05 | 47 |
| 6.18 | Force-time series for Specimen10 | 47 |
| 6.19 | Force impulse for Specimen00 | 49 |
| 6.20 | Force impulse for Specimen05 | 49 |
| 6.21 | Force impulse for Specimen10 | 50 |
| 6.22 | Shear crack top corner Specimen00 | 51 |
| 6.23 | Bending cracks at impact location Specimen05 | 51 |
| 6.24 | Connection crack on Specimen00 | 51 |
| 6.25 | Bottom corner crack Specimen10 | 51 |
| 6.26 | Major crack at Specimen10 | 52 |
| 6.27 | Major cracks at Specimen00 | 53 |
| 6.28 | Deformation of Specimen00 | 53 |
| 6.29 | Deformation of Specimen05 | 53 |
| 6.30 | Deformation of Specimen10 | 53 |
| 7.1 | Illustration of the FEM used further in the numerical analysis | 58 |
| 7.2 | Strain at maximum deflection | 60 |
| 7.3 | Stain at the end of the simulation | 60 |
| 7.4 | Crack formation at the impact location | 60 |
| 7.5 | Crack formation at the footing of column | 60 |
| 7.6 | Crack formation at impact location of the beam | 60 |
| 7.7 | Crack formation at the footing of the column | 60 |
| 7.8 | Comparison of the numerical displacement and the experimental | 61 |
| 7.9 | Impact force from experimental results and the numerical model | 62 |

Abbreviations

| | |
|-------------|----------------------------------|
| RC | Reinforced Concrete |
| FRC | Fibre reinforced concrete |
| SFRC | Steel fiber reinforced concrete |
| BFRC | Basalt fiber reinforced concrete |
| ALS | Accidental Limit State |

List of symbols

| Symbol | Unit | Description |
|---------------|-------------------|---|
| A | [m ²] | Area |
| Δ | [-] | Change of value |
| dl | [m] | Length of the center line of a beam fraction |
| E | [Pa] | Young's modulus |
| f | [Varies] | Global force vector |
| G | [Pa] | Shear modulus |
| γ | [-] | Level of confidence |
| $\gamma(x)$ | [°] | Rotation of a beam due to shear |
| γ_{xy} | [-] | Shear strain |
| I | [m ⁴] | Moment of inertia |
| k | [N/m] | Stiffness factor |
| k_{EB} | [Varies] | Local stiffness matrix for Euler-Bernoulli beam element |
| k_T | [Varies] | Local stiffness matrix for Timoshenko beam element |
| K | [Varies] | Global stiffness matrix |
| l | [m] | Length |
| L | [m] | Length |
| M | [Nm] | Moment |
| n | [-] | Amount of data in the sample |
| N | [N] | Normal force |
| ν | [-] | Poisson's ratio |
| $p(x)$ | [N/m] | Transverse line load |
| r | [m] | Radius |
| σ_{xx} | [Pa] | Normal stress |
| τ_{xy} | [Pa] | Shear stress |
| u | [Varies] | Element nodal displacement vector |

| | | |
|--------------------|------|--|
| $u(x)$ | [m] | Horizontal displacement |
| $v(x)$ | [m] | Vertical displacement |
| ε_{xx} | [-] | Axial strain |
| x_i | [Pa] | Value of an element in the sample |
| \bar{X} | [Pa] | Mean value of the sample |
| y' | [m] | Vertical distance to the center line of the beam |

This chapter will give the reader an introduction to the thesis, how the topic was determined, and the focus of the thesis with its limitations.

1.1 Background

Concrete is a widely used structural material combined with steel reinforcement bars. Even though concrete has great compressive strength, it lacks significant strength when it comes to tension. A steel re-bar can therefore be placed in the zones where the structure are in tension, thus creating a combinations that can be used for almost any structure.

Even though reinforced concrete (RC) is most common, some concrete structures are built using fibre reinforcement in addition to the traditional reinforcement, or as a replacement. Fibre reinforced concrete (FRC) is a composite material that is characterized by an enhanced post-cracking tensile residual strength, which is described later in the thesis [1]. The mechanical properties of the hardened concrete is changed with the presence of fibers, with higher fracture resistance and an increase in tensile strength.

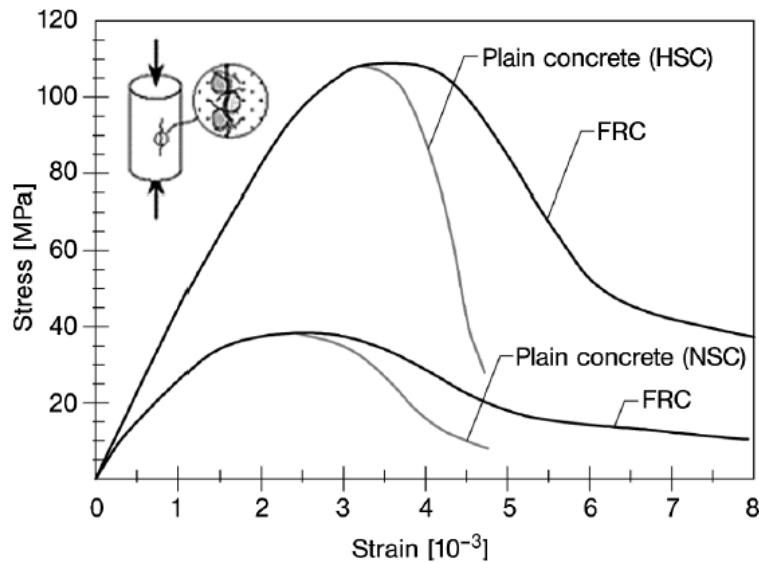


Figure 1.1. Main difference between regular concrete and FRC. [2]

Today's concrete structures are designed to account for accidental loads such as explosions, earthquakes, or vehicle collision. Bridge piers are a great example of such structure, where the structural safety is of great importance. There is much research on impact on RC columns or beams, but not as much for FRC.

1.2 Scope

The scope of the thesis is to design and build a scaled FRC pier and perform an impact experiment and evaluate the structural response. The results from the experiment are used to develop and calibrate a finite element model of the experiment.

1.3 Thesis structure

The thesis is structured such that it consists of two parts, the main report and the appendix. In the appendix, all available data sheets, raw data, and testing protocols are presented. Whereas, the main report presents the problem of the thesis.

An introduction was made in chapter one, where the background for the thesis is discussed, including the scope of the thesis.

Chapter two includes the literature review that is relevant for the thesis, while chapter three presents the relevant theory.

The experimental work, in form of the mechanical properties of the fibre concrete can be found in chapter four, as the testing procedures and results are presented together. The experimental work continues in chapter five, as the specimen design and test setup are presented. The data from the pendulum experiment is found in chapter six, together with the calculated results used further in chapter 7.

Chapter seven includes the development of the numerical model, and comparison between the experimental results and the numerical can be found here.

The different results are discussed in chapter eight, together with the concluding marks of the thesis, and recommendations for further work.

2.1 Fiber reinforced Concrete

Fiber reinforced concrete consists of normal concrete where small pieces of a material is added to increase the integrity of the structure. Fibers vary in size but are commonly between 10-60 mm in length, and 5-1000 μm in diameter [3]. During the past time many different types of fiber have been used for different structures. Some disadvantages follows when adding fibre in the concrete mix, such as reduced workability, increased dead-load, and fibers clumping instead of spreading evenly in the concrete mix. The most common types of fiber used today are steel fibers, glass fibers, carbon fibers, basalt fibers, polypropylene fibers, and natural fibers.

The shape and length of fibers plays a crucial role in the effectiveness of the fibers. Usually three different parameters determine the performance of the fibre; the shape of the fibre, aspect ratio, and the surface treatment [4]. The steel fibers most common cross section was circular, with some type of end hook as anchorage at the end for better bond strength. The bond strength of a fiber determines if the fiber will slip out from the concrete or break. It is beneficial if the fiber tears before it slips out from the concrete.

With current technology it is possible to make fibers of any desired cross section, shape, and diameter. Synthetic fibers can be produced with a diameter down to 5 μm , like glass fibers. The most common fiber shapes are presented in figure 2.1. Instead of only the traditional end-hook type of fibre, it is common to improve the bond strength by modify the fiber along its length with small bumps, indentations, twists or other anchorage methods [4]. It is also noticed that the ratio between the cross-sectional area and its circumference plays a major role, as a larger surface creates better bond conditions.

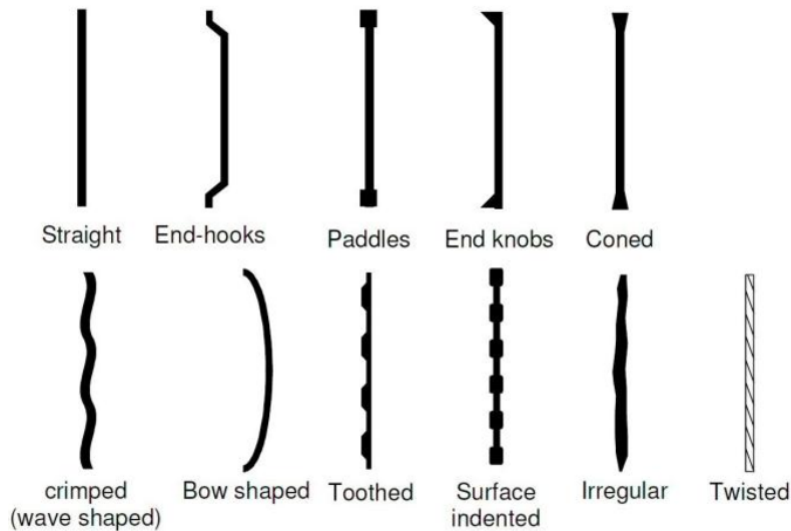


Figure 2.1. Different types of fiber shapes [5]

Steel fibers have for a long time been the most common fiber used in reinforced concrete. It have been an additional reinforcement together with normal re-bar, or replaced the reinforcement completely. Total replacement usually occurs in concrete slabs resting on the ground, or slabs with a relative short span between the supports [6]. Because of the favorable mechanical similarities between steel and concrete, steel fibers have been the optimal choice over the years. The surface of a steel fiber is changed to have a rougher surface, or different shapes, to enhance bond between the fiber and concrete. Figure 2.2 displays the effect of steel fibers in the post cracking, as it is carrying load after the initial fracture of the concrete.

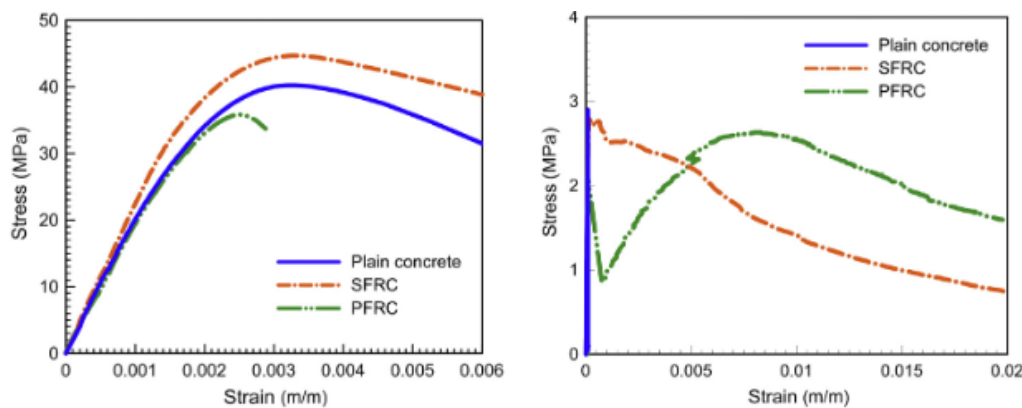


Figure 2.2. Compression (left) and tension strength (right) of plain concrete versus steel fiber reinforced concrete [7]

There are two forms of polypropylene fibers, monofilament fiber and film fibers. Film fibers is made by extruding the polypropylene trough a nozzle, that produces a flat film. The film are chopped into strings and stretched trough a roller system

to elongate and twist the fiber to form different types of shapes. Monofilament are made on the more traditional method, by extruding the polyethylene with a spinner and the cut to the desired length. Polyethylene fibers have a relatively high alkaline resistance. This together with a high melting point and a low production cost, makes it an interesting product for further optimizations. The problems with polyethylene is that it degrades with oxygen and sunlight compared to other materials. It has also a low bond strength with the cement matrix [8].

Glass fiber is made by a molten glass that is squeezed through a small valve to produce a small filament of glass fiber. The glass fiber is then either chopped to small fibers or made into a continuous roll. Glass fibers have been used to make durable ornamental concrete, but in the later years, studies have investigated its structural abilities [9]. The biggest disadvantages of the first glass fiber used in concrete was its low resistance to an alkaline environment, which you find in a concrete mix. The cement matrix causes rapid decay of glass fiber, and therefore was not suited for such purpose. Because of its lack of resistance, a new type of glass fiber was developed with a higher resistance to the cement matrix environment [10].

Basalt fibers are made out of an igneous rock that is formed by the rapid cooling of a thick flowing lava. Depending on the location of where the basalt rock is extracted the chemical composition are diverse [11]. The basalt fiber is made in a similar method as glass fiber, as it is melted and a thin filament is produced and chopped. Basalt fibers are often a popular choice regarding those concerns, as they are lighter than steel fibers, and significantly more environmentally friendly to produce.

Basalt fibers are used as normal chopped fibers, or as smaller fibers called minibars. As for normal chopped basalt fiber, studies suggest that a fiber content above 0.5% is not beneficial for the concrete's mechanical properties. On the other hand, it has been suggested that minibars can benefit the mechanical properties with a fiber content of up to 4% [12]

High et. al have performed a research program to evaluate the flexural behavior of concrete reinforced with basalt fibers. They discovered that basalt fibers slightly increased the flexural strength, but require a high reinforcement ratio to prevent slipping of the fiber [13].

John and Dharmar conducted an investigation on the behavior of BFRC under static and dynamic condition. Their experiments used basalt fibers of chopped fibers,

minibars, re-bar, and meshes. All types was found to be promising in improvement of toughness, energy absorption capacity, bending properties, tensile strength and bond strength. The basalt minibars performed better for flexural members because of its ductile nature [14].

Kirthika and Singh have performed a systematic investigation regarding BFRC, where one of the performed test was a impact test. They concluded that the basalt fiber is a potential building material with its high thermal stability and higher mechanical properties [15]. They observed a major increase in compressive, splitting tensile, flexural strength, of concrete with 5% fibre content. The measured impact strength was drastically increased with fibre, as it was found to be more than double of the reference concrete [15].

2.2 Impact test on concrete

A bridge pier needs to be designed for many types of accidental loads, as car impacts, or boat collisions. This determines the dynamic load as "Force that varies with time, and can cause significant dynamic effect on the structure" [16]. It provides guidelines as how to of accidental loads that is cause by vehicles on land, as well as water vessels. The methods in the Eurocode are simplified methods where the dynamic force is replaces with a equivalent static force.

To investigate the dynamic response of a structure, the most common methods are experimental laboratory test, or by numerical analysis. Laboratory test usually involves having a mass either dropped or swung at a specimen, for then to measure the vibrations and deflections. Numerical analysis uses a software to simulate the dynamic problem. The only limitation of a simulation is its computational power, as the structure takes no physically space. When a physically model is investigated it is usually scaled down, as it would be inefficient to build a full scale structure in the laboratory.

When designing concrete structures simplified methods are used to predict the structures response to impact loads. Impact happens over a short duration, and the structures ability to resist the impact forces without structural failure are determined by the mechanical properties of the design. It is therefore important that the dynamic response of the structure can be determined with certainty. The simplified methods do not capture any of the brittle damage that can occur with

high impulse loads.

Sohel et. al investigated the behaviour of a reinforced concrete column subjected to low-velocity car impact. Their experimental program was a drop test on a column and developed a numerical model. They concluded with that the Eurocode underestimates the equivalent static force that shall replace the dynamic loads when resisting a collision [17]. Wu et al. performed a similar numerical analysis, but for vehicles with higher speed and more mass. They found that the dominated factors concerning pier damage was vehicle velocity, section size of piers, and height of the pier. The peak bending moment and peak shear force decreases with height of the column [18].

Bin Liu et. al. performed a drop test on a reinforced concrete column. They discovered that the reinforcement ratio affect the global and the local impact damages. Local failures are greatly reduced with larger reinforcement ratio, e.g The transverse and the longitudinal reinforcement help to reduce the impact damages [19].

Sha and Hao investigated an impact between a barge and a circular bridge pier. A scaled specimen was examined in an experimental investigation, before a numerical model was calibrated and a full-scale simulation were performed. A parametric study was carried out to determine the different impact energies on impact force. They discovered that the impact velocity influenced the impact force, while the impact duration was affected by the mass of the barge [20].

Impact energy and Dynamic response

3

The purpose of this chapter is to review the relevant theory for this thesis. In the beginning, impact energy and its formulas are explained, while the dynamic response after impact are explained at the end.

3.1 Impact energy

As mentioned in the section above, impact is when an object is hit by a force from a moving object for a short duration. The kinetic energy that the moving object carries gets transferred between itself and the target object. In physics there are two types of collisions, elastic and inelastic. In an elastic all the kinetic energy is conserved in the collision, while an inelastic loses some of the kinetic energy. In reality the kinetic energy is never completely conserved, as some will become heat, sound, or other forms of energy [21]. If the colliding objects merge together after collision, it is a perfectly inelastic collision.

To determine the velocity of a dropped object, the principle of conservation of energy can be utilized. Since the potential energy of the dropped object should be equal to the kinetic energy we can set up a set of equation to determine its velocity:

$$E_i = E_f \quad (3.1)$$

$$E_{p,i} + E_{k,i} = E_{p,f} + E_{k,f} \quad (3.2)$$

$$mgh_i + \frac{1}{2}m\vec{v}_i^2 = mgh_f + \frac{1}{2}m\vec{v}_f^2 \quad (3.3)$$

If we assume that the object is starting from rest, the initial velocity, \vec{v}_i , is zero, equation 3.3 becomes:

$$mgh_i = mgh_f + \frac{1}{2}m\vec{v}_f^2 \quad (3.4)$$

$$\vec{v}_f = \sqrt{2g(h_i - h_f)} = \sqrt{2g\Delta h} \quad (3.5)$$

With the final velocity of the object, one can derive its momentum. Momentum is a vector quantity, which has a direction, which is the same direction as the velocity, and a magnitude. Momentum is equal to the objects mass times the velocity, thus have the unit $\text{kg}\cdot\text{m}\cdot\text{s}^{-1}$ [22].

$$P = m\vec{v} \quad (3.6)$$

A force is applied to a mass over a period of time. By assuming that its mass does not change, Newton's Second Law yields [22]:

$$\vec{F} = m\vec{a} = m\frac{d\vec{v}}{dt} = \frac{dm\vec{v}}{dt} = \frac{d\vec{p}}{dt} \quad (3.7)$$

The impulse of a force acting on a particle during a time interval is defined as the definite integral of the force from the time interval. For the time period $[t, t + \Delta t]$, we get [22]:

$$\vec{I} = \int_{t'=t}^{t'=t+\Delta t} \vec{F}(t') dt' \quad (3.8)$$

The units of impulse is $\text{N}\cdot\text{m}$, which is the same units as momentum, and can then apply Newton's Second Law [22]:

$$\vec{I} = \int_{t'=t}^{t'=t+\Delta t} \vec{F}(t') dt' = \int_{t'=t}^{t'=t+\Delta t} \frac{d\vec{p}}{dt'} dt' = \int_{\vec{p}'=\vec{p}(t)}^{\vec{p}'=\vec{p}(t+\Delta t)} d\vec{p}' = \vec{p}(t+\Delta t) - \vec{p}(t) = \Delta\vec{p} \quad (3.9)$$

The equation represents the integral version of Newton's Second Law: the impulse applied by a force during a time interval, is equal to the momentum of the particle during that time interval. The average force of the time interval Δt can be derived by the following expression [22]:

$$\vec{F}_{\text{ave}} = \frac{1}{\Delta t} \int_{t'=t}^{t'=t+\Delta t} \vec{F}(t') dt' \quad (3.10)$$

The product of the average force acting on the object and the time interval over which it is applied is called the average impulse [22],

$$\vec{I}_{\text{ave}} = \vec{F}_{\text{ave}}\Delta t \quad (3.11)$$

Multiply each side with equation 3.10 by Δt , it states that the average impulse applied to the particle during the time interval is equal to the change in momentum of the particle. Thus, impulse does not cause momentum, but it is the change in momentum [22]

$$\vec{\mathbf{I}}_{\text{ave}} = \Delta \vec{\mathbf{p}} \quad (3.12)$$

3.2 Dynamic response

After an initial impact, a structure is said to undergo free vibrations when it oscillates, if no external loads take place afterwards. If external dynamic loads are applied during the vibrations, it is forced vibrations. If the amplitude of the motion stays the same after the initial impact, the system is an undamped system. However, in reality some energy will often dissipate, and decrease the amplitude of the system and make it damped [23].

For a system which is vibrating freely, it will vibrate in it's natural frequency. The natural frequency of a system is depended on it's mass and it's stiffness. The natural frequency can using equation 3.13. If the system are applied a dynamic force where the frequency of the force approaching the systems natural frequency, we get resonance, which is an amplification of the applied force. This phenomenon can cause severe damage to the system, and is generally avoided in a structural sense.

$$f_n = \frac{\omega}{2\pi} = \frac{1}{2\pi} \sqrt{\frac{k}{m}} \quad (3.13)$$

Many structural systems can be assumed to be a single-degree-of-freedom system (SDOF), even if the mass is distributed along the system. The mass can be set as a single point mass, with the elasticity which also is distributed along the system. If we take a tall structure that have an initial displacement. The displacement from its original position can be denoted x , and the systems stiffness k , an SDOF system can be created and written as an equivalent spring-mass system [23]:

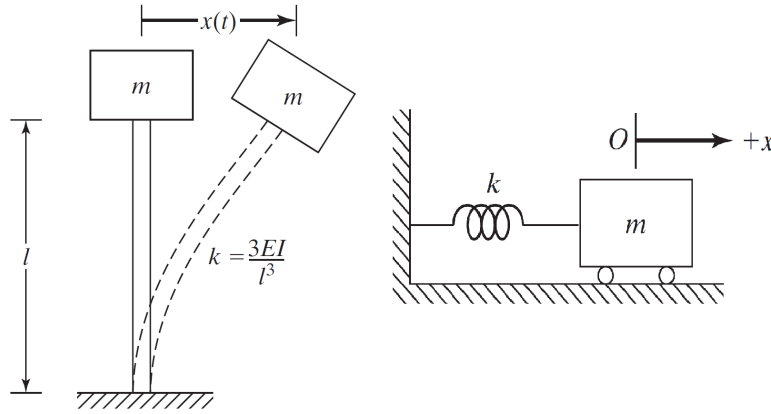


Figure 3.1. Example of a simplification from a tall structure to a spring mass system [23]

Using Newton's second law of motion it is possible to derive the equation of motion. The states as following: "The rate of change of momentum of a mass is equal to the force acting on it". If the mass m is displaced a distance $\vec{x}(t)$ when a resultant force $\vec{F}(t)$ is influencing the mass in the same direction, Newton's second law of motion gives [23]:

$$\vec{F}(t) = \frac{d}{dt} \left(m \frac{d\vec{x}(t)}{dt} \right) \quad (3.14)$$

If the mass m is constant, the equation becomes:

$$\vec{F}(t) = m \frac{d^2\vec{x}(t)}{dt^2} = m \ddot{\vec{x}} \quad (3.15)$$

where

$$\ddot{\vec{x}} = \frac{d^2\vec{x}(t)}{dt^2} \quad (3.16)$$

is the acceleration of the mass. From equation 3.15 can be written as:

$$\text{Resultant force on the mass} = \text{mass} \times \text{acceleration}$$

The procedure is applied to the SDOF system showed in figure 3.1. The mass is supported from frictionless roller and have move in the horizontal direction. when the mass is displacement in a distance $+x$ from equilibrium, the spring force is kx . The application of equation 3.15 to the mass m yields:

$$\vec{\mathbf{F}}(t) = -kx = m\ddot{\vec{\mathbf{x}}} \quad (3.17)$$

or

$$m\ddot{\vec{\mathbf{x}}} + kx = 0 \quad (3.18)$$

To take account for the damping of the system, the damping constant c is included. It is proportional to the velocity of the mass, and in the opposite direction of the stiffness. Then the equation of motion becomes:

$$m\ddot{\vec{\mathbf{x}}}(t) - c\dot{\vec{\mathbf{x}}} + kx = 0 \quad (3.19)$$

This means that when the initial displacement is at the maximum, the force in the spring will pull the mass back. until it passes statically equilibrium at maximum velocity, before it compresses the spring and returns. This process continues while some of the energy dissipates, until the the systems stops.

The following chapter describes the mix-design for the concrete formula and the mechanical properties of the hardened concrete are then presented.

4.1 Mix design

The concrete mix is made out of NORCEM Lavvarme cement, which has a 70% content of slag. This might reduce the strength of the concrete in the early curing phase, but after 28 days the strength should be as high as expected. The Superplastiziser used is Dynamon SX-N, while the sand and gravel are Årdal 0/8 mm, and Årdal 8/16 mm. The specification for each component can be found in appendix B.

To ensure an even distribution of fibres between the rebar, a sand/gravel ratio of 70/30 is chosen compared to the normal 55/45 ratio. A high content of reinforcement together with the fibers a concern rises regarding formations of air pockets during the casting. To reduce the chance of the development of thees pocket, a matrix dominant concrete mix is preferred. A matrix volume of 600 l/m^3 [24] is chosen to ensure a sufficient flow during casting.

Three separate batches are made with a fiber content of 0.0%, 0.5%, and 1.0%. Each batch is 115 liter of fresh concrete, which is distributed as follows:

Table 4.1. Distribution of concrete

| | |
|--------------------------|------------|
| Main specimen | 50 liters |
| 6 x 100x100x100 mm cubes | 6 liters |
| 3 x 100x100x500 mm beams | 15 liters |
| 2 x 150x150x550 mm beams | 38 liters |
| +5% spillage | 5.5 liters |
| Total | 115 liters |

The concrete mix is made using NORCEMs mixing procedure: The dry components are mixed together, followed by water and superplasticizer. The mixer continues for three to five minutes, before the fibres are added. 4.2.

Table 4.2. Concrete formula [kg/m³]

| Concrete Component | 0.0% | 0.5% | 1.0% |
|------------------------|-------|-------|-------|
| Cement | 805.3 | 804.5 | 805.6 |
| Årdal 0/8 mm | 720.6 | 711.1 | 701.7 |
| Årdal 8/16 mm | 307.9 | 303.8 | 399.8 |
| Water | 322.1 | 322.2 | 322.2 |
| Mapei Dynamon SX-N [g] | 157.0 | 235.0 | 241.0 |

After casting the molds are sealed to prevent moisture loss, while the forms that can't be sealed are covered with polyethylene. After 4 days the smaller specimens are removed from the molds and placed submerged in water. When the column was removed from the mold, some formation of small cracks were observed. Thus, it was decided to wait longer before taking the specimens out of the molds, to ensure that no more cracks developed.

4.2 Mechanical properties of hardened concrete

In this section the properties of the hardened concrete is presented. The test specimen are denoted with the fibre content, with a following specimen number. For instance, cube number 2 with fibre content of 0.5% is denoted as 0.05% S2. The protocols from all the test performed can be found in appendix C

4.2.1 Compression test

The most important criteria for concrete is its compressive strength, which is it's ability to withstand pressure without any failure. Three cubes from each batch are tested after seven days, and the rest are tested at 28 days. The cubes are places in a compression test machine and applied continuous loading until failure. The average stress at failure for all cubes will determine the compressive strength of the concrete. The stresses are determined from equation 4.1 [25]

$$f_c = \frac{F}{A_c} \quad (4.1)$$

where,

- f_c Compressive strength [MPa]
- F Maximum force at fracture [N]
- A_c Cross sectional area [mm²]

Result from the test

The result from the compressive test are presented in figure 4.1. One can observe from the figure that the average compressing strength is 73 MPa, and according to Table 3.1 in EC2, the concrete mix is classified to B55 concrete.

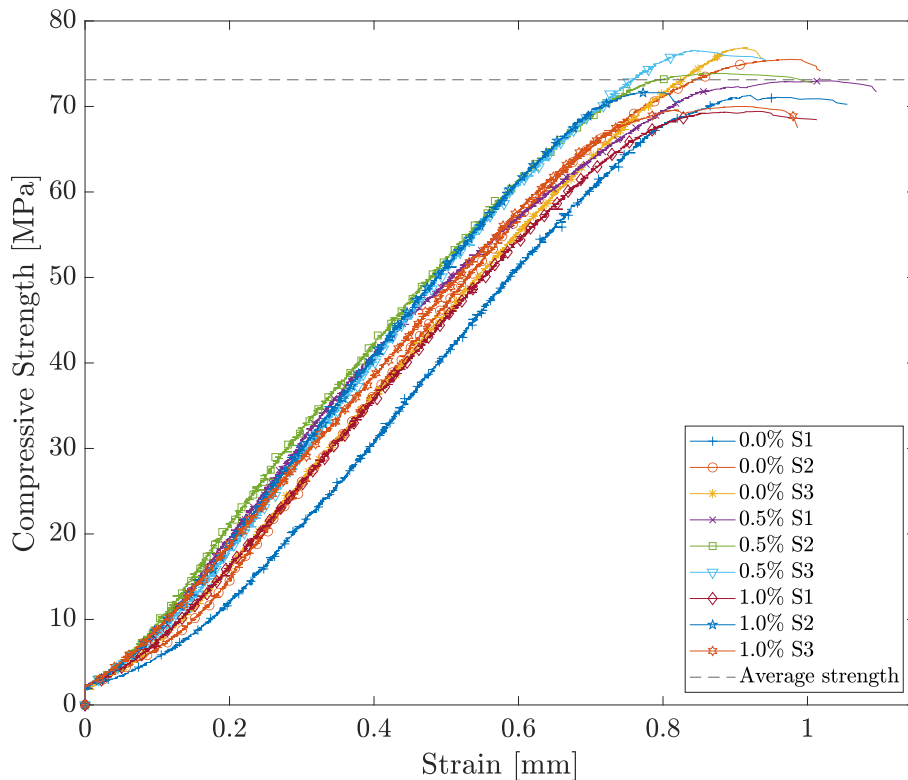


Figure 4.1. Result from the compression test [MPa]

4.2.2 Tensile splitting strength

The split tensile strength is calculated according to *NS-EN 12390-6: Testing hardened concrete - Part 6: Tensile splitting strength of test specimens*. 150x300 mm cylinders are placed in a vertical jig (see figure 4.2) in the center of the machine. Continuous load are applied until fracture. Ideally the specimen is split into two equal

parts, by its longitudinal axis. Assuming the specimen behaves elastic, the tensile strength is calculated from equation 4.2.

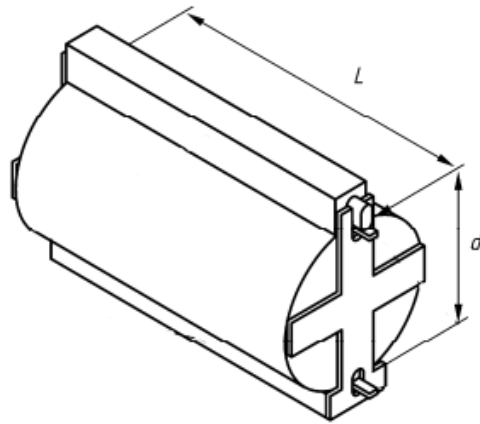


Figure 4.2. Jig for performing the tensile split test [26]

$$f_{ct} = \frac{2 \times F}{\pi \times L \times d} \quad (4.2)$$

where,

| | |
|----------|----------------------------------|
| f_{ct} | Tensile splitting strength [MPa] |
| F | Force at fracture [N] |
| L | Contact length [mm] |
| d | Cross-sectional diameter [mm] |

Result from the test

The result from the tensile splitting test can be found in table 4.3. From the table one can observe a small increase of tensile strength with an increase of fibre content. The average strength is calculated to be 3.43 MPa. It was also observed during testing of the specimen with fibres, that small fractures happened before a the concrete specimen itself fractured. This small fracture would trigger the stopping-mechanism of the testing equipment to early. After examining the specimen and no fracture was detected another test was performed on the specimen that had premature fracture.

Table 4.3. Tensile splitting strength of all tested specimens

| Specimen ID | Maximum force F [kN] | Tensile strength f_{ct} [MPa] |
|-------------|------------------------|---------------------------------|
| 0.0%S1 | 202.25 | 2.86 |
| 0.0%S2 | 228.60 | 3.23 |
| 0.0%S3 | 179.99 | 2.55 |
| 0.5%S1 | 253.71 | 3.59 |
| 0.5%S2 | 257.82 | 3.65 |
| 0.5%S3 | 212.26 | 3.00 |
| 1.0%S1 | 294.63 | 4.17 |
| 1.0%S2 | 312.87 | 4.43 |

4.2.3 Flexural tensile strength

The flexural tensile strength is calculated using *NS-EN 12390-6: Testing hardened concrete - Part 5: Flexural strength of test specimens*. [26] The small beams with dimensions of 100x100x500 mm are placed in the center of two roller supports with a mid span of 450 mm. A third roller support is lowered at constant speed at the mid span of the beam. The applied force is noted and the flexural tensile strength is calculated with equation 4.3.

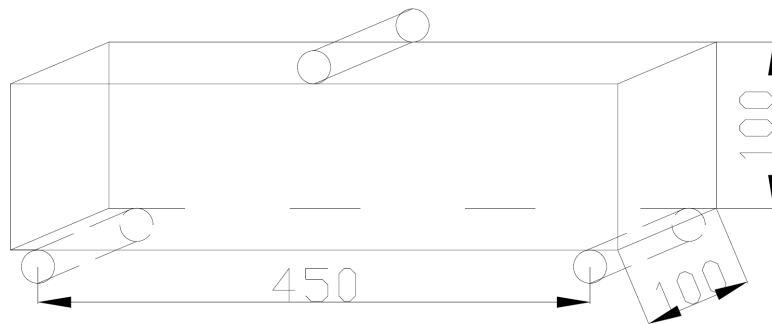


Figure 4.3. Specimen for flexural tensile strength test

$$f_{ct,fl} = \frac{3 \times F \times l}{2 \times d_1 \times d_2^2} \quad (4.3)$$

where,

| | |
|-------------|--|
| $f_{ct,fl}$ | Flexural tensile strength [MPa] |
| F | Load at fracture [N] |
| l | Distance between the roller support [mm] |
| d_1, d_2 | Cross sectional dimensions [mm] |

Results from the test

The results from the test is illustrated in figure 4.4, and the calculated flexural tensile strength are presented in table 4.4. From the figure it is a clear difference between the specimens containing fibres, versus the three without any fibres, which has a clear straight fracture around 1.5 mm strain. The three next specimen with 0.5% fiber have a small decrease in force before the fibres can resist the load with an increase in load before fracture. For the last three specimens the fibers resists the load immediately. The average flexural tensile strength for the mixes with 0.0%, 0.5%, and 1.0% is 7.38 MPa, 6.86 MPa, and 8.83 MPa, respectively.

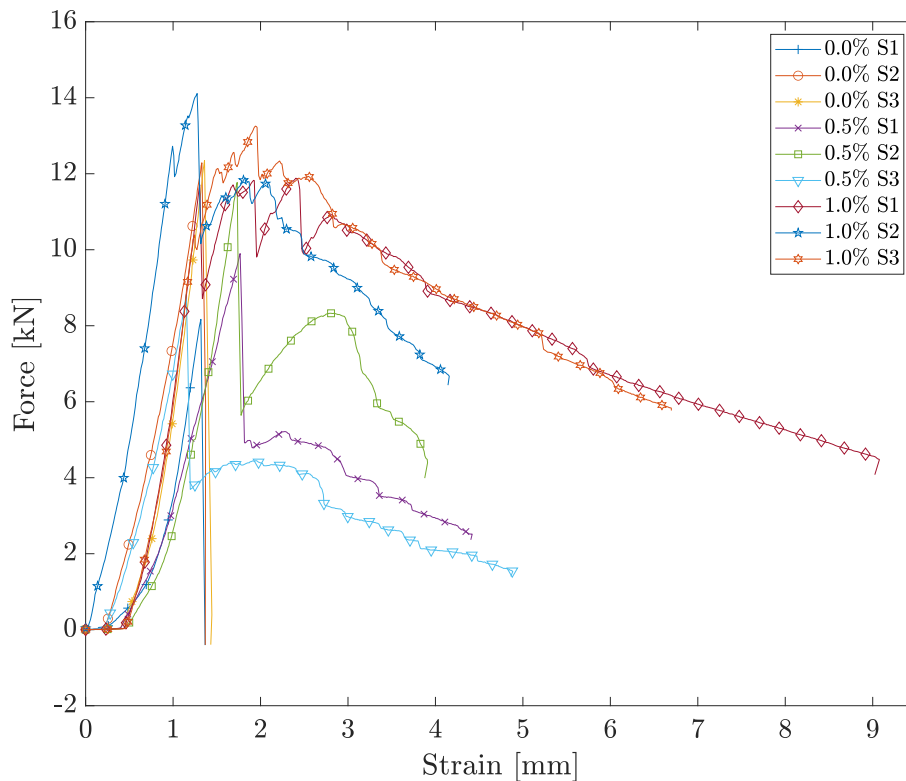


Figure 4.4. Applied force - Strain diagram

Table 4.4. Flexural tensile strength of all tested specimens

| Specimen ID | Fracture force F [kN] | Flexural tensile strength $f_{ct,fl}$ [MPa] |
|-------------|-------------------------|---|
| 0.0%S1 | 8.167 | 5.514 |
| 0.0%S2 | 12.288 | 8.294 |
| 0.0%S3 | 12.345 | 8.333 |
| 0.5%S1 | 9.899 | 6.682 |
| 0.5%S2 | 11.771 | 7.946 |
| 0.5%S3 | 8.829 | 5.959 |
| 1.0%S1 | 11.881 | 8.020 |
| 1.0%S2 | 14.112 | 9.525 |
| 1.0&S3 | 13.234 | 8.946 |

4.2.4 Residual strength test

Residual strength are determined after NS-EN 14651:2005+A1:2007. Two 150x150x550 mm beams from each batch are prepared 25 days after casting. The specimens are rotated over 90° around their longitudinal axis and a notch is sawn trough the width of the specimen at mid-span. the notch have a depth of 25 mm. At the edge of the notch, two knife blades are glued on as showed in figure 4.5. The specimens are placed under polyethylene for the remaining three days tucked in wet towels.

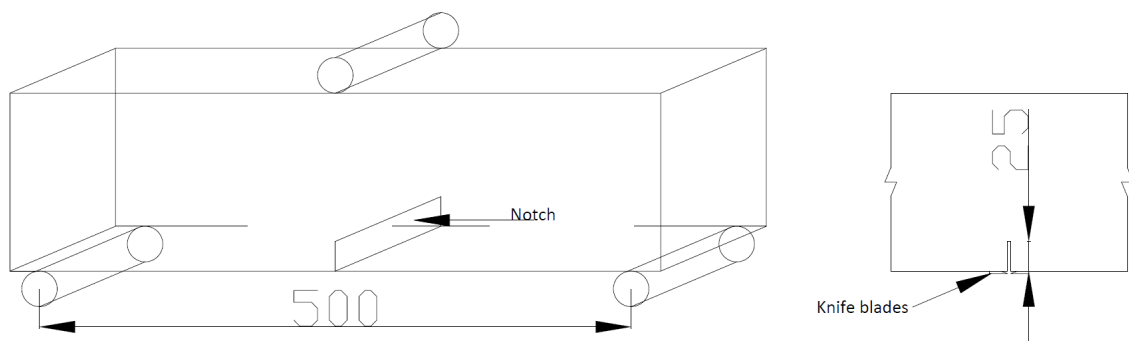


Figure 4.5. Setup for the residual test

After 28 days the specimens are placed, with the notch down, on two roller supports with a span of 500 mm. A third roller support is lowered with a constant speed at the mid span of the beam, directly above the notch. A clip-gauge is fastened at the knife blades to measure the CMOD (Crack Mouth Opening Displacement), together with a transducer to measure the downward displacement.

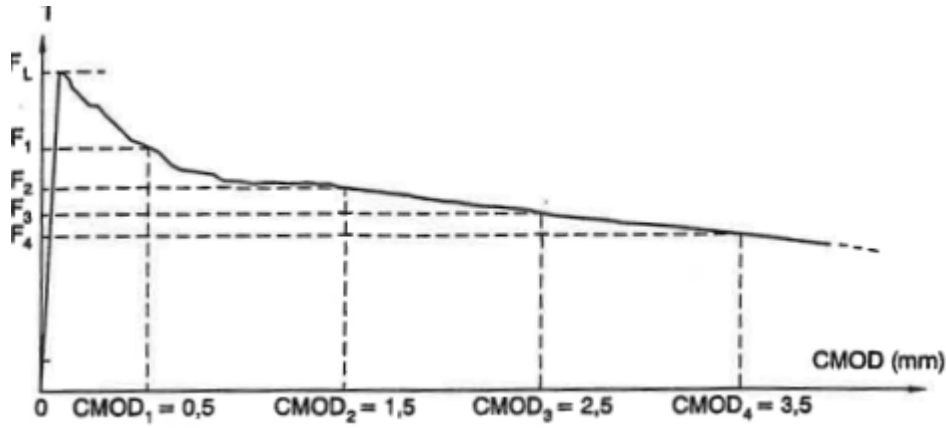


Figure 4.6. Example of Force-CMOD diagram with the corresponding $CMOD_j$ [27]

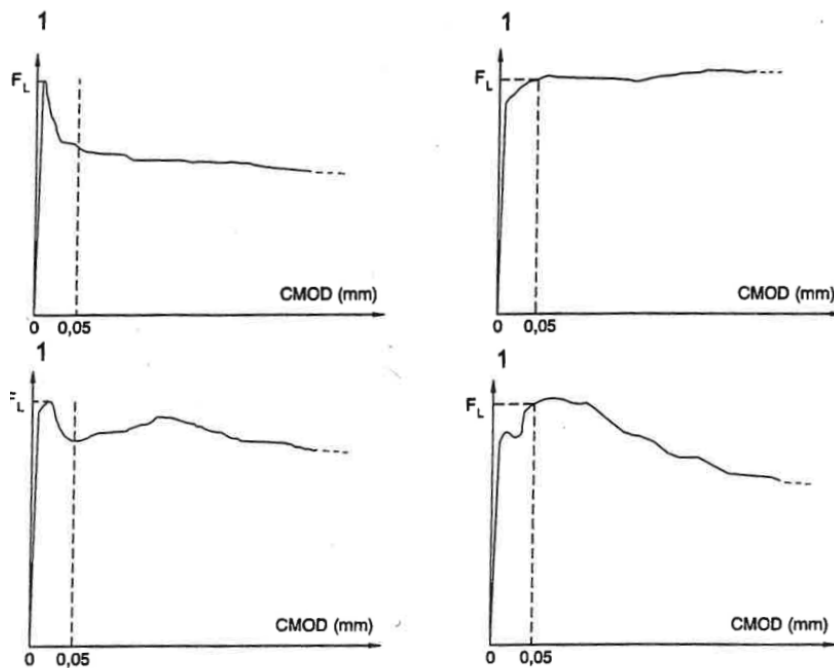
The residual strength is calculated using equation 4.4, and the Limit of proportionality (LOP) is calculated using equation 4.5. The load F_L is determined at the highest point of the curve before $CMOD = 0.05\text{mm}$. Examples of different F_L situations can be found in figure 4.7. Equation 4.4 derives the strength from the force at specific CMOD's after fracture. The specific CMOD that are used is showed in figure 4.6.

$$f_{R,j} = \frac{3F_j l}{2bh_{sp}^2} \quad (4.4)$$

$$f_{ct,L}^f = \frac{3F_L l}{2bj_{sp}^2} \quad (4.5)$$

where,

| | |
|--------------|--|
| $f_{R,j}$ | Residual flexural strength corresponding with $CMOD_j$ ($J=1,\dots,4$) [MPa] |
| F_j | Load corresponding with $CMOD_j$ [N] |
| l | Span length [mm] |
| b | Width of the specimen [mm] |
| h_{sp} | Distance between the tip of the notch and the top of the specimen [mm] |
| $f_{ct,L}^f$ | Limit of proportionality [MPa] |
| F_L | Load corresponding to the LOP [N] |

Figure 4.7. Load-CMOD diagram with F_L [27]

Results from the test

The Force-CMOD diagram from each test is illustrated in figure 4.8. One can see from the figure that the three specimens with 0.5% fibre have a significant smaller resistance to the applied force after fracture of the concrete. All three have a drop in applied force before tackling further load. The three specimens with 1.0% load manages to resist a much higher force after fracture of the concrete.

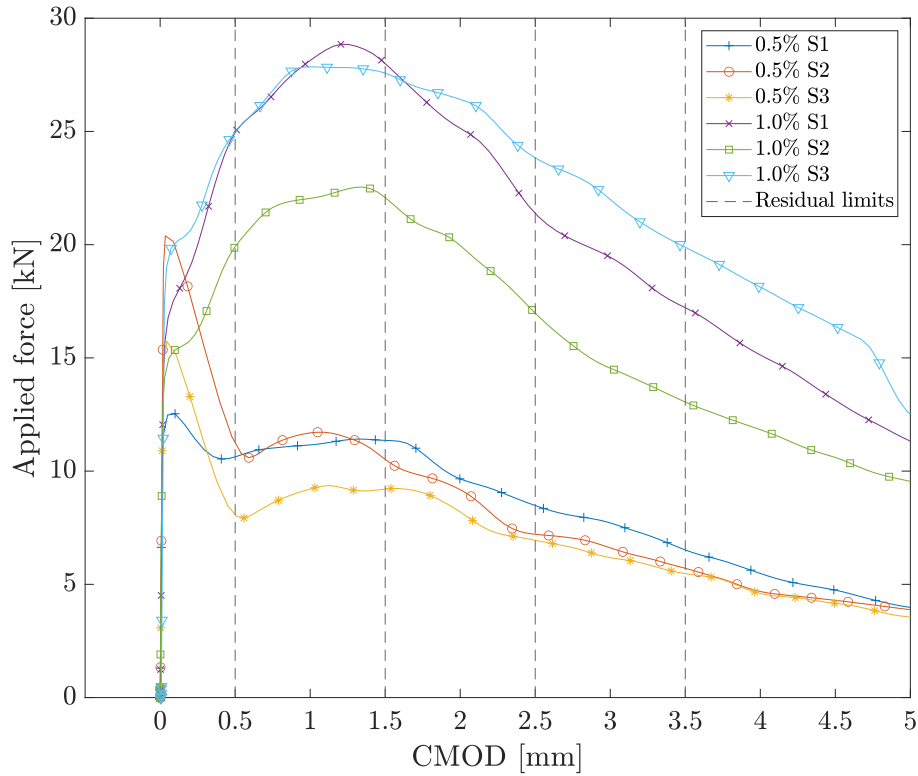


Figure 4.8. Applied force - CMOD diagram

Using equation 4.5 and equation 4.4 we obtain the limit of proportionality and residual strength, which is illustrated in the figure 4.9.

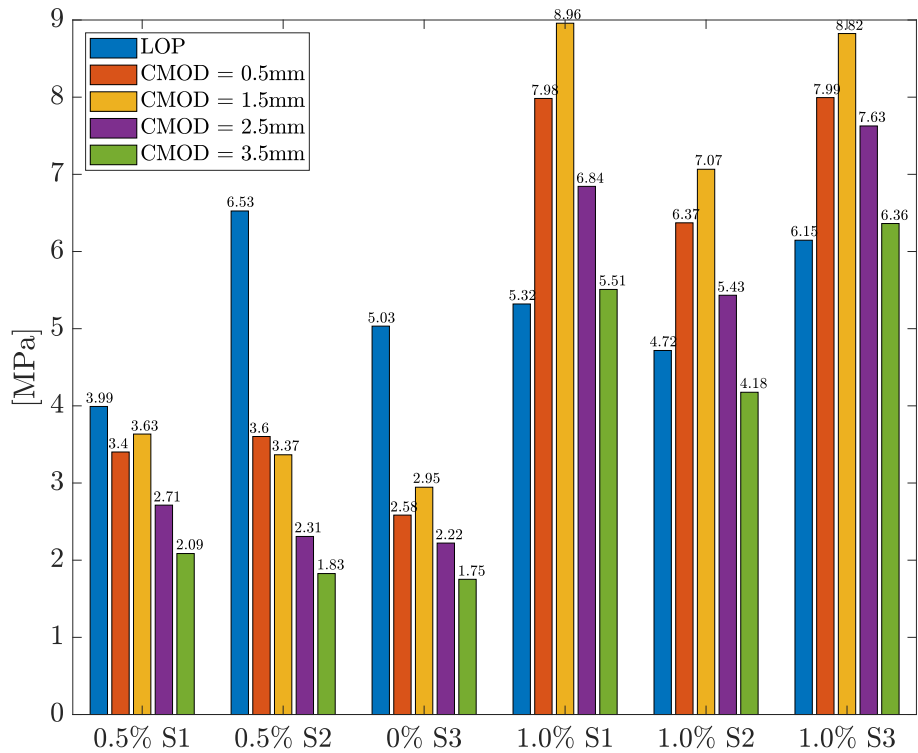


Figure 4.9. Limit of proportionality followed by the residual strength for the four CMOD's for all specimens

This chapter aims to describe the specimen design for the impact test, together with the measuring equipment used, and the test setup

5.1 Column design

To be able to investigate the impact resistance and response fibre-reinforced bridge piers, a scaled down specimen is made. The design is based on a square column which is supported on both sides with a small slab.

An already existing pendulum rig exist in the testing facilities, and therefore the column is designed to fit the testing rig. The dimensions of the column is 100x100x1500mm, which is centered on the 400x400x100 mm slabs. A detailed drawing of the slabs can be found in figure 5.1. The figure also includes the placement of the reinforcement of the whole specimen.

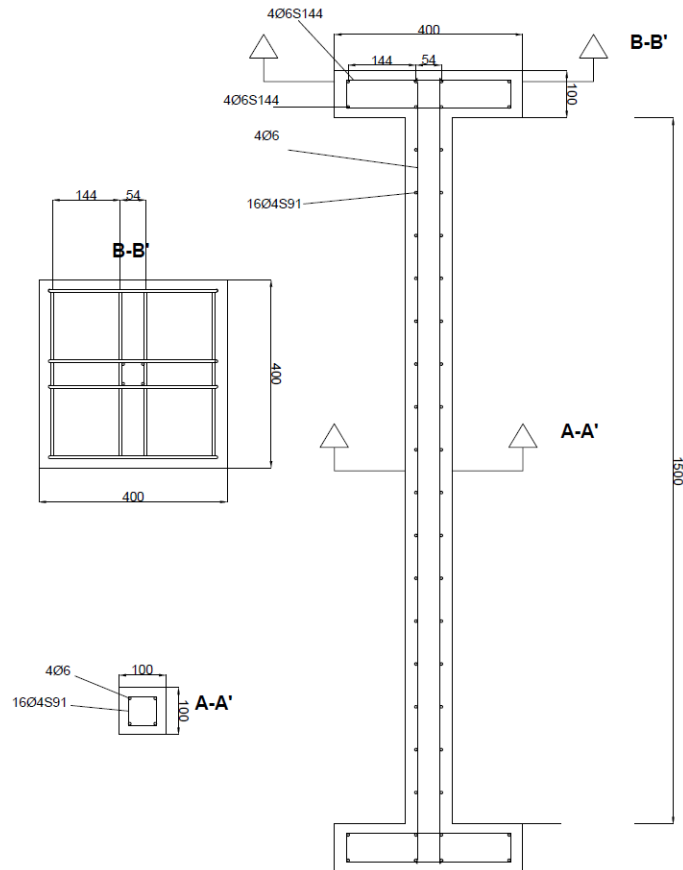


Figure 5.1. Dimensions of designed specimen

The reinforcement used in the specimens are B500NC steel bars. The column have $\text{Ø}6$ re-bar in the corners with end hooks connected to the slab reinforcement. $\text{Ø}4$ re-bar is used for the stirrups. A small web of $\text{Ø}6$ re-bar constitutes the slab reinforcement. Because of the small dimensions of the steel bar, smooth bars were delivered instead of steel bars with ribs. This will lower the bond strength between the concrete and reinforcement. The reinforcement calculations are performed according to Eurocode 2: Design of concrete structures (EC2) [28].

5.2 Pendulum setup for impact test

The purpose of the experiment is to investigate the dynamic response of a fibre reinforced concrete column under impact loading. The results of the test are presented, and used to calibrate the numerical model in chapter 7.

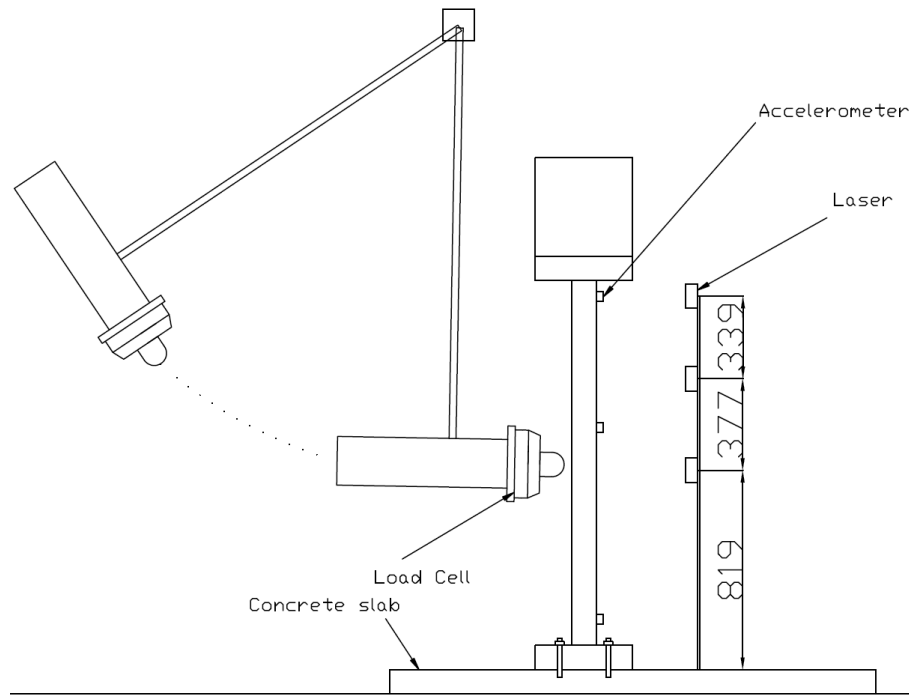


Figure 5.2. Setup for impact experiment [mm]

To determine such response a pendulum setup is needed. As shown in figure 5.2 the concrete column is fastened to a concrete slab with four bolts, to create a fixed boundary condition. A concrete cube with a mass of 208 kg is placed on top and fastened with straps. The pendulum is made of a one meter long square hollow steel beam. On the end an load cell is fastened with a indenter at the end. The steel beam is fastened to an crossing steel beam with four adjustable turnbuckles. A rope with hoops at different intervals is fastened to the back of the pendulum, where each hoop represent a different drop height for the experiment. Each concrete column is tested from the same heights. The total mass of the pendulum is measured to 183 kg.

5.2.1 High speed camera

A high-speed camera where used to capture impact. The camera are of the model Photron FASTCAM mini AX100, and captures up to 4000 frames per seconds (FPS). With maximum frame-rate the camera can capture footage of 2.7 seconds each time, which means that the release of the pendulum must be within this range. The camera comes equipped with its own lighting, as filming with such high frame-rate gets very dark.

5.2.2 Accelerometer

Three accelerometers are fastened to the concrete column, to measure the vibrations after impact. One accelerometer is fastened to the top, one in the middle, and one on the bottom of the column. Each accelerometer are fastened to a steel plate which can be screwed into the concrete or taped using thin double sided tape.

The accelerometers are of the model Dytran 3200B6M, and records data up to 24500 m/s^2 , with a frequency of 1 kHz. The software used to record data from the accelerometers are Quickdaq. The sensors needed to be calibrated with a reference value that followed each accelerometer. The value where given in unit mV/g , but converted to $\text{mV}/(\text{m/s}^2)$.



Figure 5.3. Accelerometer fastened with double sided tape

5.2.3 Laser displacement equipment

Three OptoNCDT 1220 laser displacement sensors were equipped to measure the backwards deflection. The sensors have a measuring range of 50 mm, and records data with a frequency of 1 kHz. The lasers where mounted on a separate wood frame that was fastened in the walls of test area, to avid the vibrations from the impact

to disturb the measurement. The laser sensors were mounted in the middle of the concrete column, at the heights of 819 mm, 1196 mm, and 1535 mm.

The software used to collect the data is sensorTOOL V1.7.0, which can record with multiple sensors at the same time. Each laser is connected to its own amplifier, and then is connected to the computer.



Figure 5.4. Laser displacement equipment used

5.2.4 Load-Cell

The load-cell that is mounted on the end of the pendulum is a HBM U10M 500 kN, which has a range up to 500 kN. The load cell are connected to an MX840B amplifier and records data with a frequency of 300 Hz. CATMAN Easy is used to store and process the data afterwards.



Figure 5.5. 500 kN Load Cell mounted with a steel tip on the end of the pendulum

5.2.5 Testing procedure

Each column is to be tested with three impacts from three different heights, where the release height are increased for each impact. The impact height remains the same for all nine tests, and is 0.86 m above the concrete slab. The three release height is measured to be 0.005 m, 0.045 m, and 0.165 m, respectively. The result are presented in the next chapter, and the influence from different factor on the response of the structure is investigated.

Impact test results

6

"Numbers numbers numbers, exactly what we want" - Kollbjørn Adolfsen

The following chapter contains the results obtained from the impact test. In this chapter the testing specimens are denoted with a specimen-ID which consist of the fibre content in percentage, followed by the corresponding run. e.g column with a fiber content of 0.5% and run number two is denoted Specimen00 run2, or S05R2 for short.

Table 6.1 has a summary of the key from the results. During the test of Specimen00, the impact height of the pendulum was increased directly from 0.005 m to 0.165 m. Thus, the column fractured on run number two instead of number three. Since the height of the run two corresponds to the height of run 3 on the other specimens, the label is changed to make comparison easier.

Table 6.1. Summary of the results

| SpecimenID | Velocity [m/s] | Peak Impact force [kN] | Impulse [kNs] | Max. displace- ment [mm] |
|-----------------|-------------------|---------------------------------|------------------|-----------------------------------|
| Specimen00 run1 | 0.313 | 5.93 | 0.158 | 11.17 |
| Specimen00 run3 | 1.799 | 21.51 | 1.000 | 16.65 |
| Specimen05 run1 | 0.313 | 10.07 | 0.218 | 3.60 |
| Specimen05 run2 | 0.939 | 20.93 | 0.642 | 21.02 |
| Specimen05 run3 | 1.799 | 29.09 | 1.204 | 45.63 |
| Specimen10 run1 | 0.313 | 7.67 | 0.223 | 6.30 |
| Specimen10 run2 | 0.939 | 19.49 | 0.686 | 28.78 |
| Specimen10 run3 | 1.799 | 32.73 | 1.280 | 45.25 |

6.1 Data processing

All data processing is done using the MATLAB Signal processing toolbox. The raw data is imported and the different timestamps are synchronized by locating the peak of the first impact and align the time series thereafter. The raw data before any processing can be found in appendix E.

As mentioned in chapter 4, the lasers have a range of 50 mm, however the deflection on the beams appeared to be greater than 50 mm. After discovering this some adjustments were done to the laser rig, so that most of the response could be captured, but some of the initial peaks were lost. When the column was out of range the laser recorded data that was nonsense. Those values are therefore removed to make the analysis of the data as simple as possible. An example of this removal is found in figure 6.1. Afterwards the initial displacement between the laser and the concrete column are removed. Thus, one can examine the residual displacement with great ease.

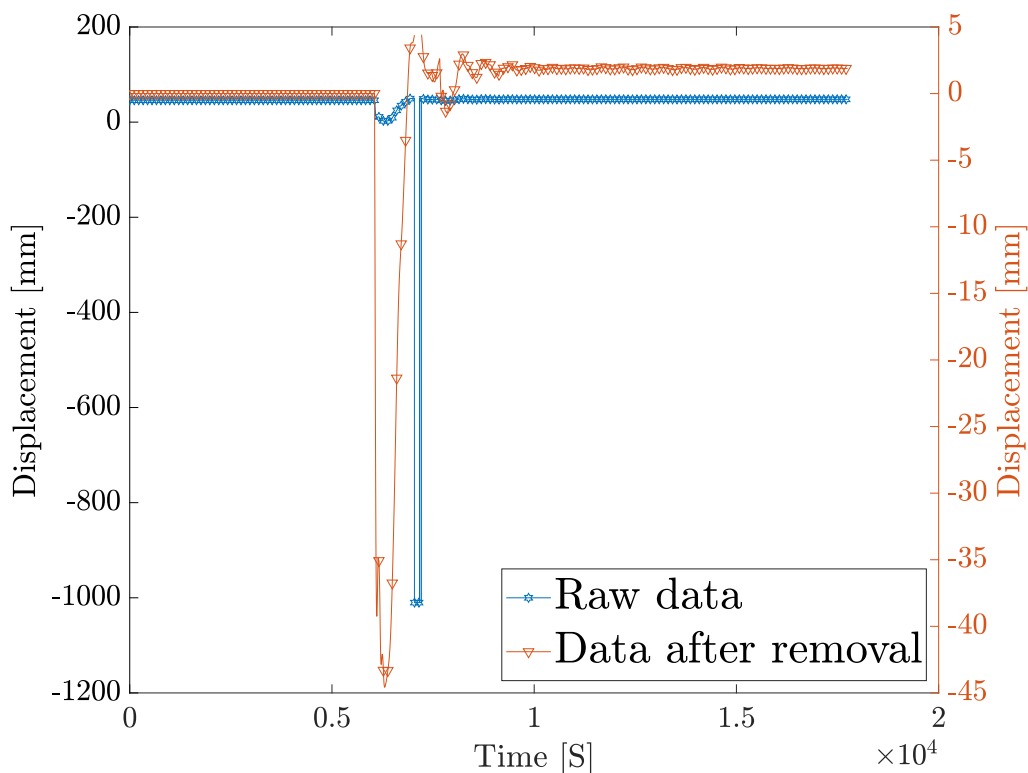


Figure 6.1. Removal of unusable data from Specimen05 run3

The data from the accelerometers was expected to be in m/s, but after further investigation, the conversion from mV/g to mV/(m/s²) was in fact not correct. The

data are converted back, but because of the insecurities in the unit, the data is not used in the results. The plots from the accelerometers can be found in appendix D.

The data from the load cell were stored and analyzed, but it was revealed that the scale of the data was unusual low. To be sure that the load cell was giving the correct data, a static test of the load cell were performed. A object of known weight were placed on top of the load cell, and it was discovered that the load cell measure was not correct. The load-cell data were scaled with the results found in the static test and used further in the analysis.

6.2 Results

This section aims to present the measured forces, accelerations, and displacements, and the relevant calculations.

6.2.1 Displacement

The displacement of the concrete column where measured with three lasers at three different heights. The laser mouthed highest of the three had the largest variations in displacement. Since the column where fixed at the bottom and free to move at the top, the large variation was as expected. As mentioned above, the range of the lasers where not large enough to capture the full specter of fluctuations of the beam at top, thus the maximum deflection was hard to determine. A summary of the maximum deflections and the residual displacement can be found in table 6.2.

The largest deflection on all cases appears right after the initial impact, before a small vibration occurs. The natural frequency of the structure is determined by the first run, since the force of the impact was not large enough to crack the column. The displacement from Specimen05 run1 is presented in figure 6.2, to illustrate the calculation process for the natural frequency.

Table 6.2. Maximum and residual displacements. Negative number denotes inwards deflection. Red numbers indicate maximum value are at range limit of lasers [mm]

| Specimen ID | Top | | Middle | | Bottom | |
|-----------------|-------|----------|--------|----------|--------|----------|
| | Max | Residual | Max | Residual | Max | Residual |
| Specimen00 run1 | 11.17 | 2.13 | 8.57 | 1.91 | 5.53 | 1.60 |
| Specimen00 run3 | 16.65 | 13.06 | 20.74 | 18.01 | 24.52 | 17.42 |
| Specimen05 run1 | 3.60 | 0.04 | 2.73 | 0.25 | 2.52 | 0.38 |
| Specimen05 run2 | 21.02 | 1.45 | 16.39 | 2.64 | 11.76 | 2.65 |
| Specimen05 run3 | 45.62 | n/a | 44.58 | -1.9 | 31.83 | -1.0 |
| Specimen10 run1 | 6.30 | 0.00 | 4.67 | 0.10 | 2.27 | 0.12 |
| Specimen10 run2 | 28.78 | 1.45 | 21.65 | 3.04 | 13.32 | 2.48 |
| Specimen10 run3 | 45.25 | 12.21 | 45.47 | 9.57 | 39.48 | 4.47 |

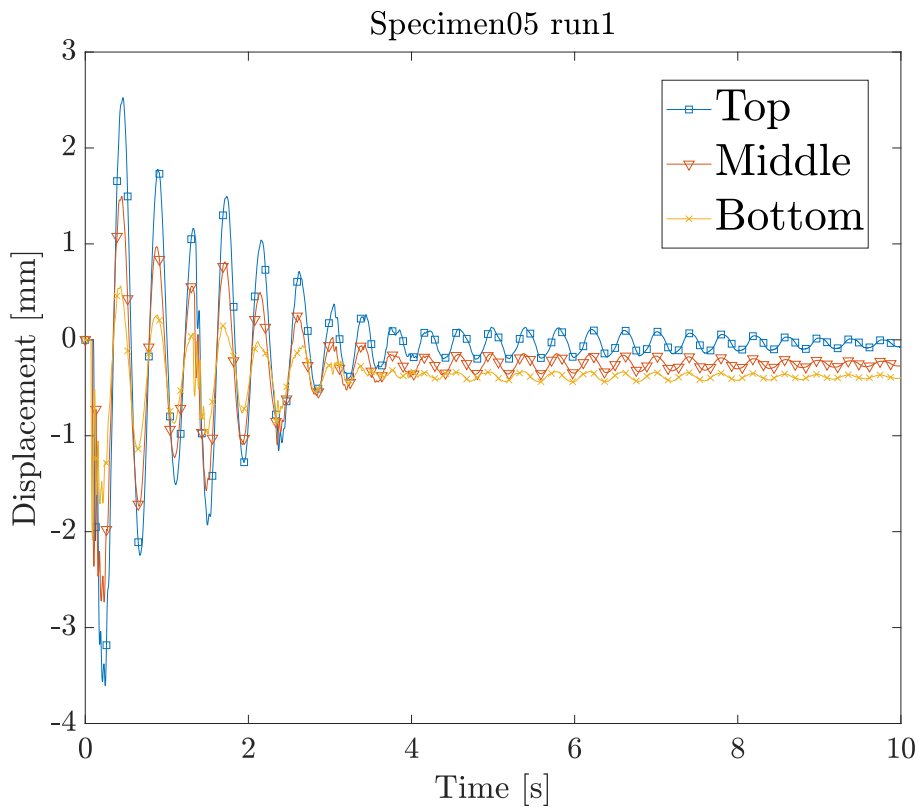


Figure 6.2. displacement response of Specimen05 run1

Unfortunately, the pendulum was not captured as it swung back after the initial impact, which resulted in a second impact. This can be seen in figure 6.2 at 1.40 s, as the amplitude increases after a steadily decrease.

The natural frequency of the column are derived from the period between the displacement peaks. Since the pendulum had multiple impacts, the peaks between

two impact are chosen for this calculation. Figure 6.3 displays where the period is obtained, and the natural frequency is derived using equation 6.1.

$$f_{n,S05} = \frac{1}{T} = \frac{1}{0.432} = 2.32 \text{ Hz} \quad (6.1)$$

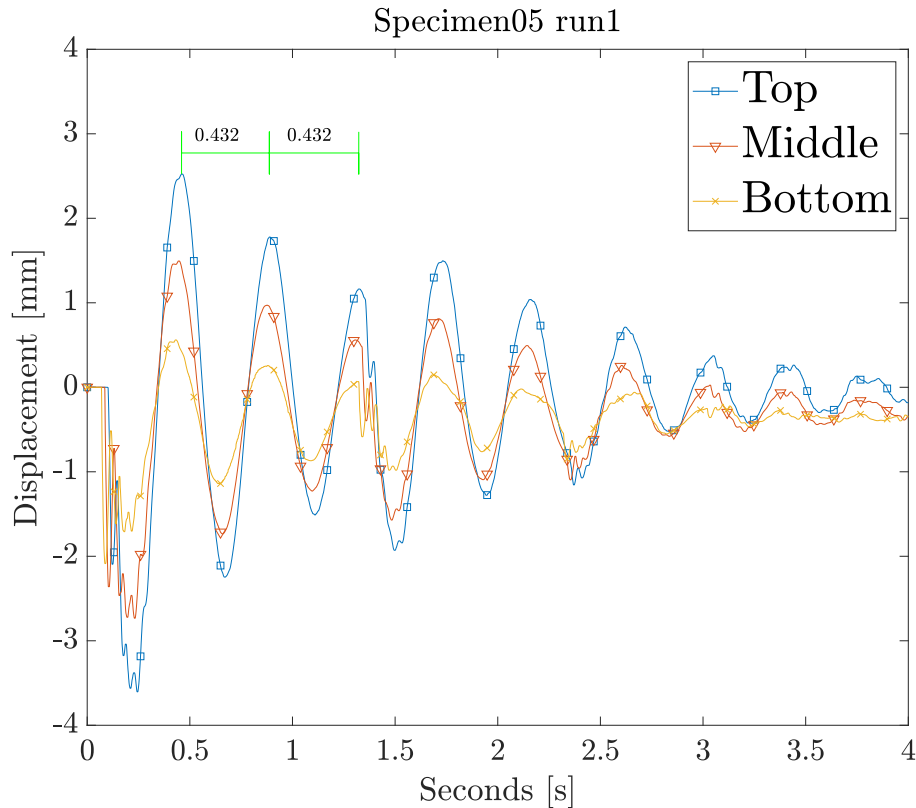


Figure 6.3. Period calculation of Specimen05 run1

For Specimen00 and Specimen10, the natural frequency was not so easily obtained. Figure 6.4 shows Specimen00 run1, and one can observe that a considerable larger displacement is observed compared to the other two Specimens with the same velocity. Figure 6.5 displays run 1 from Specimen10. The response from Specimen00 is quite different from the two others. It has a odd response, as the initial displacement is significantly large, and a residual displacement from the lowest release height.

For Specimen10 run1 the lasers where places such that the initial peaks, thus missing out of the peaks of the return of the column. The problem here was that the second impact of the pendulum hit exactly at one of the peaks, which disturbed the response. This meant that the period was not consistent throughout with the decent of the amplitude.

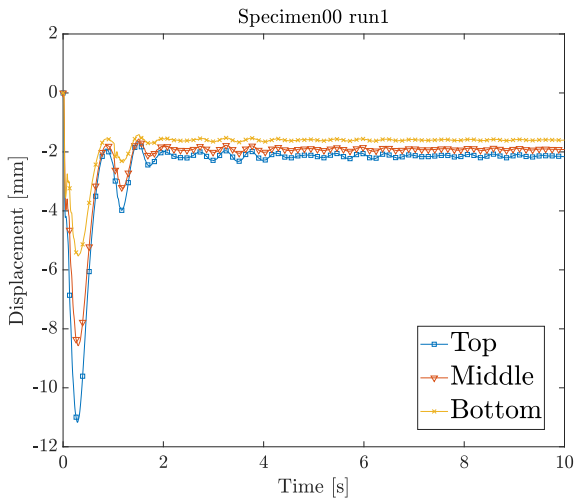


Figure 6.4. Displacement response of Specimen00 run1

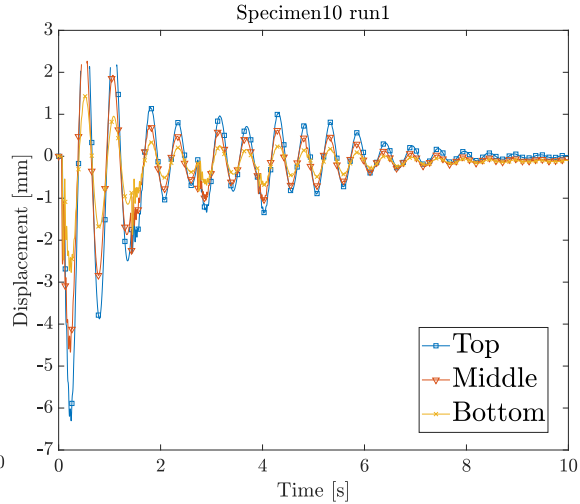


Figure 6.5. Displacement response of Specimen10 run1

To calculate a frequency that represented the structure without the interference from the pendulum, peaks that occurred after the pendulum went to a halt. This frequency cant perfectly represent the natural frequency of the structure, but is an adequate assumption. The time periods found for the Specimen00 and Specimen10 are 0.478 s and 0.506 s, respectively. Using equation 6.1, the natural frequency for for Specimen00 and Specimen10 are calculated below.

$$f_{n,S00} = \frac{1}{0.481} = 2.079 \quad (6.2)$$

$$f_{n,S10} = \frac{1}{0.553} = 1.808 \quad (6.3)$$

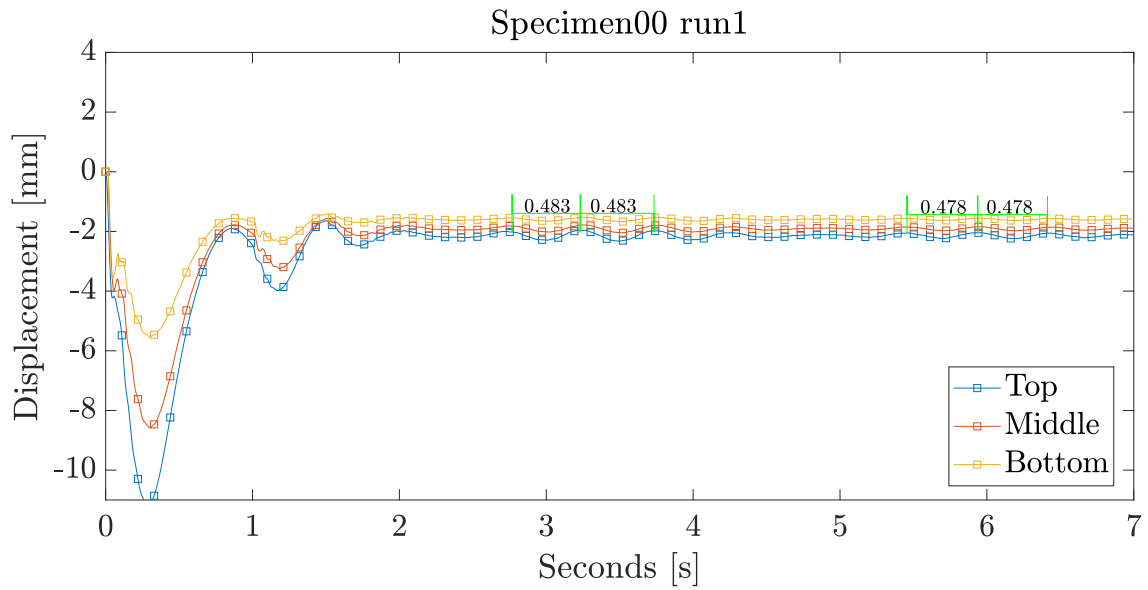


Figure 6.6. Period calculation of Specimen00 run1

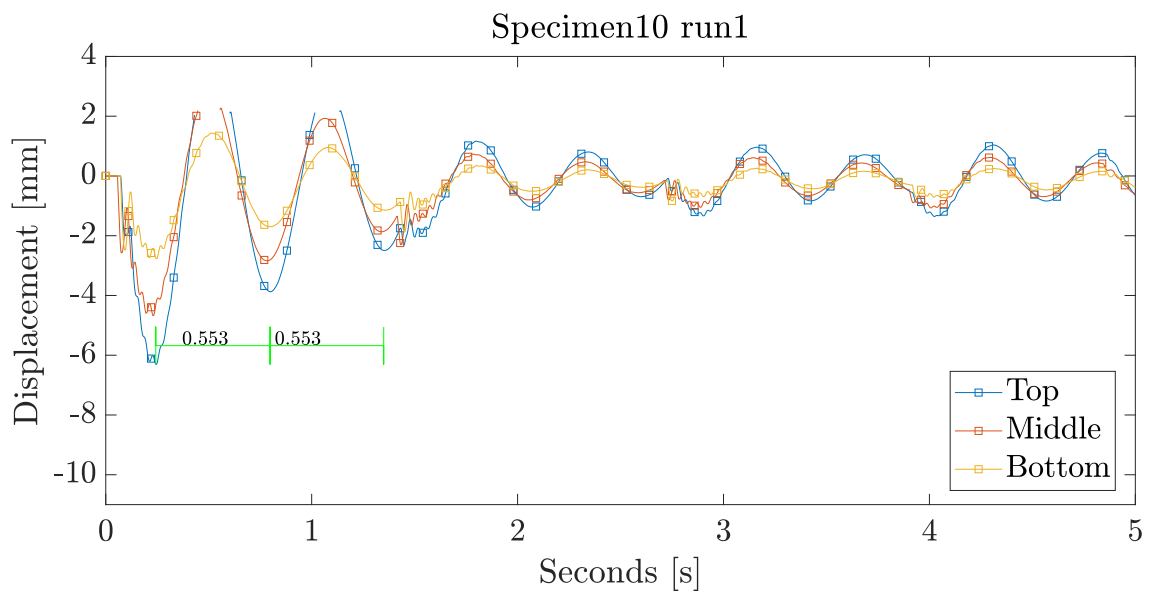


Figure 6.7. Period calculation of Specimen10 run1

The displacement response from all the impacts can be found below.

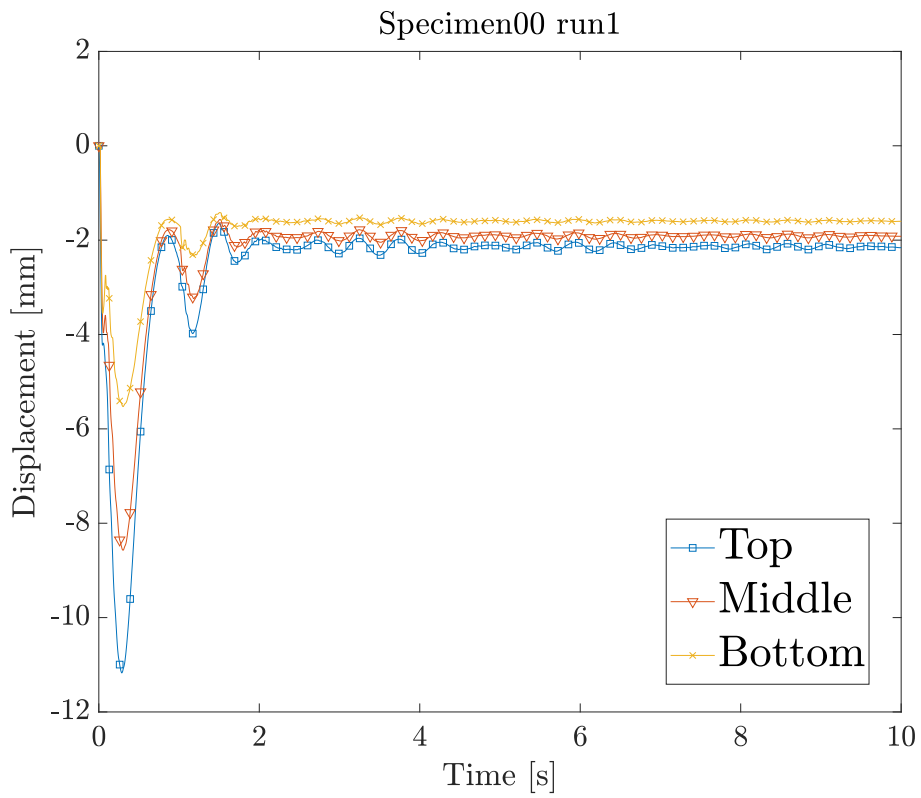


Figure 6.8. Laser Specimen00 run1

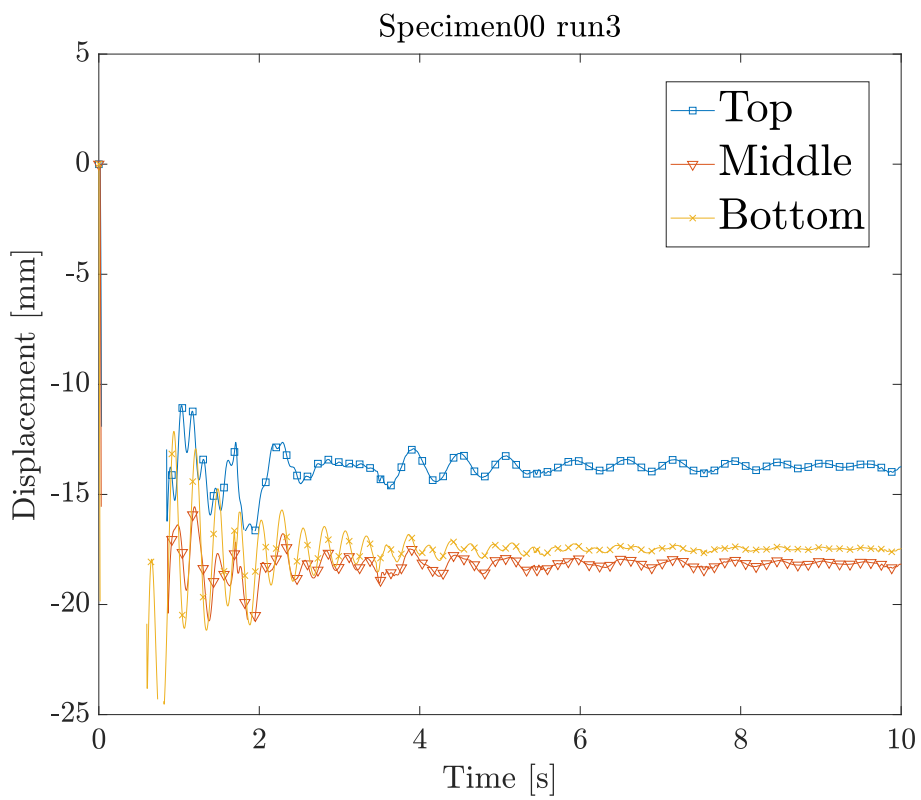


Figure 6.9. Laser Specimen00 run3

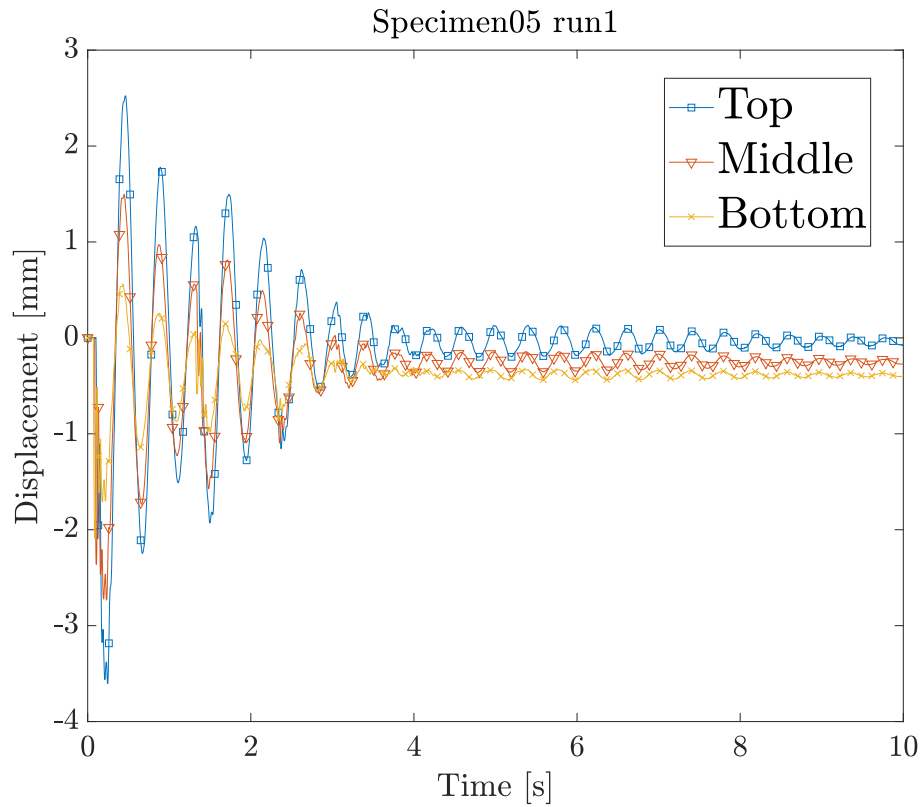


Figure 6.10. Laser Specimen05 run1

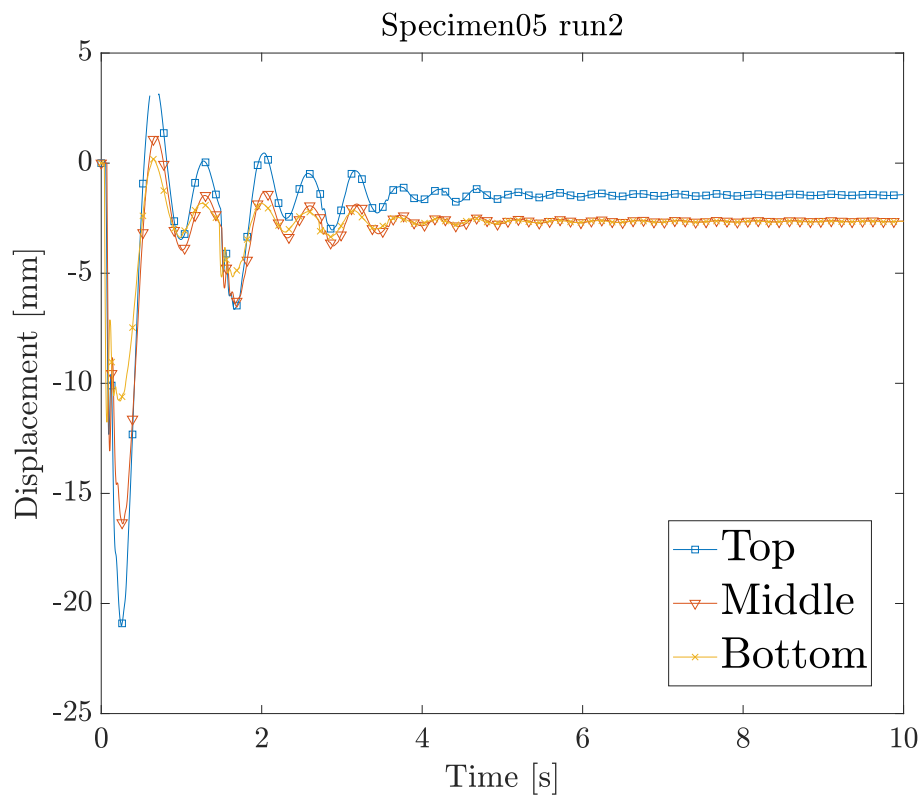


Figure 6.11. Laser Specimen05 run2

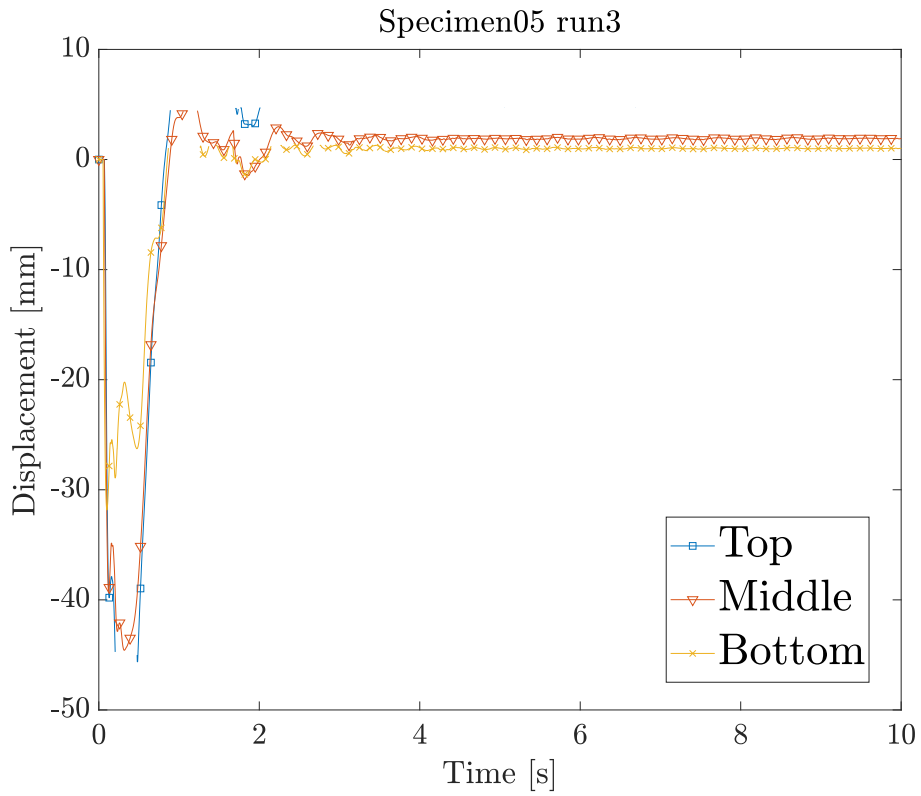


Figure 6.12. Laser Specimen05 run3

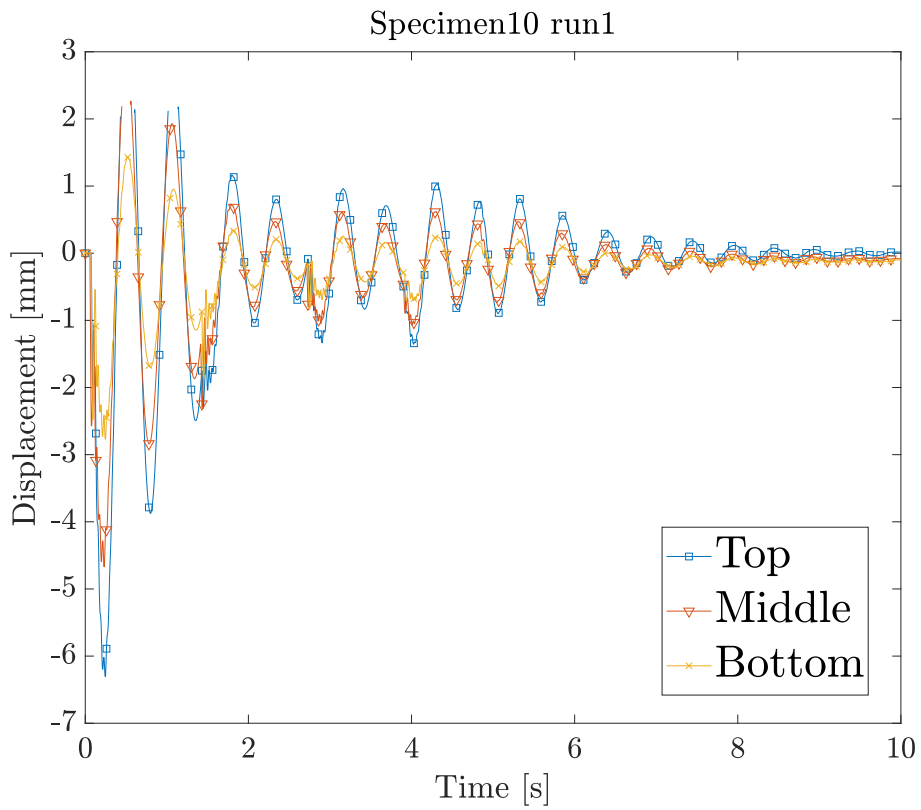


Figure 6.13. Laser Specimen10 run1

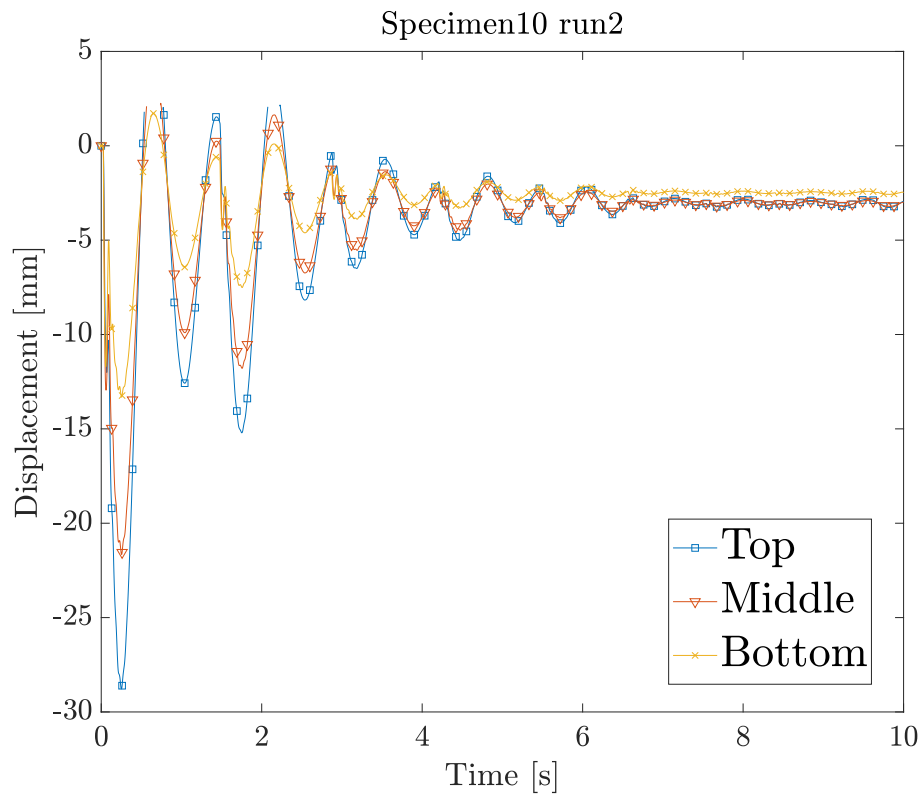


Figure 6.14. Laser Specimen10 run2

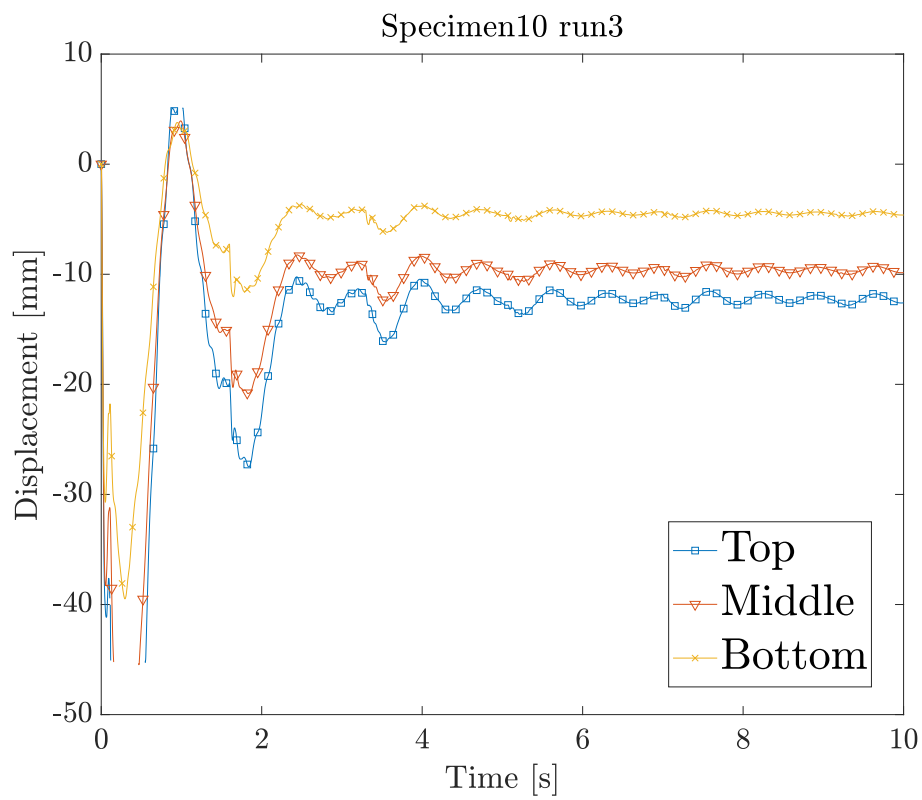


Figure 6.15. Laser Specimen10 run3

6.2.2 Impact force

The impact force for all impact sequences were obtained by the load cell. The maximum measured force for Specimen00 is $F_{00} = 21.51$ kN, for Specimen05 $F_{05} = 29.09$ kN, and for Specimen10 $F_{10} = 32.73$ kN. The measured force for the three specimens can be found in figure 6.16, 6.17, and 6.18. The similarities that can be found from the figures are the impact force for Specimen05 run2 and Specimen10 run2, as they had a peak of 20.93 kN and 19.49 kN, respectively. A dent in the concrete at the impact location were observed at run3 for all specimens. This can explain the small decrease in force at the peak of run3 at all specimens.

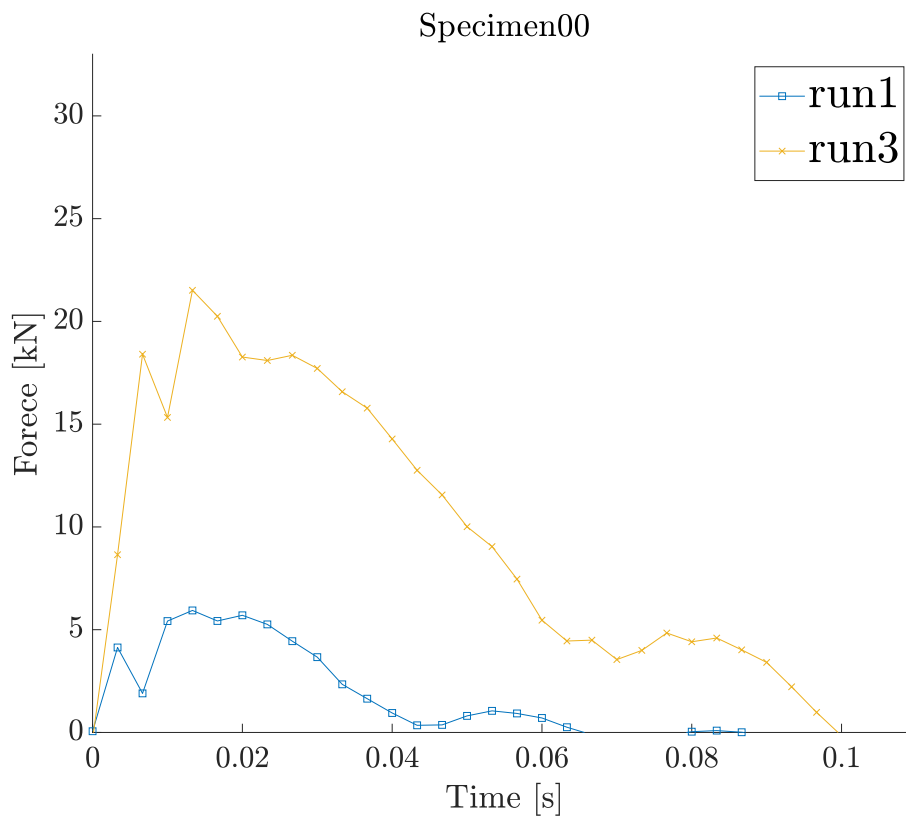


Figure 6.16. Force-time series for Specimen00

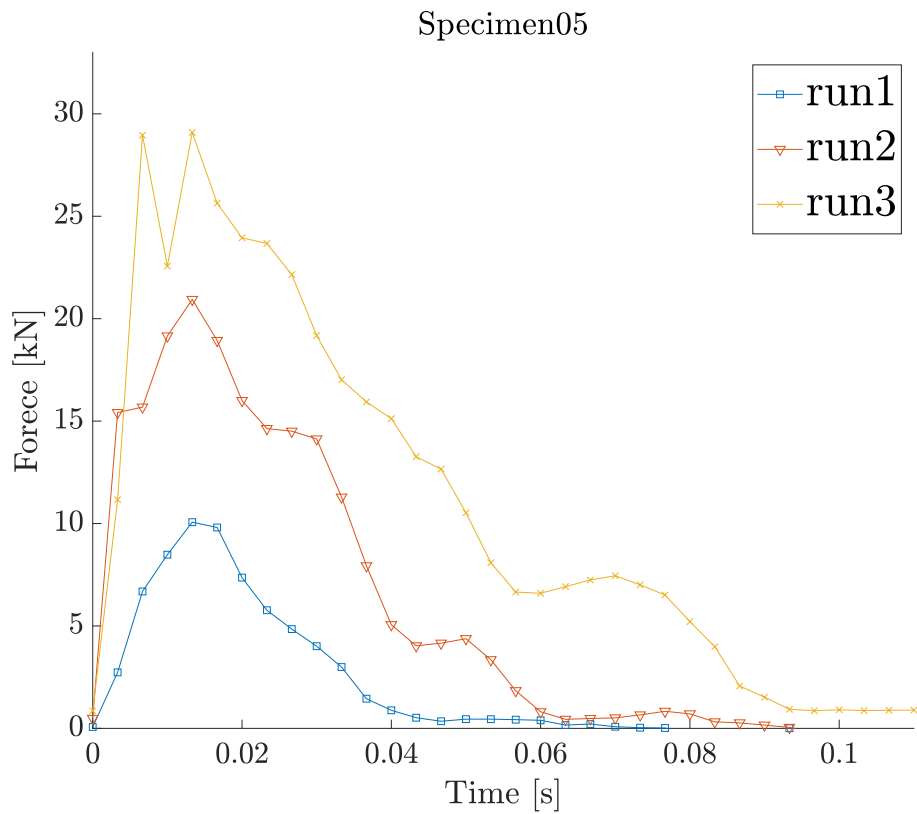


Figure 6.17. Force-time series for Specimen05

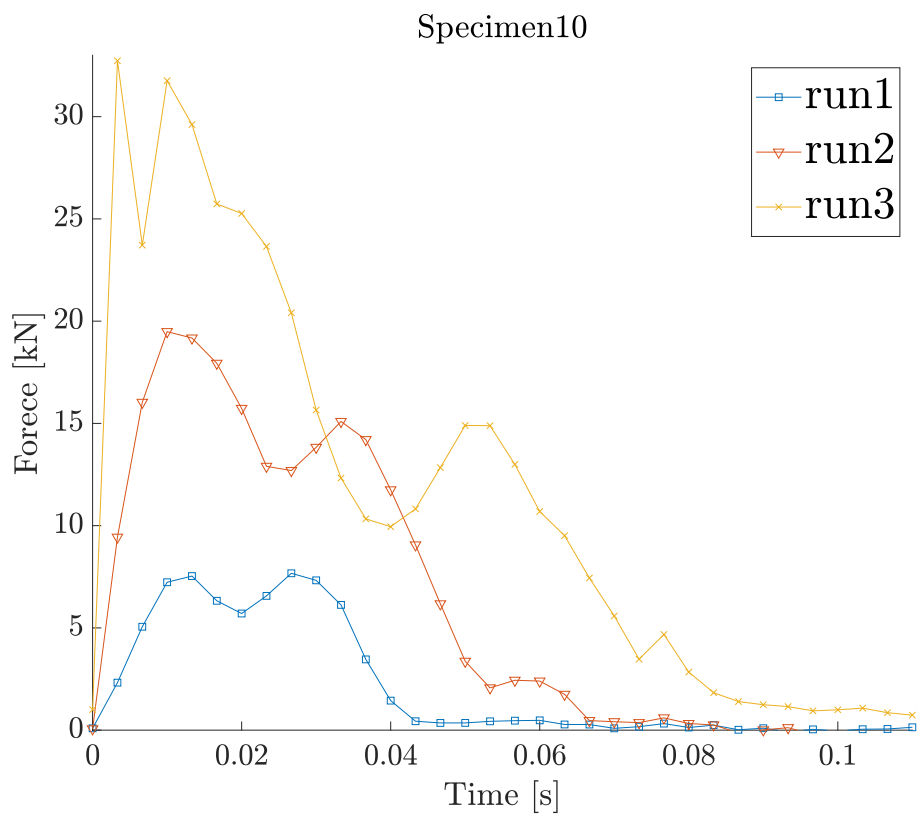


Figure 6.18. Force-time series for Specimen10

The impulse of the impact can be determined by the integrating the force-time graph from the load cell. Impulse describes the change in momentum that is caused during the impact. The impact duration for all specimens were approximately 100 ms for run3, 60 ms for run2, and 40 ms for run1. With the duration of impact an integration can be performed. The force impulses are calculated with its corresponding average force, and presented in table 6.3. In addition the impulse are illustrated in figures 6.19, 6.20, and 6.21.

Table 6.3. Results from impulse calculations

| Specimen ID | Impact duration [ms] | Peak Force [kN] | Impulse [kNs] | Avg. Force [kN] |
|-----------------|----------------------|-----------------|---------------|-----------------|
| Specimen00 run1 | 46.7 | 5.93 | 0.158 | 3.44 |
| Specimen00 run3 | 100 | 21.51 | 1.000 | 10.0 |
| Specimen05 run1 | 43.3 | 10.07 | 0.218 | 5.07 |
| Specimen05 run2 | 63.3 | 20.93 | 0.642 | 14.8 |
| Specimen05 run3 | 93.3 | 29.09 | 1.204 | 12.9 |
| Specimen10 run1 | 43.3 | 7.67 | 0.223 | 5.19 |
| Specimen10 run2 | 66.7 | 19.49 | 0.686 | 10.3 |
| Specimen10 run3 | 120 | 32.73 | 1.280 | 10.7 |

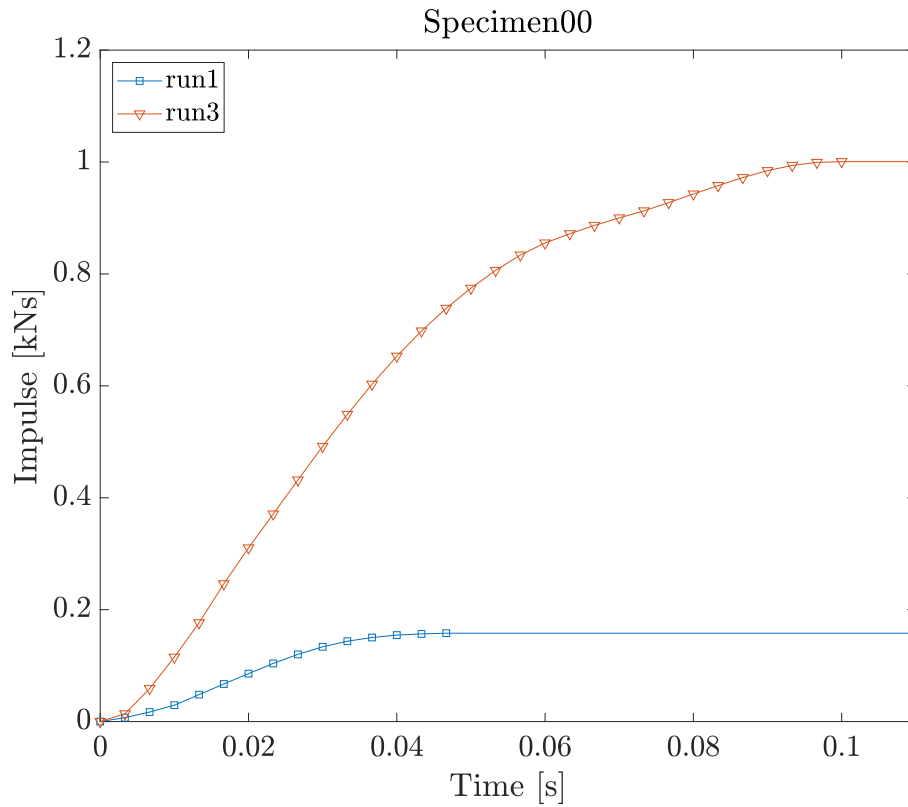


Figure 6.19. Force impulse for Specimen00

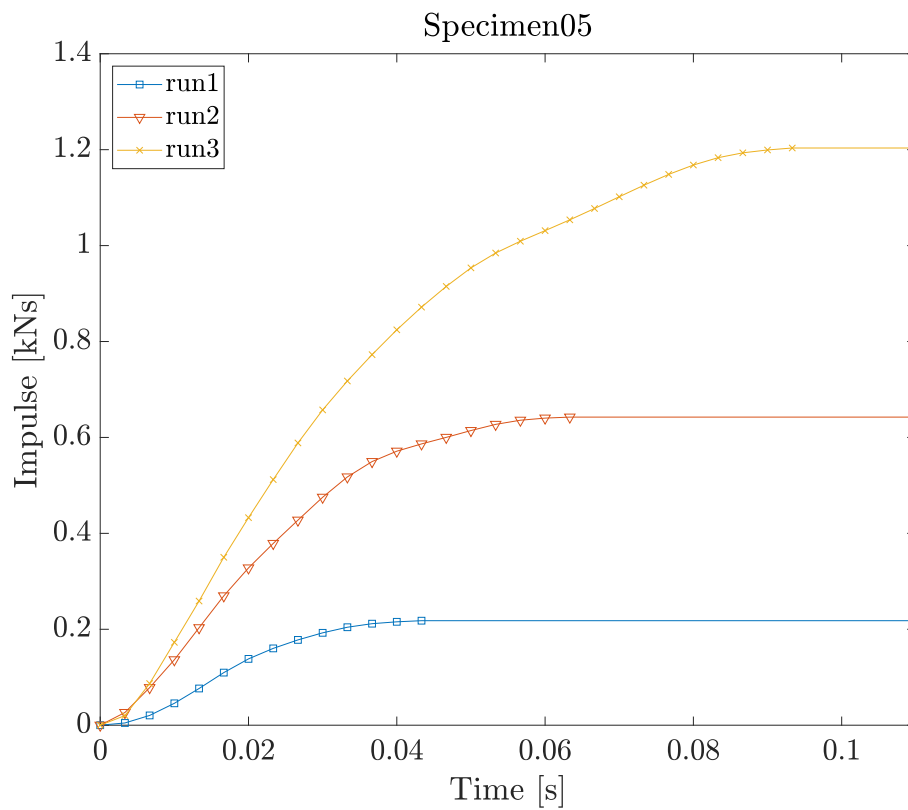


Figure 6.20. Force impulse for Specimen05

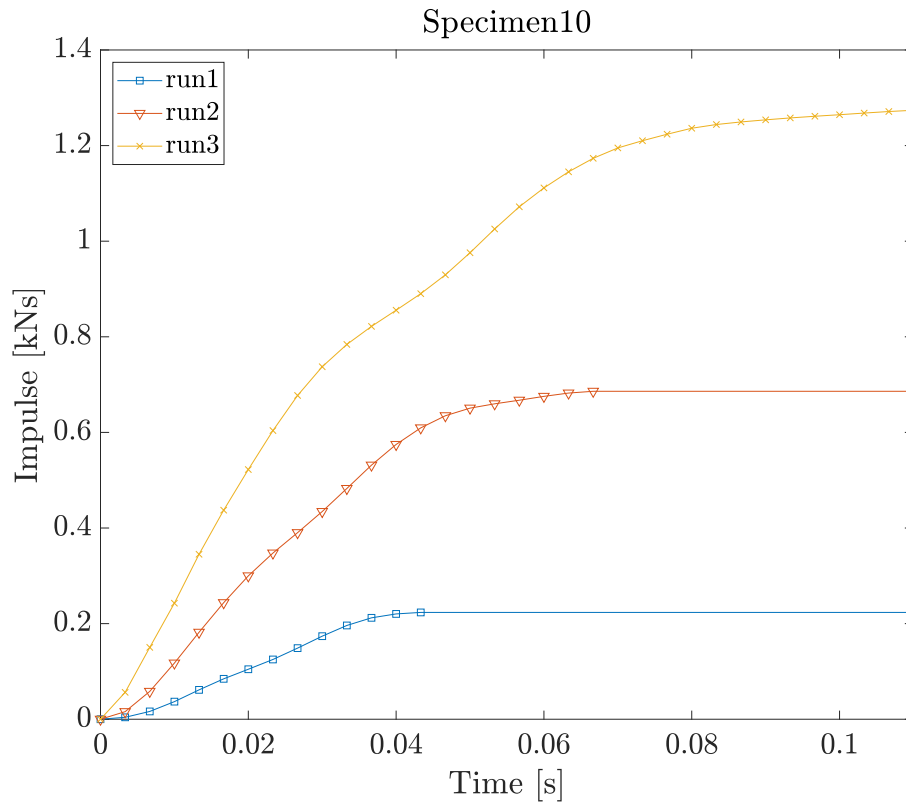


Figure 6.21. Force impulse for Specimen10

6.2.3 Cracks

No cracks occurred on the specimens before the second run. The most common cracks were cracks at the middle of the column where the pendulum hit together with cracks at the slab-column connections. Figure 6.22 to 6.25 shows some examples of these cracks. To distinguish between the cracks at the different runs, red marker where used on run2, while green marker was used for run3. Specimen00 had only one run before fracture, and therefore has no markings on the cracks.



Figure 6.22. Shear crack top corner Specimen00

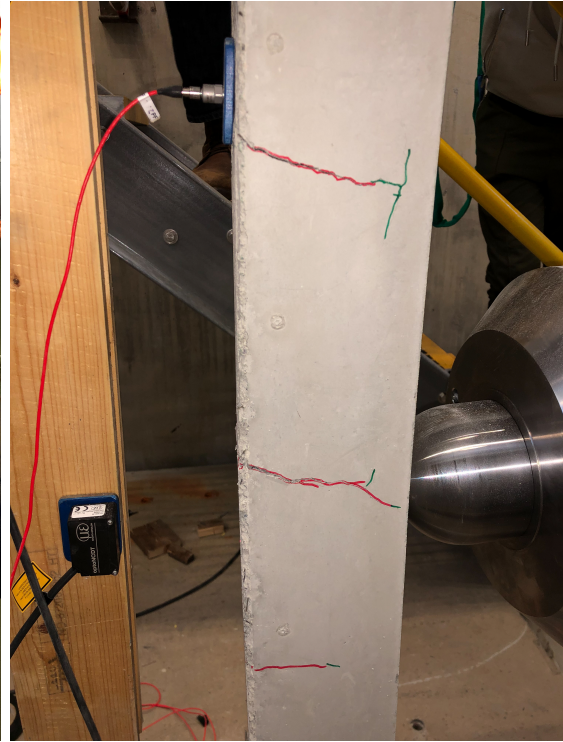


Figure 6.23. Bending cracks at impact location Specimen05



Figure 6.24. Connection crack on Specimen00



Figure 6.25. Bottom corner crack Specimen10

Some of the smaller cracks had little signs of any propagation, while other cracks went fully through. Many of the cracks from run2 did not pierce deep in the concrete, before run3 enlarged the cracks greatly. No bending cracks were discovered on the compression side, except at the corner between the column and the bottom slab. On Specimen10, close to the top slab, a small crack from run2 grew increasingly larger with every impact, that at the last run the whole column snapped in two. This is illustrated in figure 6.26, one can see that the crack grew larger with every marker color. It is possible that a weakness in the concrete was the reason for an extensive crack of this magnitude.



Figure 6.26. Major crack at Specimen10

Specimen05 also endured some major cracks in run3, as two cracks with an opening of 5 mm propagated as the force increased. This resulted in a major deflection of the column. This is illustrated in figure 6.27, together with the deflection for all three specimens.

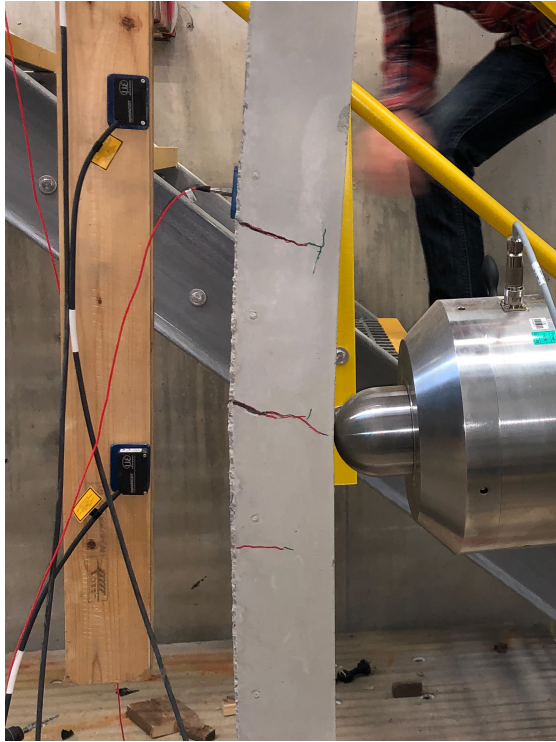


Figure 6.27. Major cracks at Specimen00



Figure 6.28. Deformation of Specimen00

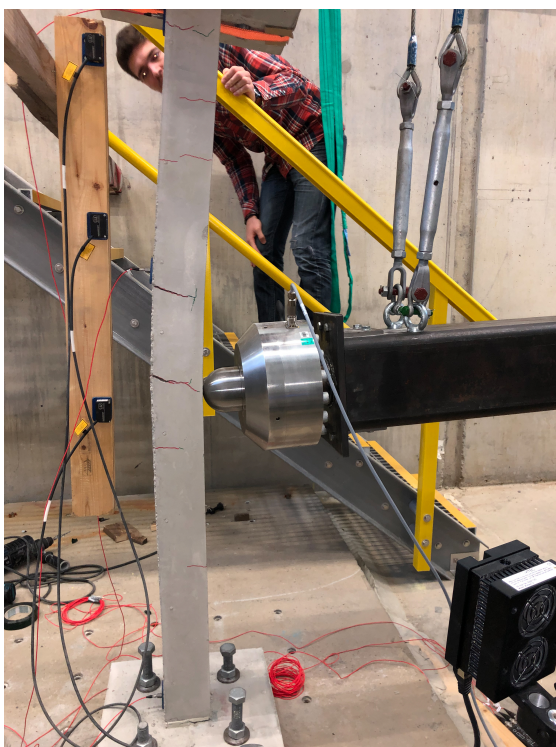


Figure 6.29. Deformation of Specimen05



Figure 6.30. Deformation of Specimen10

6.3 Influence of fibres on the results

This section aims to look at the influence of fibres on the different results presented in the chapter above.

Displacement response

Specimen00 had a larger displacement than the two other specimens for all three laser positions. Specimen00 run1 also have a residual deflecting after the initial impact, while the rest of the Specimens run1 have close to zero residual deflection. Specimen00 run1 also have a one sided response, as deflect to 11 mm before the vibrations disappears after 2 seconds. When including that the measured force for Specimen00 is considerable lower that for Specimen05 run1, and slightly lower than Specimen10 run1.

Specimen05 run3 is the only that has a displacement towards the pendulum, at the middle and the bottom lasers. This run were the fracturing run for the specimen and a residual displacement is not recorded as the column fractured and tilted out of range. A general increase in amplitude of the vibration are observed from Specimen05 to Specimen10. This might be an indication on that stiffness decreases with fiber content.

Crack distributing

The specimen with that developed most cracks was Specimen00. Specimen05 had several small cracks in middle of the column, behind the impact location, that grew to larger cracks at run3. The increase of fibers reduces the presence of cracks for the earlier impact runs, while also reduces the size of the cracks that appear in the later runs. The only exception is the crack presented in figure 6.26.

6.4 Source of errors

Throughout the laboratory testing it was discovered different factors that would lead to incorrect or invalid data. The calibration of the accelerometers where not done in a correct manner, as the result was beyond reasonable. a conversion back to was attempted but without knowing without doubt what data we had the data was not usable.

It was quickly discovered that the laser displacement equipment had a shorter range than the experiment required. With a range of only 50 mm the displacements peaks on one of the sides could be captured. Another problem with the displacements was discovered during the data processing. The pendulum was not captured on its return, thus interfering with the vibration column. This lead to an uncertainty regarding the calculations of the column response.

Furthermore, to properly use the CATMAN software together with the load cell, is was calibrated using the included calibration sheet. However, Specimen00 was calibrated using a signal value on the calibration sheet, while Specimen05 and Specimen10 was calibrated using a table on the calibration sheet. The single value was derived from the table, so the magnitude of the results should be comparable, but the unit were missing on the second two Specimens. It does not change the result, but raises an uncertainty regarding the data.

In the following chapter, the results from all tests are used to develop a finite element model in LS-dyna and run simulations of the same impact experiment.

7.1 Model development

The modelling is performed using LS-DYNA, which is a finite element program that is capable of simulation advanced real-world problems and specialises in collision problems.

The model is built using the same material parameters are the specimen used in the impact test. The model is built from four main parts; The concrete column, with slabs on the bottom and top, concrete mass on top of the column, reinforcement bars, and the pendulum impact. A simulation with the same conditions will be performed, and the results are compared with the results from the impact experiment to validate the numerical model.

The concrete column is made out of one part with a mesh size of 5 mm. The same mesh size is used for the concrete mass and the reinforcement. The reinforcement is modelled as bar elements, while the concrete is modelled from solid elements. To save computational time, the pendulum is not modelled completely, as the indenter is the only part that has any contact with the concrete. The density of the indenter is scaled to match the weight of the whole pendulum. The dimensions of the indenter are equal to the dimensions of the tip of the pendulum in the experiment. Figure 7.1 illustrates the FEM model in its entirety.

The connections between concrete and reinforcement are determined by the keyword card *LAGRANGE_IN_SOLID*. It makes sure that the forces are transferred from the concrete and through the re-bar. The interaction between the indenter and the concrete column is determined by the keyword card *CONTACT_AUTOMATIC_SURFACE_TO_SURFACE*. The card has a dynamic

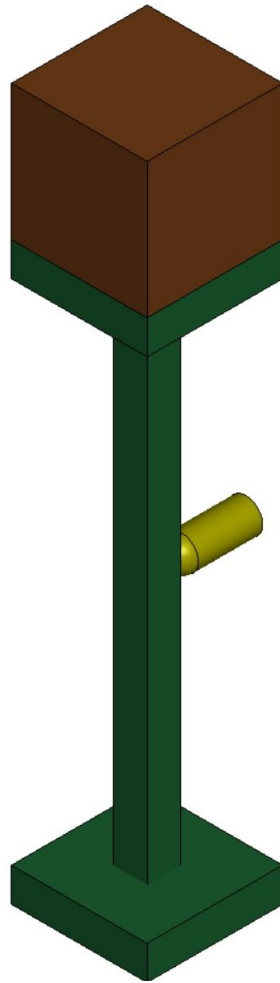


Figure 7.1. Illustration of the FEM used further in the numerical analysis

coefficient of friction and a static coefficient of friction, that need to be given. Both of the parameters are set to 0.3. To resemble the boundary conditions in the impact experiment the nodes underneath the bottom slab are restrained from any displacement in all directions. The top mass is fixed at the connected nodes between itself and the top slab.

The material card for concrete is *MAT_CONCRETE_DAMAGE_REL3*. This material card requires the concrete density, its Poisson ratio, and the compressive strength. For the reinforcement bars, the material card *PIECEWISE_LINEAR_PLASTICITY* is used. This material card takes into account strain hardening of the material and requires yield strength and E-modulus, instead of compressive strength. In the laboratory experiment, it was noted that the pendulum had no significant deformation, so a rigid material card is used for the indenter. The parameters for each material card can be found in the table below.

Table 7.1. Material parameters used in the numerical model

| Material Card | Input | | Value |
|-----------------------------|------------|----------------------|--------------------|
| MAT_CONCRETE_DAMAGE_REL3 | Density | [kg/m ³] | 2400 |
| | Poisson | [-] | 0.2 |
| | f_c | [MPa] | 71 |
| PIECEWISE_LINEAR_PLASTICITY | Density | [kg/m ³] | 7850 |
| | Poisson | [-] | 0.3 |
| | E-mod | [MPa] | 200 |
| | σ_y | [MPa] | 587.8 |
| RIGID | Density | [kg/m ³] | 1.04e ⁵ |

One simulation was performed with an impact velocity of 1.799 m/s, which corresponds to run3 from the experiment. The simulation did not account for the damage from run1 and run2, thus losing some of its accuracies. The simulation has a duration of 1 second after impact to extract the full response from the column.

7.2 Numerical results

The following numerical results are shown from the simulation of the impact test. The plastic strain distribution is presented and compared with the cracks of the pendulum test, and the displacement and impact force is analyzed.

7.2.1 Strain distribution

The strain distribution around the column at maximum deflection is illustrated in figure 7.2, followed by the strain distribution when the response is finished in figure 7.3. One can see the development of plastic hinges at the centre of the column, and the top and bottom. The strain fields that appear just after impact becomes larger after the vibration of the column, especially at the bottom of the column. The effective plastic strain aligns with where the small crack formation of the experimental specimens.

Figure 7.4 and 7.5 displays the major crack formation at the centre of the column, and at the bottom of the specimen. Comparing figure 7.4 with 7.6, one can observe that the crack formation aligns with the numerical model.

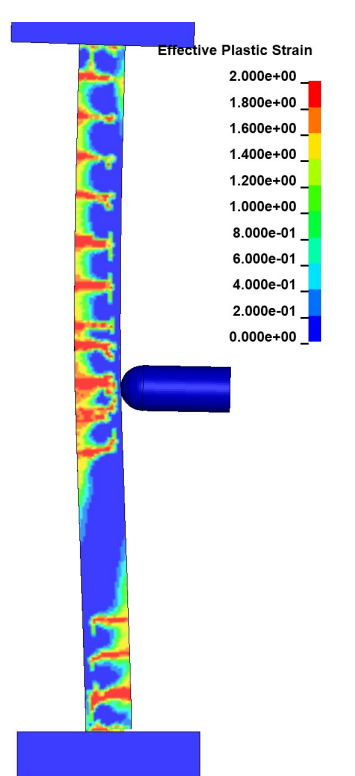


Figure 7.2. Strain at maximum deflection

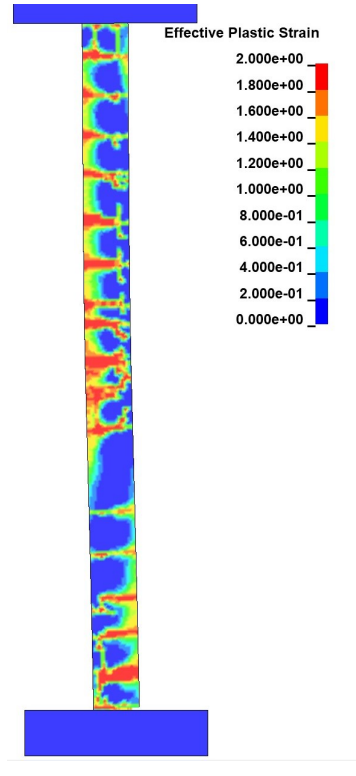


Figure 7.3. Strain at the end of the simulation

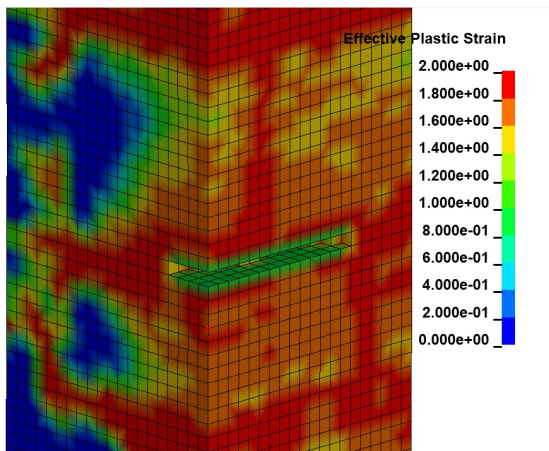


Figure 7.4. Crack formation at the impact location

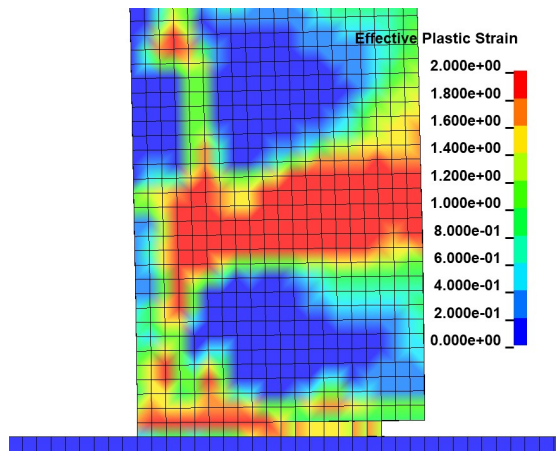


Figure 7.5. Crack formation at the footing of column

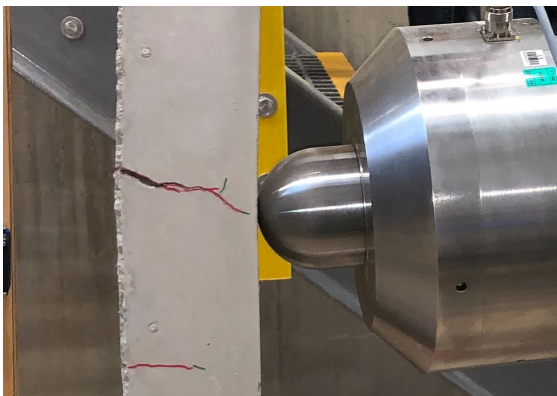


Figure 7.6. Crack formation at impact location of the beam



Figure 7.7. Crack formation at the footing of the column

7.2.2 Displacement response

The displacement obtained from the numerical is compared with the corresponding displacement obtained from the laser in figure 7.8. The result from the numerical model has some similarities with the experiments. It can be observed at around 0.1 seconds the numerical model have the same high-frequency vibrations that are observed on the experimental graph before the displacement exceeds the range of the lasers. The high-frequency vibrations stop at the return peak, which is equal to the results from the impact test.

It can be seen that the period of the numerical model is slightly lower compared to the results from the experimental test. This might be a result of the cumulative damage the column from the impact test has endured, which makes the column less stiff and increases the period of the vibrations. The magnitude of the top laser seems to be equal to the numerical model at the return peak, while the magnitude of the middle and bottom laser is slightly higher than the model.

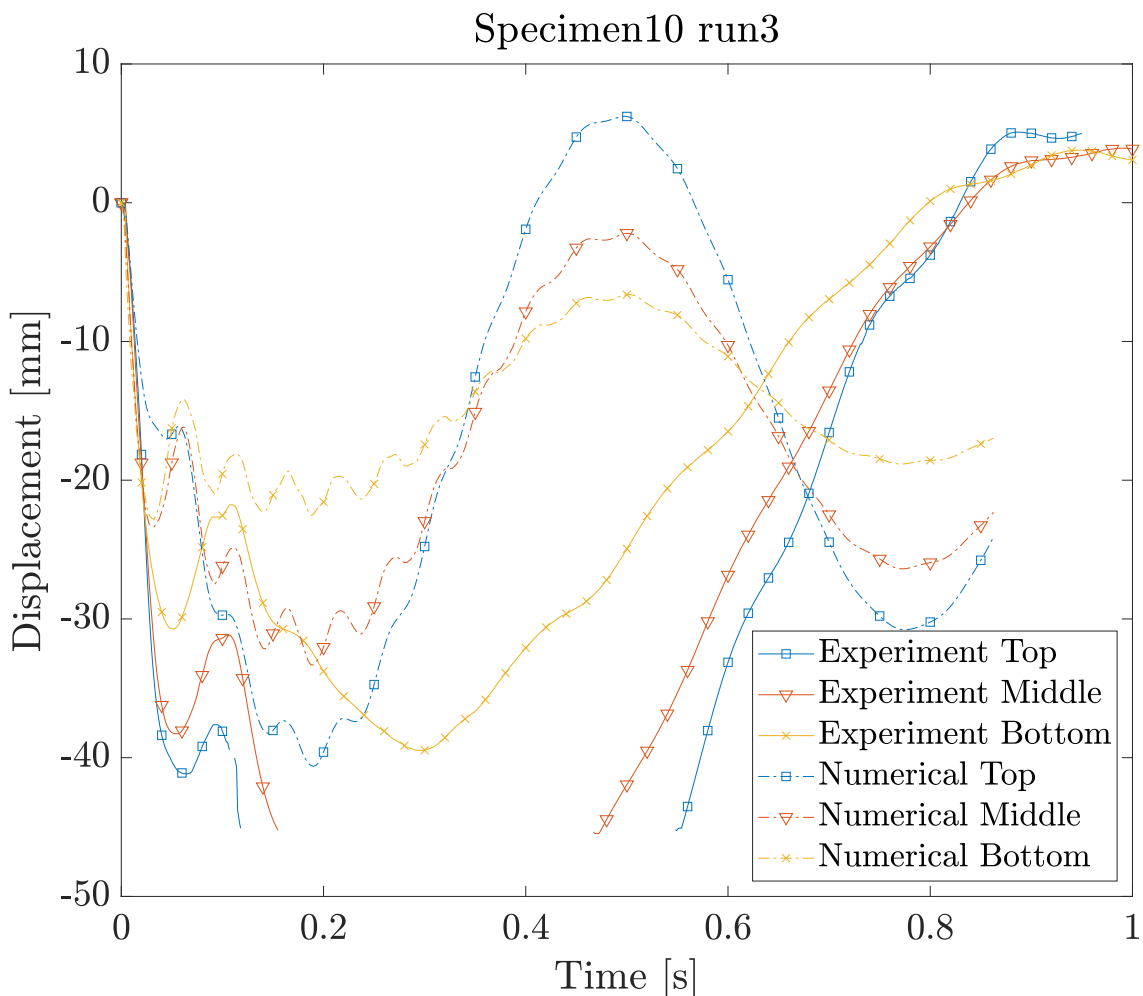


Figure 7.8. Comparison of the numerical displacement and the experimental

7.2.3 Impact force

Figure 7.9 illustrates the impact force from the pendulum experiment and the numerical simulation. From the figure it can be observed that the numerical force follows the experimental force up to approximate the same peak force, before it has a rapid decline, before a slight increase in force again. As mentioned earlier, this is where the concrete gets crushed by the impactor, before the concrete resists and more force is applied. The impact duration in the numerical simulation is much shorter than in the experiment and is measured to be 50 ms.

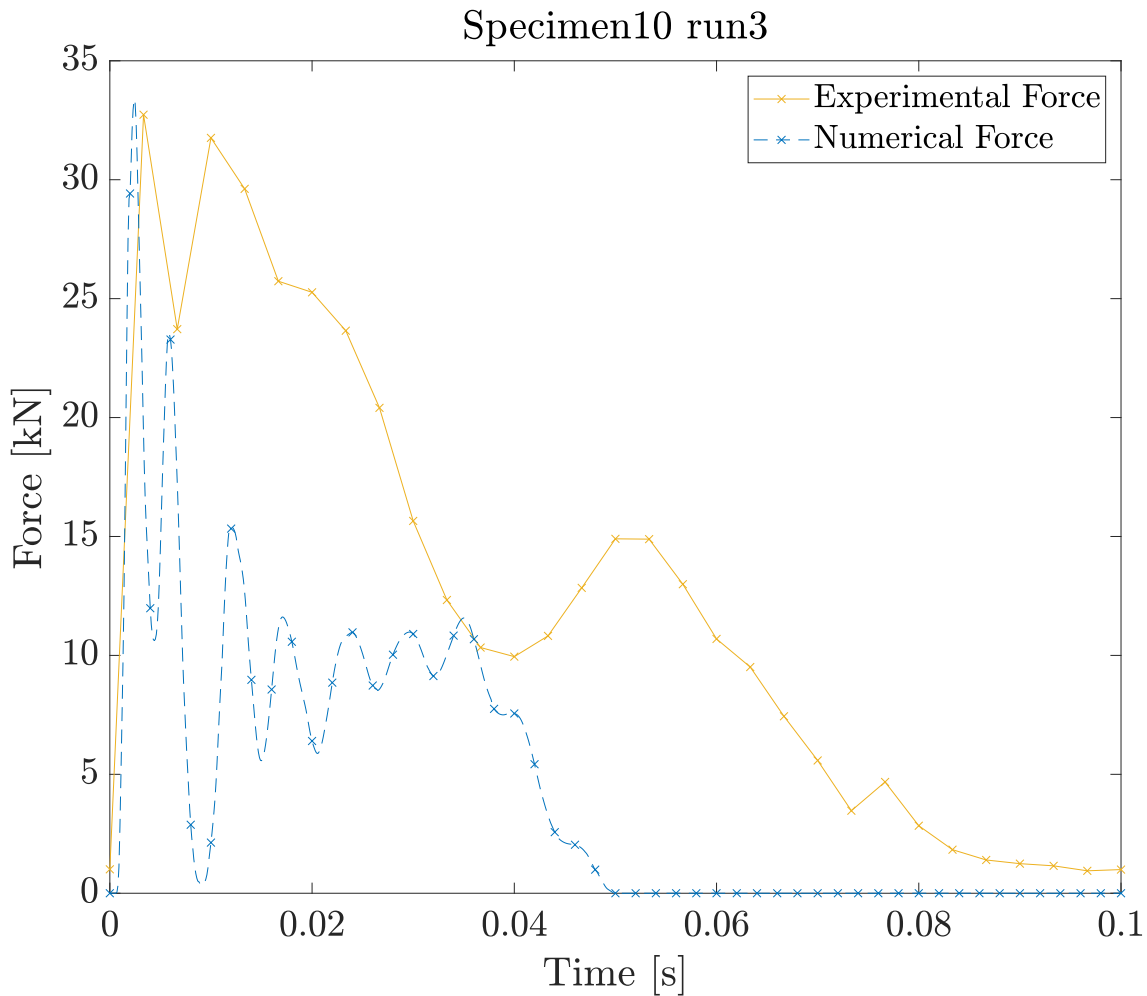


Figure 7.9. Impact force from experimental results and the numerical model

7.3 Sources of inaccuracies

There are some factors in the numerical analysis that unfortunately influence the accuracy of the simulated result. The concrete modelled in LS-dyna does not take account of the content in the concrete. The concrete card in the model is configured with the mechanical properties of the fibre concrete, but still, it is modelled as normal concrete.

Another inaccuracy is the cumulative damage that occurs on the specimen for testing. The numerical model have no damage before the simulation of run3 was performed, and the results can deviate from the experiment. This can be noticed in the period of the numerical displacement compared to the experimental, and the impact duration.

In the model, the nodes between the top mass and the column top slab were fixed to each other, while in the experiment the top mass was fastened to the top slab with straps. Even though the straps were tightened as good as possible, the top mass could have moved slightly thus changing the vibrations compared to a fully restrained top mass.

In the following chapter, the results acquired from the use of experimental and numerical analysis will be compared and discussed in the first section. The findings of the thesis are addressed in the second section, and recommendations for future work is suggested.

8.1 Discussion

8.1.1 Expectations

The objective of this thesis was to investigate the effect of basalt fiber on a structural columns impact response, and implement the results into a finite element model for further investigations. The literature review revealed that researches are confident that the implementation of fiber in structures where accidental impacts can occur, could influence its durability in the years to come. Fiber reinforced concrete is known for its ability to enhance the fracture strength of concrete, and is therefore expected to better its performance under impact loading.

8.1.2 Observations

During the execution of the experimental work, it was noticed that the equipment used for measured data gave inconsistent readings. The issue of having measurement that differentiate between test is the difficulties of making proper comparisons and correct conclusions. The displacement data, measured force, and accelerations all had problems of some sort that was discovered either during the experiments, or in the post processing of the data. The issue with the laser displacement equipment were quickly discovered, as the first impact testing revealed that the displacement of the column were greatly underestimated, and the range of the laser were not sufficient. Adjustments were made to be able to collect as much usable data as possible,

which can be seen in the difference of the displacement series from Specimen00 to Specimen05. Another issue occurred when processing the displacement data, as the pendulum were not captured after the initial impact, thus interfering with the vibrations.

During the post process of the accelerometer data, it was discovered that an error have occurred in the conversion of the electrical data to accelerations. This lead to an uncertain regarding the magnitude of the data, and further investigation concluded that the data could not be used as it raised to many uncertainties. In the same process the measured force from the load cell were analyzed, and it was believed that the same issue occurred here as with the accelerometers. This was easily checks, as an static test with an object of known mass could be placed on the load cell, thus confirms or denies any presumption of inaccurate data. It was discovered that the load cell readings were smaller that it should be, and the data were scaled before further analyze were performed.

From comparing the displacement response of all test specimens, a reduction of residual strength is observed. Specimen00 with no fibre content had an residual displacement after run1, with a peak impact force of 5.93 kN. Compared to Specimen05 run1 which had close to zero residual displacement (0.04 mm), and an peak impact force of 10.07 kN, an argument can be made that the content of fiber strengthen its ability to withstand strength considerably. Taking Specimen10 run1 into account, the same pattern emerges, as the residual displacement is measured to 0.00 mm, with a peak impact force of 7.67 kN. It should be noted that Specimen00 suffered some initial cracks during the disassembly of the form work, which can be a cause of the larger residual displacements during the first impact. Further, the calculated natural frequency of the columns have a decreasing tendency with an increasing fiber content, which indicates that a higher content of fiber reduces the stiffness of the column. This is an important factor to be considered, as the natural frequency of a column is avoided in a design perspective, as when reached causes resonance and can lead to major damage of the structure, and in worst case structural failure. It should be mentioned that after all impact test for all specimens were performed, it was discovered that the connection between the column and bottom slab of Specimen10 was not as attached as the other two test specimens. This might indicate that the reinforcement in the connections had a weakness, which resulted in a larger displacement that the other two.

Comparing the numerical results with the experimental results, it becomes clear

that modeling of a fiber reinforced concrete column under impact loading is within the limits of reason. Comparing the displacement response from the laboratory test and the numerical model, one can draw several similarities. The high-frequency vibrations that can be seen on figure 6.10 to 6.15 are present in the model. The high levels of plastic strain in the model are located roughly the same locations as the experimental, and the major cracks that were observed in the experiment also present. The only exception is the major crack at the top of Specimen10, but it is expected that this crack is due to a weakness in the concrete reinforcement. The force-time series compared in figure 7.9 have matching amplitude, but the impact duration does not match very well, as the experimental duration is twice as long as in the numerical. It is assumed that the cumulative damage from the multiple impacts in the experiment is the reason for the elongated impact duration. This is also assumed to be the reason for that the period of the numerical model don't align very well with the experimental results.

8.2 Conclusion

8.2.1 Findings

An investigation on the effect of basalt fiber on the dynamic response of a concrete column under impact loading has been performed. The findings has been presented, discussed, and the following conclusions are presented.

A relationship between fiber content and natural frequency is definitely present, as the results indicate that a increase in fiber content reduces the stiffness of the column. This effect cannot be determined with certainty, as there is to many factors that could have influenced the results.

The results from the numerical model seems to applicable to a certain degree, as peak impact forces and displacement amplitude align with the experimental result. However, the the impact duration and the period of the displacement response from the simulation does not match very well with the pendulum experiment.

The developed numerical model could with high accuracy predict some important attributes of the pendulum test, while other results deviated from the experimental result to some extend. With further improvement, the numerical model could predict the response of an real life impact test with high accuracy.

8.2.2 Further research

The effect of fiber on the natural frequency of a column should be instigated further. As mentioned in section 6.4, the reinforcement bar were without any ribs, and bent by hand. With reinforcement bars that is bent using machinery, higher accuracy are achieved and the chances for weak spots in the column are significantly reduced.

The laser displacement equipment did not have sufficient range to capture the full displacement of the column, and acquiring laser with sufficient range should be considered.

The finite element model could not be validated properly, because of restrained time schedule and delays in the laboratory, and further simulations could improve the quality of the model. To eliminate the uncertainty regarding the cumulative damage in the model, more laboratory test specimens should be casted, and one impact should be performed for each height without any previously impacts.

The top mass which aim was to mimic load from a superstructure should be fastened with similar bolts as the bottom slab, to better mimic the fixed boundary condition that you find in a full scale bridge pier.

Before further use the calibration of the load cell and the accelerometers should be completed with certainty, to eliminate any doubt in the experimental results.

Bibliography

- [1] M. di Prisco, G. Plizzari, and L. Vandewalle, “Fibre reinforced concrete: new design perspectives,” *Materials and Structures*, vol. 42, no. 9, pp. 1261–1281, Nov. 2009. [Online]. Available: <http://link.springer.com/10.1617/s11527-009-9529-4>
- [2] F. internationale du béton, *Fibre-reinforced concrete: from design to structural applications: technical report: proceedings of a workshop held in Montréal, Canada on 24 and 25 July 2014*, ser. fib CEB-FIP bulletin, B. Massicotte, A. C. Institute, and I. F. for Structural Concrete, Eds. Lausanne, Switzerland: Fédération internationale du béton (fib), 2016, no. 79, meeting Name: FRC International Workshop.
- [3] S. Paul, G. van Zijl, and B. Šavija, “Effect of Fibers on Durability of Concrete: A Practical Review,” *Materials*, vol. 13, no. 20, p. 4562, Oct. 2020. [Online]. Available: <https://www.mdpi.com/1996-1944/13/20/4562>
- [4] I. Löfgren, *Fibre-reinforced concrete for industrial construction: a fracture mechanics approach to material testing and structural analysis*, ser. Doktorsavhandlingar vid Chalmers Tekniska Högskola. Göteborg: Chalmers Univ. of Technology, 2005, no. N.S., 2378.
- [5] J. Karlovsek, N. Wagner, and A. Scheuermann, “Frequency-dependant dielectric parameters of steel fiber reinforced concrete,” in *2012 14th International Conference on Ground Penetrating Radar (GPR)*. Shanghai: IEEE, Jun. 2012, pp. 510–516. [Online]. Available: <http://ieeexplore.ieee.org/document/6254918/>
- [6] N. T. Nguyen, T.-T. Bui, and Q.-B. Bui, “Fiber reinforced concrete for slabs without steel rebar reinforcement: Assessing the feasibility for 3D-printed individual houses,” *Case Studies in Construction Materials*, vol. 16, p. e00950, Jun. 2022. [Online]. Available: <https://linkinghub.elsevier.com/retrieve/pii/S2214509522000821>
- [7] Y.-S. Choun and H.-K. Park, “Containment performance evaluation of prestressed concrete containment vessels with fiber reinforcement,” *Nuclear*

- Engineering and Technology*, vol. 47, no. 7, pp. 884–894, Dec. 2015. [Online]. Available: <https://linkinghub.elsevier.com/retrieve/pii/S1738573315001746>
- [8] M. V. Mohod, “Performance of Polypropylene Fibre Reinforced Concrete,” *IOSR Journal of Mechanical and Civil Engineering*, p. 10, 2015.
- [9] B. Palmer, “Gfrc - glass fiber reinforced concrete,” Jan 2021. [Online]. Available: <https://www.concretenetwork.com/glass-fiber-reinforced-concrete/>
- [10] B. Singh and A. J. Majumdar, “The effect of fibre length and content on the durability of glass reinforced cement ? ten-year results,” *Journal of Materials Science Letters*, vol. 4, no. 8, pp. 967–971, Aug. 1985. [Online]. Available: <http://link.springer.com/10.1007/BF00721095>
- [11] R. S. Selbekk, “Basalt,” Jan 2020. [Online]. Available: <https://snl.no/basalt>
- [12] J. Branston, S. Das, S. Y. Kenno, and C. Taylor, “Mechanical behaviour of basalt fibre reinforced concrete,” *Construction and Building Materials*, vol. 124, pp. 878–886, Oct. 2016. [Online]. Available: <https://linkinghub.elsevier.com/retrieve/pii/S0950061816312727>
- [13] C. High, H. M. Seliem, A. El-Safty, and S. H. Rizkalla, “Use of basalt fibers for concrete structures,” *Construction and Building Materials*, vol. 96, pp. 37–46, Oct. 2015. [Online]. Available: <https://linkinghub.elsevier.com/retrieve/pii/S0950061815301653>
- [14] V. J. John and B. Dharmar, “Influence of basalt fibers on the mechanical behavior of concrete—A review,” *Structural Concrete*, vol. 22, no. 1, pp. 491–502, Feb. 2021. [Online]. Available: <https://onlinelibrary.wiley.com/doi/10.1002/suco.201900086>
- [15] S. K. Kirthika and S. K. Singh, “Experimental Investigations on Basalt Fibre-Reinforced Concrete,” *Journal of The Institution of Engineers (India): Series A*, vol. 99, no. 4, pp. 661–670, Dec. 2018. [Online]. Available: <http://link.springer.com/10.1007/s40030-018-0325-4>
- [16] S. Norge, “NS-EN 1991-1-7:2006+NA:2008: Eurocode 1: Actions on structures - part 1-7: General actions - accidental actions,” 2008. [Online]. Available: <https://www.standard.no/no/Nettbutikk/produktkatalogen/Produktpresentasjon/?ProductID=330044>

- [17] K. Sohel, K. Al-Jabri, and A. Al Abri, “Behavior and design of reinforced concrete building columns subjected to low-velocity car impact,” *Structures*, vol. 26, pp. 601–616, Aug. 2020. [Online]. Available: <https://linkinghub.elsevier.com/retrieve/pii/S2352012420302101>
- [18] M. Wu, L. Jin, and X. Du, “Dynamic responses and reliability analysis of bridge double-column under vehicle collision,” *Engineering Structures*, vol. 221, p. 111035, Oct. 2020. [Online]. Available: <https://linkinghub.elsevier.com/retrieve/pii/S0141029620316151>
- [19] B. Liu, W. Fan, W. Guo, B. Chen, and R. Liu, “Experimental investigation and improved FE modeling of axially-loaded circular RC columns under lateral impact loading,” *Engineering Structures*, vol. 152, pp. 619–642, Dec. 2017. [Online]. Available: <https://linkinghub.elsevier.com/retrieve/pii/S0141029617301761>
- [20] Y. Sha and H. Hao, “Laboratory tests and numerical simulations of barge impact on circular reinforced concrete piers,” *Engineering Structures*, vol. 46, pp. 593–605, Jan. 2013. [Online]. Available: <https://linkinghub.elsevier.com/retrieve/pii/S0141029612004750>
- [21] H. Ormestad, “Støt – fysikk,” Dec 2019. [Online]. Available: https://snl.no/st%C3%B8t_-_fysikk
- [22] P. Dourmashkin, “10.2: Momentum (quantity of motion) and average impulse,” Dec 2020. [Online]. Available: [https://phys.libretexts.org/Bookshelves/Classical_Mechanics/Classical_Mechanics_\(Dourmashkin\)/10%3A_Momentum_System_of_Particles_and_Conservation_of_Momentum/10.02%3A_Momentum_\(Quantity_of_Motion\)_and_Average_Impulse](https://phys.libretexts.org/Bookshelves/Classical_Mechanics/Classical_Mechanics_(Dourmashkin)/10%3A_Momentum_System_of_Particles_and_Conservation_of_Momentum/10.02%3A_Momentum_(Quantity_of_Motion)_and_Average_Impulse)
- [23] S. S. Rao and P. Griffin, *Chapter 2: Free vibration of Single-Degree-of-Freedom system*, 6th ed. Pearson, 2018, p. 153–296.
- [24] R. H. Brenden, “Steel fiberin self compacting concrete,” 2018.
- [25] S. Norge, “NS-EN 12390-3:2019: Testing hardened concrete - part 3: Compressive strength of test specimens,” 2019. [Online]. Available: <https://www.standard.no/no/Nettbutikk/produktkatalogen/Produktpresentasjon/?ProductID=1107001>
- [26] —, “NS-EN 12390-6:2009: Testing hardened concrete - part 6: Tensile splitting strength of test specimens,” 2010. [Online]. Available:

[https://www.standard.no/no/Nettbutikk/produktkatalogen/
Produktpresentasjon/?ProductID=418911](https://www.standard.no/no/Nettbutikk/produktkatalogen/Produktpresentasjon/?ProductID=418911)

- [27] —, “NS-EN 14651:2005+A1:2007: Test method for metallic fibre concrete - measuring the flexural tensile strength (limit of proportionality (lop), residual),” 2008. [Online]. Available: <https://www.standard.no/no/Nettbutikk/produktkatalogen/Produktpresentasjon/?ProductID=312614>
- [28] —, “NS-EN 1992-1-1:2004+NA:2010: Eurocode 2 — design of concrete structures — part 1-1: General rules and rules for buildings,” 2019. [Online]. Available: [https://www.standard.no/no/Nettbutikk/produktkatalogen/
Produktpresentasjon/?ProductID=411303](https://www.standard.no/no/Nettbutikk/produktkatalogen/Produktpresentasjon/?ProductID=411303)

Part I

Appendix

Concrete Matrix



Blandeskjema**SKANSKA**

| | |
|---------------------------|--|
| Prosjekt | Prøvemix 0.5% Basaltfiber, 30/70 grus/sand |
| Reseptnummer | Resept 1 |
| Tilsiktet kvalitet | B70 M40 |

| | |
|--------------------------------------|-----------|
| Blande volum | 135 liter |
| Dato: | |
| Tidspunkt for vanntilsetning: | |
| Ansvarlig: | |
| Utført av: | |

| Materialer | Resept kg/m³ | Sats kg | Fukt* % | Korr. kg | Oppveid** kg |
|-------------------------|------------------------------------|--------------------|--------------------|---------------------|-------------------------|
| Norcem Industri | 0.0 | 0.000 | | | 0.000 |
| Lavvarme | 805.3 | 108.716 | | | 108.716 |
| | 0.0 | 0.000 | | | 0.000 |
| Elkem Microsilica | 0.0 | 0.000 | 0.0 | 0.000 | 0.000 |
| Normineral flyveaske | 0.0 | 0.000 | | | 0.000 |
| | 0.0 | 0.000 | | | 0.000 |
| Fritt vann | 322.1 | 43.487 | | -2.003 | 41.484 |
| Absorbent vann | 6.1 | 0.819 | | | 0.819 |
| Årdal 0/8 mm nat. vask. | 720.6 | 97.283 | 1.0 | 0.973 | 98.256 |
| Årdal 0/2 mm nat. vask | 0.0 | 0.000 | 0.0 | 0.000 | 0.000 |
| Årdal 8/16mm | 307.9 | 41.569 | 0.5 | 0.208 | 41.777 |
| Årdal 16/22 mm | 0.0 | 0.000 | 0.5 | 0.000 | 0.000 |
| Velde 0/8 Industri S | 0.0 | 0.000 | 0.0 | 0.000 | 0.000 |
| Velde 8/16 Industri | 0.0 | 0.000 | 0.0 | 0.000 | 0.000 |
| | 0.0 | 0.000 | 0.0 | 0.000 | 0.000 |
| | 0.0 | 0.000 | 0.0 | 0.000 | 0.000 |
| | 0.0 | 0.000 | 0.0 | 0.000 | 0.000 |
| | 0.0 | 0.000 | 0.0 | 0.000 | 0.000 |
| Mapei Dynamon SX-N | 7.2 | 0.978 | 84 | 0.822 | 0.978 |
| Mapei Dynamon SX-23 | 0.0 | 0.000 | 0 | 0.000 | 0.000 |
| Mapeair 25 1:19 | 0.0 | 0.000 | 0 | 0.000 | 0.000 |
| | 0.0 | 0.000 | 0 | 0.000 | 0.000 |
| Stålfiber | 0.0 | 0.000 | | | 0.000 |
| Basaltfiber | 0.0 | 0.000 | | | 0.000 |

42.303

*Se fotnote på delark "Resept"

** NB! Våte mengder, også for silikaslurry

| Fersk betong | | | | | |
|--------------------------|--|--|--|--|--|
| Tid etter vanntilsetning | | | | | |
| Synkmål | | | | | |
| Utbredelsesmål | | | | | |
| Luft | | | | | |
| Densitet | | | | | |

| Prøvestykker (antall) | | | | | |
|------------------------------|--|--|--|--|--|
| Utstøpningstidspunkt | | | | | |
| Terninger | | | | | |
| 150x300 sylindre | | | | | |
| 100x200 sylindre | | | | | |

Blandeskjema**SKANSKA**

| | |
|---------------------------|--|
| Prosjekt | Prøvemix 0.5% Basaltfiber, 30/70 grus/sand 0.9% SP |
| Reseptnummer | Resept 2 |
| Tilsiktet kvalitet | B70 M40 |

| | |
|--------------------------------------|-------------------------|
| Blande volum | 135 liter |
| Dato: | Onsdag 3 uker før påske |
| Tidspunkt for vanntilsetning: | |
| Ansvarlig: | |
| Utført av: | Einar Mesloe |

| Materialer | Resept kg/m³ | Sats kg | Fukt* % | Korr. kg | Oppveid** kg |
|-------------------------|------------------------------------|--------------------|--------------------|---------------------|-------------------------|
| Norcem Industri | 0.0 | 0.000 | | | 0.000 |
| Lavvarme | 805.4 | 108.733 | | | 108.733 |
| | 0.0 | 0.000 | | | 0.000 |
| Elkem Microsilica | 0.0 | 0.000 | 0.0 | 0.000 | 0.000 |
| Normineral flyveaske | 0.0 | 0.000 | | | 0.000 |
| | 0.0 | 0.000 | | | 0.000 |
| Fritt vann | 322.2 | 43.493 | | -1.987 | 41.506 |
| Absorbent vann | 6.0 | 0.808 | | | 0.808 |
| Årdal 0/8 mm nat. vask. | 711.1 | 96.003 | 1.0 | 0.960 | 96.963 |
| Årdal 0/2 mm nat. vask | 0.0 | 0.000 | 0.0 | 0.000 | 0.000 |
| Årdal 8/16mm | 303.9 | 41.022 | 0.5 | 0.205 | 41.227 |
| Årdal 16/22 mm | 0.0 | 0.000 | 0.5 | 0.000 | 0.000 |
| Velde 0/8 Industri S | 0.0 | 0.000 | 0.0 | 0.000 | 0.000 |
| Velde 8/16 Industri | 0.0 | 0.000 | 0.0 | 0.000 | 0.000 |
| | 0.0 | 0.000 | 0.0 | 0.000 | 0.000 |
| | 0.0 | 0.000 | 0.0 | 0.000 | 0.000 |
| | 0.0 | 0.000 | 0.0 | 0.000 | 0.000 |
| Mapei Dynamon SX-N | 7.2 | 0.979 | 84 | 0.822 | 0.979 |
| Mapei Dynamon SX-23 | 0.0 | 0.000 | 0 | 0.000 | 0.000 |
| Mapeair 25 1:19 | 0.0 | 0.000 | 0 | 0.000 | 0.000 |
| | 0.0 | 0.000 | 0 | 0.000 | 0.000 |
| Stålfiber | 0.0 | 0.000 | | | 0.000 |
| Basaltfiber | 10.5 | 1.418 | | | 1.418 |

42.314

*Se fotnote på delark "Resept"

** NB! Våte mengder, også for silikaslurry

| Fersk betong | | | | | |
|--------------------------|--|--|--|--|--|
| Tid etter vanntilsetning | | | | | |
| Synkmål | | | | | |
| Utbredelsesmål | | | | | |
| Luft | | | | | |
| Densitet | | | | | |

| Prøvestykker (antall) | | | | | |
|------------------------------|--|--|--|--|--|
| Utstøpningstidspunkt | | | | | |
| Terninger | | | | | |
| 150x300 sylindre | | | | | |
| 100x200 sylindre | | | | | |

Blandeskjema**SKANSKA**

| | |
|---------------------------|--|
| Prosjekt | Prøvemix 0.5% Basaltfiber, 30/70 grus/sand |
| Reseptnummer | Resept 3 |
| Tilsiktet kvalitet | B70 M40 |

| | |
|--------------------------------------|-----------|
| Blande volum | 135 liter |
| Dato: | |
| Tidspunkt for vanntilsetning: | |
| Ansvarlig: | |
| Utført av: | |

| Materialer | Resept kg/m³ | Sats kg | Fukt* % | Korr. kg | Oppveid** kg |
|-------------------------|------------------------------------|--------------------|--------------------|---------------------|-------------------------|
| Norcem Industri | 0.0 | 0.000 | | | 0.000 |
| Norcem lavvarme | 805.6 | 108.749 | | | 108.749 |
| | 0.0 | 0.000 | | | 0.000 |
| Elkem Microsilica | 0.0 | 0.000 | 0.0 | 0.000 | 0.000 |
| Normineral flyveaske | 0.0 | 0.000 | | | 0.000 |
| | 0.0 | 0.000 | | | 0.000 |
| Fritt vann | 322.2 | 43.500 | | -1.972 | 41.528 |
| Absorbent vann | 5.9 | 0.797 | | | 0.797 |
| Årdal 0/8 mm nat. vask. | 701.7 | 94.723 | 1.0 | 0.947 | 95.670 |
| Årdal 0/2 mm nat. vask | 0.0 | 0.000 | 0.0 | 0.000 | 0.000 |
| Årdal 8/16mm | 299.8 | 40.475 | 0.5 | 0.202 | 40.677 |
| Årdal 16/22 mm | 0.0 | 0.000 | 0.5 | 0.000 | 0.000 |
| Velde 0/8 Industri S | 0.0 | 0.000 | 0.0 | 0.000 | 0.000 |
| Velde 8/16 Industri | 0.0 | 0.000 | 0.0 | 0.000 | 0.000 |
| | 0.0 | 0.000 | 0.0 | 0.000 | 0.000 |
| | 0.0 | 0.000 | 0.0 | 0.000 | 0.000 |
| | 0.0 | 0.000 | 0.0 | 0.000 | 0.000 |
| Mapei Dynamon SX-N | 7.2 | 0.979 | 84 | 0.822 | 0.979 |
| Mapei Dynamon SX-23 | 0.0 | 0.000 | 0 | 0.000 | 0.000 |
| Mapeair 25 1:19 | 0.0 | 0.000 | 0 | 0.000 | 0.000 |
| | 0.0 | 0.000 | 0 | 0.000 | 0.000 |
| Stålfiber | 0.0 | 0.000 | | | 0.000 |
| Basaltfiber | 21.0 | 2.835 | | | 2.835 |

42.325

*Se fotnote på delark "Resept"

** NB! Våte mengder, også for silikaslurry

| Fersk betong | | | | | |
|--------------------------|--|--|--|--|--|
| Tid etter vanntilsetning | | | | | |
| Synkmål | | | | | |
| Utbredelsesmål | | | | | |
| Luft | | | | | |
| Densitet | | | | | |

| Prøvestykker (antall) | | | | | |
|------------------------------|--|--|--|--|--|
| Utstøpningstidspunkt | | | | | |
| Terninger | | | | | |
| 150x300 sylindre | | | | | |
| 100x200 sylindre | | | | | |

Data sheets

B

Teknisk datablad

Lavvarmesement

CEM III/B 42,5 L-LH/SR (na)

Rüdersdorf

| | |
|----------------|--|
| Sammensetning: | Slaggsement |
| Bruk: | Til bruk i betongproduksjon. Elementindustri, ferdigbetong og injeksjon. |
| Egenskaper: | Lav varme- og herdeutvikling. Lavt CO2 avtrykk. |

Tilfredsstill kravene ihht. EN 197-1: CEM III/B 42,5 L-LH/SR (na)
Produktet er sertifisert (CE-merket) ihht. EN 197-1 av VDZ, Tyskland

Typiske data:

Fysiske data

| | |
|----------------|-------------------------|
| Finhet(blaine) | 4700 cm ² /g |
| Densitet | 2,98 g/cm ³ |
| Bulkdensitet | 1,1g/cm ³ |
| Andel slagg | Ca 70% |
| Bindetid | 230 min |
| Ekspansjon | 0,3 mm |

Trykkfasthet

| | |
|-----|--------|
| 2d | 28 Mpa |
| 7d | 36 MPa |
| 28d | 58 MPa |
| 56d | 64 MPa |

Kjemiske data

| | | vekt % |
|--------------------|-----------------------------------|-----------|
| Kalk | (CaO) | 49 |
| Silisium | (SiO ₂) | 31 |
| Aluminium | (Al ₂ O ₃) | 8,3 |
| Magnesium | (MgO) | 6,1 |
| Sulfat | (SO ₃) | 2,1 |
| Jern | (Fe ₂ O ₃) | 1,6 |
| Kalium | (K ₂ O) | 0,6 |
| Natrium | (Na ₂ O) | 0,3 |
| Alkali ekv. | (Na ₂ Oekv) | 0,79 |
| (C ₃ A) | | 5,3 |
| Glødetap | (L.O.I) | 0,7 |
| Uløselig rest | (i.r) | 0,2 |
| Vannløslig klorid | (Cl ⁻) | 0,05 |
| Vannløslig krom | Cr ^(VI) | < 2 mg/kg |



0840

CEMEX Zement GmbH
Werk Rüdersdorf
Frankfurter Chaussee
15562 Rüdersdorf

0840-CPD-5520-340595-16

EN 197-1
CEM III/B 42,5 L-LH/SR (na)

Teknisk spørsmål:

Lars Busterud, tel 908 90 668

- E-Mail lars.busterud@schwenk.no

Versjon August 2019

SCHWENK Norge AS

Grønland 70A, 3045 Drammen

Telefon: +47 31 02 10 11

E-Mail: info@schwenk.no · www.schwenk.no

Informasjonen i denne publikasjonen er basert på gjeldende kunnskap og erfaring. De gir en referanseverdi for grunnleggende egnethet og må matches av tester og forsøk av prosessoren til den spesifikke applikasjonen. For dette må de tilsvarende gyldige lover, standarder og retningslinjer samt de generelt anerkjente reglene for byggeteknikk overholdes. Ved publisering av dette tekniske databladet mister tidligere tekniske datablad deres gyldighet. Endringer i rammeproduktet og applikasjonsteknikkutviklingen er reservert. Våre salgs- og leveringsbetingelser i gjeldende versjon gjelder for alle forretningsforbindelser.



ENABLING INNOVATION IN CONCRETE STRUCTURES

ReforceTech Basalt Fiber Reinforced Polymer (BFRP) MiniBars™ are an engineered macrofiber designed to increase the structural tensile strength of concrete by uniform distribution of MiniBars™ throughout the matrix.

Concrete reinforced with RFT MiniBars™ demonstrates excellent flexural toughness and energy absorption capability after cracking when tested according to ASTM C78 and C1399 and EN16451.

Testing demonstrates that MiniBars™ satisfy the relevant residual strength requirements based on ASTM C1609 tests (as specified in ACI 318) using MiniBars™ as shear reinforcement in reinforced concrete slabs and beams.

ReforceTech BFRP MiniBars™ are engineered to deliver high flexural tensile strength and average residual strength in concrete in conjunction with proven alkali resistance and engineered bond strength.

Det Norske Veritas (DNV) testing has demonstrated that the unique ReforceTech process delivers a strong bond between the concrete and the BFRP bars. Further testing with the University of Akron demonstrated results of Flexural Tensile Strength (ASTM C78) enabling the increase from 4.5 MPa (653 psi) for normal concrete up to 17 MPa (2465 psi) depending on volume fraction of MiniBars™. Testing Average Residual Strength (ASTM C1399) has developed ARS from zero in normal concrete to over 17 MPa (2465 psi). The Norwegian technical university NTNU has demonstrated the bond strength of MiniBars™ in single fiber testing.

From volcanic basalt stone, thin basalt fibers are assembled in ReforceTech's patented process to create unique macro fiber called MiniBars™ cut to the prescribed length 20 to 60 mm (0.79" to 2.36") to achieve the desired concrete performance.

UNIQUE ENABLING FEATURES TO REDUCE PROJECT COSTS

- Corrosion Free allows thinner lighter structures
- Zero Conductivity, eliminates galvanic corrosion
- Improved Flexural and Average Residual Strength of Concrete allowing design freedom, elimination or reduction of normal reinforcement
- Compatible Specific Gravity of 1.9 g/cm³ means uniform distribution, MiniBars™ do not settle or float and are easily mixed
- Suitable for site work, precast or dry mix concrete
- No MiniBars protrude from Concrete; no MiniBars™ are visible on the surface
- Improved freeze thaw resistance
- Savings of labor costs and faster construction
- Improved abrasion resistance
- Improves safety on site by eliminating handling of traditional steel reinforcement
- Excellent bond related to engineered helix, rough fiber surface, bond length and diameter

MiniBars Properties

| | | |
|---------------------|------------|----------------------------|
| Diameter | 0.65mm | 0.026 inches |
| Length | 20 to 60mm | 0.8 to 2.40 inches |
| Specific Gravity | 1.9g/cc | 0.069 oz/inch ³ |
| Water Absorption | None | None |
| E modulus | 60GPa | 8700 KSI |
| Tensile Strength | 1100MPa | 159 KSI |
| Alkaline Resistance | Excellent | Excellent |



MiniBars™

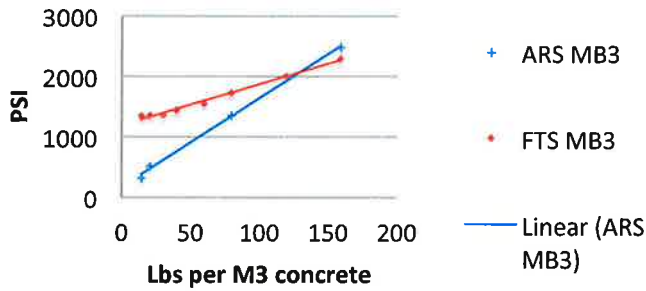
ADVANTAGES

- Greatly increases toughness and strength of concrete at low dosage
- Enables thinner sections, lighter weight products for easier installation and transportation
- Suitable for aggressive chloride environments
- Acts as minimum reinforcement to lower cost
- Transforms concrete from a brittle material requiring steel reinforcement to ductile with tensile strength capacity

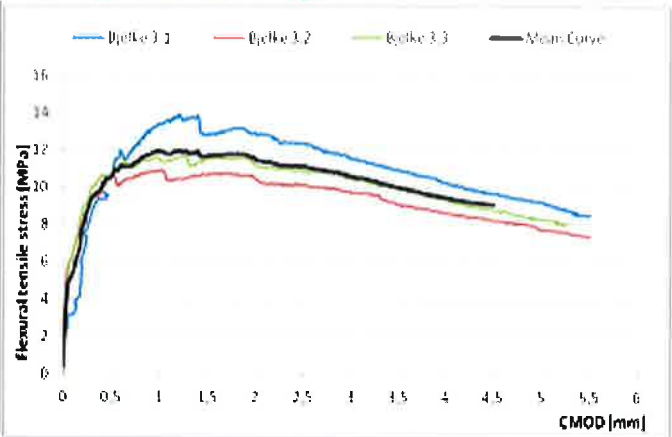
REFORCETECH IS 9001 CERTIFIED

Improved Concrete Tensile Properties

FTS and ARS versus dosage



ASTM C78 and 1399



EN 14651 at 2% VF

Typical Applications

- Submersed Concrete Products
- Structural Slab on Grade
- Thinner Precast and Cast-In-Place Facades
- Highway Slabs & Bridge Decks
- Floating Infrastructure
- Agricultural Products
- Drainage Systems
- Grout Systems
- Blast & Impact Resistance
- Inner Walls
- Bridge Beams
- Sound Walls
- Barrier Walls
- Block Walls
- Power Poles
- Barrier Poles
- High Performance Concrete
- Balconies

Specification for MiniBars™ - MasterFormat® Section 03 24 00

Generic: Use macrofibers made from Basalt FRP rods with helix winding geometry and diameters in the range of 0.65mm to 0.70mm. BFRP macrofibers should be fabricated with CBF (continuous basalt fiber) and vinyl ester resin with a minimum Heat Distortion Temperature of 235F (115C) and Modulus of Elasticity of 8700 ksi (60 GPa). The length of the fibers will be from 0.80" to 2.40" (20mm to 60mm) with exact length to be determined by trial batch with guidance from the manufacturer. Dosage will be determined by trial batch up to 130 lbs/cu.yd based on the minimum ARS (average residual strength per ASTM C1399) and FTS (flexural tensile strength per ASTM C1609) established by the engineer-of-record. The BFRP macrofiber reinforced concrete shall be capable of achieving an ARS of 2400 psi (17.2 MPa) and FTS of 2300 psi (15.8 MPa) at maximum dosage.

Specific: Use MiniBars™ by ReforceTech AS. Length of fibers and dosage to be determined by trial batch with guidance from the manufacturer per the requirements for ARS (ASTM C1399) and FTS (ASTM C1609) established by the engineer-of-record for the project.

Mixing Instructions

- Due to the MiniBars™ unique density and geometry they are very simple to mix. They do not float, ball or sink.
- MiniBars are added in either the batching plant or in the truck and follow normal practices by adding after water and add mixtures. Mix for 5 to 10 minutes.
- Higher volume fraction dosage's are possible with minor mix design adjustments
- Contact your representative for specific instructions for your mix design, application or concrete

The information shown here inclusive of all drawings and tables is for informational purposes only. Details are subject to change; every effort has been made to ensure accuracy. The user shall ensure the appropriate guidelines and building codes are followed. ReforceTech has no control over the use of their products and assumes no responsibility for the end products or uses of our materials.

ReforceTech LTD
Pamdohlen House
Dooradoyle Road
Limerick
Republic of Ireland
Phone: +47 66 76 77 80
www.reforcetech.com

ReforceTech AS
Luftveien 4
3440 Røyken
Norway
Phone: +47 66 76 77 80
www.reforcetech.com

ReforceTech Qatar
P.O. Box 3889,
Doha
Qatar
Phone +974 77 44 7732
www.reforcetech.com

Basalt Products Group LLC
2285 Botanica Circle
Melbourne, FL 32904-7340
USA
Phone +321 537 1810
www.basaltproducts.com



1111

NorStone Årdal, 4137 Årdal, Norge

19

NS-EN 12620:2002+A1:2008+NA:2016

Tilslag for betong

Ytelseserklæring nr / Entydig identifikasjonskode

164102 001

NK 60-20-20

0/8mm (B)

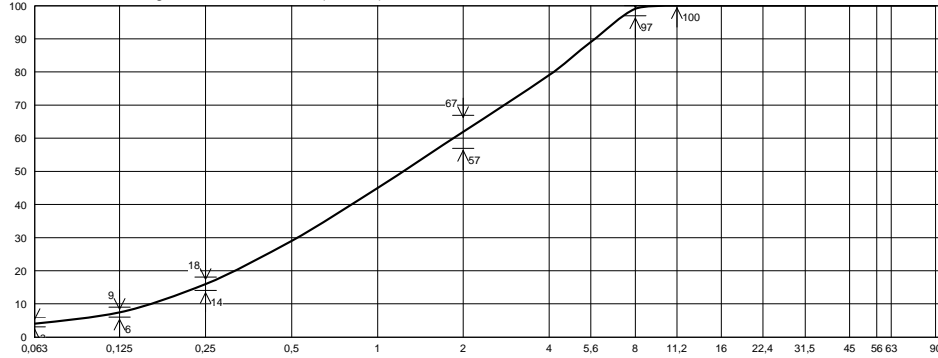
Gneis-Granitt

| Standarder | | Verdier | Kategorier |
|-------------------|---|--|---|
| NS EN 933-1 | Kornstørrelse Gradering Toleransekategori | | 0/8 G _{NG90} - |
| NS EN 933-3 | Kornform Flisighetsindeks | - | |
| NS EN 1097-6 | Korndensitet | 2,68 Mg/m ³ | 2,66 Mg/m ³ - 2,70 Mg/m ³ |
| NS EN 1097-6 | Vannabsorpsjon | 0,3% | WA ₂₄₁ |
| NS-EN12620 F.2.3 | Motstand mot frysing og tining | 0,3 | F ₁ |
| | Renhet | | |
| NS EN 933-1 | Finstoffinnhold | 3% | f ₁₀ |
| NS EN 933-7 | Skjellinnhold | | - |
| NS EN 933-5 | Prosentandel knuste korn | | C _{IK} |
| | Sammensetning / innhold | | |
| NS EN 1744-1§ 7 | Klorider | 0 | |
| NS EN 1744-1§ 11 | Totalt innhold av svovel | 0,02 | |
| NS EN 1744-1§ 12 | Syreløselige sulfater | 0,01 | AS _{0,1} |
| NS-EN 1744-1§ 15 | Bestanddelene som endrer størknings- og herdingstiden av betong | | Lysere |
| NB 21 | Alkalireaktivitet (sammelningsverdi) | 4,8% | |
| ASTM C1260-14 | Accelerert utvidelse | 0,01% | <0.10% |
| NS EN 932-3 | Petrografisk beskrivelse | Sand med knuste korn fra løssmasseforekomst. Hovedsakelig sammensatt av kubisk rundede/skarpkantede korn av granitt, gneis, feltspatiske bergarter og mørke bergarter. Løst belegg på kornoverflater, enkelte forvitrede korn og enkelte meget svake korn. | |

| | | | |
|-----------------|----------------|-------------|-----------------|
| Material | Vare nr | Dato | Avdeling |
| 0/8 | 164102 | 18.09.2019 | NorStone Årdal |

| | Gjennomgang(%) | | | | | | | | | | | | | | | | |
|------------------|----------------|-------|------|------|------|------|------|------|-------|-------|----|------|------|----|----|----|----|
| | 0,063 | 0,125 | 0,25 | 0,5 | 1 | 2 | 4 | 5,6 | 8 | 11,2 | 16 | 22,4 | 31,5 | 45 | 56 | 63 | 90 |
| Typisk gradering | 4,0 | 7,5 | 16,0 | 29,0 | 45,0 | 62,0 | 79,0 | 89,0 | 99,0 | 100,0 | | | | | | | |
| Min. | 3,0 | 6,0 | 14,0 | | | 57,0 | | | 97,0 | 100,0 | | | | | | | |
| Max. | 6,0 | 9,0 | 18,0 | | | 67,0 | | | 100,0 | | | | | | | | |

Gneis-Granitt/Naturlig Gradert 0/8 60/20/20 (164102)



| | |
|--------------------|-----------------------------|
| 18.09.2019 Dato | S. Tengesdal Prepared by |
|--------------------|-----------------------------|

Ytelseserklæring

I henhold til forordning (EU) nr. 305/2011 (byggevarer), vedlegg III

Side - 3 -

| | | | | |
|---|-------------------|---------------|---|---------------|
| Ytelseserklæring nr: | 164102 001 | | | |
| NK 60-20-20 | 0/8mm (B) | Gneis-Granitt | Vare nr: | 164102 |
| Bruksområder for byggevaren(e): | | | Tilslag for betong | |
| Det eller de systemer for vurdering og kontroll av byggevarens konstante ytelse | | | System 2+ | |
| Dersom ytelseserklæringen gjelder en byggevarer som omfattes av en harmonisert Standard | | | NS-EN 12620:2002+A1:2008+NA:2016 | |
| Sertifiseringsorganet: | | | Kontrollrådet-1111 | |
| har utstedt sertifikat for produksjonskontrollen i samsvar med | | | System 2+ | |
| basert på førstegangsrevisjon av produksjons-anlegget og produksjonskontrollen: | | | 1111-CPD-0007 | |
| Ytelseserklæring arkiveres i ti år. | | | | |

NORSTONE
HEIDELBERGCEMENT Group

NorStone Årdal

NorStone Årdal, 4137 Årdal, Norge

www.norstone.no

Tlf:0047-51754200

Tlf:

| Harmonisert teknisk spesifisering | Standarder | Vesentlige egenskaper | Ytelse | |
|-----------------------------------|---|---|------------------------|---|
| | | | Verdier | Kategorier |
| NS EN 12620:2002+A1:2008+NA:2016 | NS EN 933-1 | Kornstruktur Gradering Toleransekategori | | 0/8 G _{NG} 90 - |
| | NS EN 933-3 | Kornform Flisighetsindeks | - | |
| | NS EN 933-4 | Shape indeks | - | NPD |
| | NS EN 1097-6 | Korndensitet | 2,68 Mg/m ³ | 2,66 Mg/m ³ - 2,70 Mg/m ³ |
| | NS EN 1097-6 §8 | Vannabsorpsjon | 0,3% | WA ₂₄ 1 |
| | NSEN 12620 F.2.3 | Motstand mot frysing og tining | 0,3 | F ₁ |
| | | Renhet | | |
| | NS EN 933-1 | Finstoffinnhold | 3 % | f ₁₀ |
| | NS EN 933-7 | Skjellinnhold | | NPD |
| | | Motstand mot knusing | | |
| | NS EN 1097-2 §5 | Los Angeles-prøving | 23 | LA ₃₀ |
| | NS EN 1097-2 §6 | Slagprøving | | NPD |
| | | Motstand mot polering/slitasje | | |
| | NS EN 1097-8 | Poleringsverdi | | NPD |
| | NS EN 1097-1 | Motstand mot slitasje for grovt tilslag | | NPD |
| | NS EN 1097-9 | Motstand mot piggdekkslitasje | | NPD |
| | | Sammensetning / innhold | | |
| | NS EN 1744-1§ 7 | Klorider | 0 | |
| | NS EN 1744-1§ 11 | Totalt innhold av svovel | 0,02 | |
| | NS EN 1744-1§ 12 | Syreløselige sulfater | 0,01 | AS _{0,1} |
| NS EN 1744-1§ 15 | Bestanddelene som endrer størknings- og herdingstiden av betong | | Lysere | |
| NB21 | Alkalireaktivitet (sammelningsverdi) | 4,8% | | |
| ASTM C1260-14 | Accelerert m,rtelprismeeekspansjon | 0,01% | <0.10% | |
| NS-EN 932-3 | Innhold av kalkstein | 0,0% | | |
| NS EN 932-3 | Petrografisk beskrivelse | Sand med knuste korn fra lyssmasseforekomst. Hovedsakelig sammensatt av kubisk rundede/skarpkantede korn av granitt, gneis, feltspatisk bergarter og mørke bergarter. Lyst belegg på kornoverflater, enkelte forvitrede korn og enkelte meget svake korn. | | |

Ytelsen for denne varen som angitt ovenfor, er i samsvar med spesifikasjonene for produktet angitt i tabellen. Denne ytelseserklæringen er utstedt på eget ansvar av produsenten, NorStone Årdal. Undertegnet for og på vegne av produsenten av:

Årdal 18.09.2019
(Sted og utstedelsesdato)

Svein Johan Mæland, Site Manager
(navn og stilling)

NORSTONE
HEIDELBERGCEMENT Group

(Underskrift)



1111

NorStone Årdal, 4137 Årdal, Norge

19

NS-EN 12620:2002+A1:2008+NA:2016

Tilslag for betong

Ytelseserklæring nr / Entydig identifikasjonskode

101712-161 006

Knust-Natur

16/22mm (B)

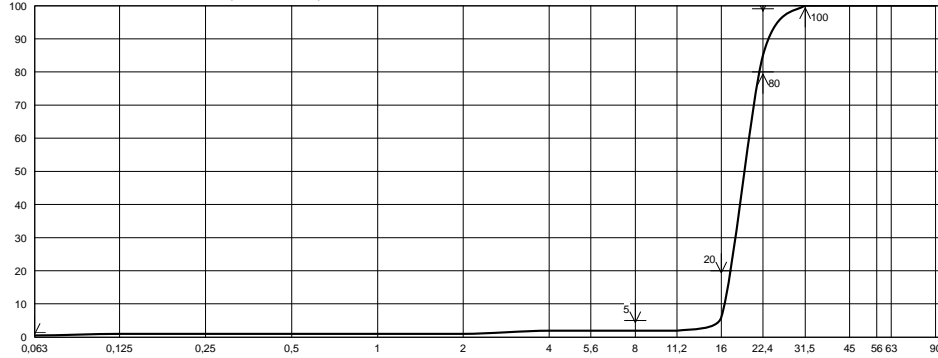
Gneis-Granitt

| <u>Standarder</u> | | <u>Verdier</u> | <u>Kategorier</u> |
|-------------------|---|--|---|
| NS EN 933-1 | Kornstørrelse Gradering Toleransekategori | | 16/22 G _C 80/20 - |
| NS EN 933-3 | Kornform Flisighetsindeks | 3% | FI ₁₀ |
| NS EN 1097-6 | Korndensitet | 2,71 Mg/m ³ | 2,69 Mg/m ³ - 2,73 Mg/m ³ |
| NS EN 1097-6 | Vannabsorpsjon | 0,3% | WA ₂₄₁ |
| NS-EN12620 F.2.3 | Motstand mot frysing og tining | 0,3 | F ₁ |
| | Renhet | | |
| NS EN 933-1 | Finstoffinnhold | 0,5% | f _{1,5} |
| NS EN 933-7 | Skjellinnhold | | SC ₁₀ |
| NS EN 933-5 | Prosentandel knuste korn | | C _{IK} |
| | Sammensetning / innhold | | |
| NS EN 1744-1§ 7 | Klorider | 0 | |
| NS EN 1744-1§ 11 | Totalt innhold av svovel | 0,02 | |
| NS EN 1744-1§ 12 | Syreløselige sulfater | 0,01 | AS _{0,2} |
| NS-EN 1744-1§ 15 | Bestanddelene som endrer størknings- og herdingstiden av betong | | Lysere |
| NB 21 | Alkalireaktivitet (sammelningsverdi) | 0,9% | |
| ASTM C1260-14 | Accelerert merkelprismekspansjon | 0,01% | <0.10% |
| NS EN 932-3 | Petrografisk beskrivelse | Singel med knuste korn fra løssmasseforekomst. Hovedsakelig sammensatt av kubisk rundede/skarpkantede korn av granitt, gneis, feltspatiske bergarter og mørke bergarter. Løst belegg på kornoverflater, ingen forvitrede korn og ingen meget svake korn. | |

| Material | Vare nr | Dato | Avdeling |
|----------|------------|------------|----------------|
| 16/22 | 101712-161 | 17.10.2019 | NorStone Årdal |

| | Gjennomgang(%) | | | | | | | | | | | | | | | | |
|------------------|----------------|-------|------|-----|-----|-----|-----|-----|-----|------|------|------|-------|----|----|----|----|
| | 0,063 | 0,125 | 0,25 | 0,5 | 1 | 2 | 4 | 5,6 | 8 | 11,2 | 16 | 22,4 | 31,5 | 45 | 56 | 63 | 90 |
| Typisk gradering | 0,5 | 1,0 | 1,0 | 1,0 | 1,0 | 1,0 | 2,0 | 2,0 | 2,0 | 2,0 | 6,0 | 85,0 | 100,0 | | | | |
| Min. | | | | | | | | | | | | 80,0 | 100,0 | | | | |
| Max. | 1,5 | | | | | | | | 5,0 | | 20,0 | 99,0 | | | | | |

Gneis-Granitt/Grovt 16/22 161 (101712-161)




| | |
|--------------------|-----------------------------|
| 17.10.2019 Dato | S. Tengesdal Prepared by |
|--------------------|-----------------------------|

Ytelseserklæring

I henhold til forordning (EU) nr. 305/2011 (byggevarer), vedlegg III

Side - 3 -

| | | | | |
|--|-----------------------|---------------|---|---|
| Ytelseserklæring nr: | 101712-161 006 | | |  |
| Knust-Natur | 16/22mm (B) | Gneis-Granitt | Vare nr: 101712-161 | |
| Bruksområder for byggevaren(e): | | | Tilslag for betong | |
| Det eller de systemer for vurdering og kontroll av byggevarens konstante ytelse | | | System 2+ | |
| Dersom ytelseserklæringen gjelder en byggevare som omfattes av en harmonisert Standard | | | NS-EN 12620:2002+A1:2008+NA:2016 | NorStone Årdal |
| Sertifiseringsorganet: | | | Kontrollrådet-1111 | NorStone Årdal, 4137 Årdal, Norge |
| har utstedt sertifikat for produksjonskontrollen i samsvar med | | | System 2+ | www.norstone.no |
| basert på førstegangsrevisjon av produksjons-anlegget og produksjonskontrollen: | | | 1111-CPD-0007 | Tlf:0047-51754200 |
| Ytelseserklæring arkiveres i ti år. | | | | Tlf: |

| Harmonisert teknisk spesifisering | Standarder | Vesentlige egenskaper | Ytelse | |
|-----------------------------------|---|--|------------------------|---|
| | | | Verdier | Kategorier |
| NS EN 12620:2002+A1:2008+NA:2016 | NS EN 933-1 | Kornstørrelse Gradering Toleransekategori | | 16/22 G _C 80/20 - |
| | NS EN 933-3 | Kornform Flisighetsindeks | 3% | Fl ₁₀ |
| | NS EN 933-4 | Shape indeks | - | Sl _{NR} |
| | NS EN 1097-6 | Korndensitet | 2,71 Mg/m ³ | 2,69 Mg/m ³ - 2,73 Mg/m ³ |
| | NS EN 1097-6 §8 | Vannabsorpsjon | 0,3% | WA ₂₄₁ |
| | NSEN 12620 F.2.3 | Motstand mot frysing og tining | 0,3 | F ₁ |
| | | Renhet | | |
| | NS EN 933-1 | Finstoffinnhold | 0,5 % | f _{1,5} |
| | NS EN 933-7 | Skjellinnhold | | SC ₁₀ |
| | | Motstand mot knusing | | |
| | NS EN 1097-2 §5 | Los Angeles-prøving | 23 | LA ₃₀ |
| | NS EN 1097-2 §6 | Slagprøving | | NPD |
| | | Motstand mot polering/slitasje | | |
| | NS EN 1097-8 | Poleringsverdi | | NPD |
| | NS EN 1097-1 | Motstand mot slitasje for grovt tilslag | | NPD |
| | NS EN 1097-9 | Motstand mot piggdekkslitasje | | NPD |
| | | Sammensetning / innhold | | |
| | NS EN 1744-1§ 7 | Klorider | 0 | |
| | NS EN 1744-1§ 11 | Totalt innhold av svovel | 0,02 | |
| | NS EN 1744-1§ 12 | Syreløselige sulfater | 0,01 | AS _{0,2} |
| NS EN 1744-1§ 15 | Bestanddelene som endrer størknings- og herdingstiden av betong | | Lysere | |
| NB21 | Alkalireaktivitet (sammelningsverdi) | 0,9% | | |
| ASTM C1260-14 | Accelerert m,rtelprismeeksponasjon | 0,01% | <0.10% | |
| NS-EN 932-3 | Innhold av kalkstein | 0,0% | | |
| NS EN 932-3 | Petrografisk beskrivelse | Singel med knuste korn fra lyssmasseforekomst. Hovedsakelig sammensatt av kubisk rundede/skarpkantede korn av granitt, gneis, feltspatiske bergarter og mørke bergarter. Løst belegg på kornoverflater, ingen forvitrede korn og ingen meget svake korn. | | |

Ytelsen for denne varen som angitt ovenfor, er i samsvar med spesifikasjonene for produktet angitt i tabellen. Denne ytelseserklæringen er utstedt på eget ansvar av produsenten, NorStone Årdal. Undertegnet for og på vegne av produsenten av:

Årdal 17.10.2019
(Sted og utstedelsesdato)

Svein Johan Mæland, Site Manager
(navn og stilling)



(Underskrift)

Dynamon SX-N

Superplastiserende tilsetningsstoff



BESKRIVELSE

Dynamon SX-N er et svært effektivt superplastiserende tilsetningsstoff basert på modifiserte akrylpolymerer. Produktet tilhører **Dynamon-systemet** basert på den Mapei-utviklede DPP-teknologien (DPP = Designed Performance Polymers), der tilsetningsstoffenes egenskaper skreddersys til ulike betongformål. **Dynamon-systemet** er utviklet på basis av Mapeis egen sammenstilling og produksjon av monomerer.

BRUKSOMRÅDER

Dynamon SX-N er et tilnærmet allround-produkt som er anvendelig i all betong for å øke støpeligheten og/eller redusere tilsatt vannmengde.

Noen spesielle bruksområder er:

- Vann tett betong med krav til høy eller svært høy fasthet og med strenge krav til bestandighet i aggressive miljøer.
- Betong med særlige krav til høy støpelighet; i konsistensklasser S4 og S5 etter NS-EN 206.
- Selvkomprimerende betong med ønske om lengre åpentid. Om nødvendig kan SKB stabiliseres med en viskositetsøker - **Viscofluid** eller **Viscostar**.
- Til produksjon av frostbestandig betong - da i kombinasjon med luftinnførende tilsetningsstoffer - **Mapeair**. Valg av type luftinnførende stoff gjøres ut

fra egenskapene til de andre delmaterialer som er tilgjengelige.

- Til golvstøp for å oppnå en smidig betong med bedret støpelighet. Store doseringer og lave temperaturer kan retardere betongen noe.

EGENSKAPER

Dynamon SX-N er en vannløsning av aktive akrylpolymerer som effektivt dispergerer (løser opp) sementklaser.

Denne effekten kan prinsipielt utnyttes på tre måter:

1. For å redusere mengden tilsatt vann, men samtidig beholde betongens støpelighet. Lavere v/c-forhold gir høyere fasthet, tetthet og bestandighet i betongen.
2. For å forbedre støpeligheten sammenlignet med betonger med samme v/c-forhold. Fastheten forblir dermed den samme, men muliggjør forenklet utstøping.
3. For å redusere både vann og sementmengde uten å forandre betongens mekaniske styrke. Gjennom denne metoden kan en blant annet redusere kostnadene (mindre sement), redusere betongens svinnpotensial (mindre vann) og redusere faren for temperaturgradienter på grunn av lavere hydrasjonsvarme. Spesielt er denne siste effekten viktig ved betonger med større sementmengder.

KOMPATIBILITET MED ANDRE PRODUKTER

Dynamon SX-N lar seg kombinere med andre Mapei tilsetningsstoffer, som f.eks. størkningsakselererende stoffer som **Mapefast** og størkningsretarderende stoffer som **Mapetard**.

Produktet lar seg også kombinere med luftinnførende tilsetningsstoffer, **Mapear**, for produksjon av frostbestandig betong.

Valg av type luftinnførende stoff gjøres ut fra egenskapene til de andre delmaterialer som er tilgjengelige.

DOSERING

Dynamon SX-N tilsettes for å oppnå ønsket resultat (styrke, bestandighet, støpelighet, sementreduksjon) ved å variere doseringen mellom 0,4 og 2,0 % av sement + flyveaske + mikrosilika. Ved økt dosering økes også betongens åpentid, dvs. tiden betongen lar seg bearbeide. Større doseringsmengder og lave betongtemperaturer gir en retardert betong. Vi anbefaler alltid prøvestøper med aktuelle parametere.

Til forskjell fra konvensjonelle melamineller naftalenbaserte superplastiserende tilsetningsstoffer, utvikler **Dynamon SX-N** maksimal effekt uavhengig av tilsetningstidspunkt, men tilsetningstidspunktet kan påvirke nødvendig blandetid.

Dersom **Dynamon SX-N** tilsettes etter at minst 80 % av blandevannet er inne vil blandetiden generelt være kortest. Det er likevel viktig med utprøvinger tilpasset eget blandeutstyr.

Dynamon SX-N kan også tilsettes direkte i automikser på bygg- eller anleggsplass. Betongen bør da blandes med maksimal hastighet på trommelen i ett minutt pr. m³ betong i lasset, men minimum 5 minutter.

EMBALLASJE

Dynamon SX-N leveres i 25 liters kanner, 200 liters fat, 1000 liter IBC-tanker og i tank.

LAGRING

Produktet må oppbevares ved temperaturer mellom +8°C og +35°C. I lukket emballasje bevarer produktet sine egenskaper i minst 12 måneder. Hvis produktet utsettes for direkte sollys, kan det føre til variasjoner i fargetonen uten at dette påvirker egenskapene til produktet.

SIKKERHETSINSTRUKSJONER FOR KLARGJØRING OG BRUK

For instruksjon vedrørende sikker håndtering av våre produkter, vennligst se siste utgave av sikkerhetsdatablad på vår nettside www.mapei.no

PRODUKT FOR PROFESJONELL BRUK.

MERK

De tekniske anbefalinger og detaljer som fremkommer i denne produktbeskrivelse representerer vår nåværende kunnskap og erfaring om produktene. All overstående informasjon må likevel betraktes som retningsgivende og gjenstand for vurdering. Enhver som benytter produktet må på forhånd forsikre seg om at produktet er egnet for tilsiktet anvendelse. Brukeren står selv ansvarlig dersom produktet blir benyttet til andre formål enn anbefalt eller ved feilaktig utførelse.

Vennligst referer til siste oppdaterte versjon av teknisk datablad som finnes tilgjengelig på vår webside www.mapei.no

JURIDISK MERKNAD

**Innholdet i dette tekniske databladet kan kopieres til andre prosjektrelaterte dokumenter, men det endelige dokumentet må ikke suppleres eller erstatte betingelsene i det tekniske datablad, som er gjeldende, når MAPEI-produktet benyttes. Det seneste oppdaterte datablad er tilgjengelig på vår hjemmeside www.mapei.no
ENHVER ENDRING AV ORDLYDEN
ELLER BETINGELSER, SOM ER GITT
ELLER AVLEDET FRA DETTE TEKNISKE
DATABLADET, MEDFØRER AT MAPEI
SITT ANSVAR OPPHØRER.**

Alle relevante referanser for produktet er tilgjengelige på forespørsel og fra www.mapei.no

TEKNISKE DATA (typiske verdier)

PRODUKTBESKRIVELSE

| | |
|--|--------------------------|
| Form: | væske |
| Farge: | gulbrun |
| Viskositet: | lettflytende; < 30 mPa·s |
| Tørrestoffinnhold (%): | 18,5 ± 1,0 |
| Densitet (g/cm³): | 1,06 ± 0,02 |
| pH: | 6,5 ± 1 |
| Kloridinnhold (%): | < 0,05 |
| Alkaliinnhold (Na₂O-ekvivalenter) (%): | < 2,0 |



STALMA Co. 20-822 Lublin, ul. Puławska 38, e-mail:office@stalma.com.pl

INSPECTION
CERTIFICATE

No. 29286/9

 3.1 EN 10204 2.2 EN 10204

| | | |
|----------|--|--|
| Customer | Steeltec Boxholm AB 590 10 BOXHOLM, Box 1 | Order No. / Confirmation No. 3549018063 |
|----------|--|--|

| | | |
|------------------|--|--------------------|
| Delivery address | Steeltec Boxholm AB 590 12 BOXHOLM, Nordenstens Väg 2 | Weight [kg] 950 |
|------------------|--|--------------------|

| Product / Specifications | Dimensions | Quality / Finished condition | Prod. batch No. |
|---|------------------------|------------------------------|-----------------|
| Cold drawn bar, rd EN-10025 EN-10277;EN-10278 | rd 4.00 h9 3000+100 | S355J2C+C | W/ 6907/1 |

I. CHEMICAL COMPOSITION

CEV: 0,40

| Charge No. | C | Mn | Si | P | S | Cr | Ni | Cu | Mo | Al | Pb | N ₂ |
|------------|------|------|------|-------|-------|------|------|------|------|-------|----|----------------|
| 221488 | 0,14 | 1,27 | 0,21 | 0,012 | 0,020 | 0,10 | 0,08 | 0,20 | 0,03 | 0,020 | | |

II. MECHANICAL TESTS

| Charge No. | R _e /R _{p0.2} [*] [Mpa] | R _m [Mpa] | A5 [*] [%] | Hardness [HB] | Other tests [*] |
|------------|---|-------------------------|------------------------|------------------|--------------------------|
| 221488 | 820 | 840 | 13,7 | 219 | . |

^{*} test is carried out under the agreement made when placing the order

III. CHARACTERISTICS AND PARAMETERS AGREED WHEN PLACING THE ORDER

Surface: class 2,
Straightness: 0,5mm/m;
Other tests: NDT-Test

| QUALITY CONTROL | | DECLARATION OF CONFORMITY | |
|--------------------|--------------------|--|--|
| Lublin | Date 2019.07.23 | STALMA Co. declares that the product satisfies requirements of documents to in this Certificate. | |
| Marcin Janiszewski | Konrad Barżał | | |
| Issued by | Approved by | | |

Applies to raw materials acc. to EN 10025 - 1,2, directive 93/68/EWG

CUSTOMER Skandistal Ab
AKÇELİK ORDER NO SE - 186982 / SH - 187126 - 10.000
CUSTOMER ORDER NO IL206326
DISPATCH NOTE / 201623

WEIGHT (kg.) 1994
QTY/BUNDLE 2998 / 2
LENGTH (mm)/TOL 3000 / -0/+200
DOCUMENT NO 96

QUALITY/HEAT T. S355J2 / -
HEAT NO 2121852
DELIVERY CONDITION Cold Drawn
DIMENSION (mm.)/TOL Ø / Round 6 / h9

| ELEMENT | C | | Si | | Mn | | P | | S | | | | | | | | | | | |
|---------|------|------|------|------|------|------|-------|-------|-------|-------|-----|-----|-----|-----|-----|-----|-----|-----|-----|-----|
| | Min | Max | Min | Max | Min | Max | Min | Max | Min | Max | Min | Max | Min | Max | Min | Max | Min | Max | Min | Max |
| RANGE | 0.00 | 0.20 | 0.00 | 0.55 | 0.00 | 1.60 | 0.00 | 0.030 | 0.00 | 0.030 | | | | | | | | | | |
| % | 0.18 | | 0.21 | | 0.70 | | 0.019 | | 0.030 | | | | | | | | | | | |

| MECHANICAL PROPERTIES | | | | | | | |
|------------------------|--------------------------|----------------|---------------|--|--|--|--|
| YIELD STRENGTH (N/mm2) | TENSILE STRENGTH (N/mm2) | ELONGATION (%) | HARDNESS (HB) | | | | |
| 654 | 775 | 6,3 | 225 | | | | |

STATEMENTS

APPROVED BY
Quality Engineer
Neslihan ÖZTÜRK



We hereby certify, material described has been complied with the term of order contract

Akcelik guarantee that the test values mentioned above, has same values with which determined in suppliers document.

Çayırova : Tel : 0262 658 89 52

Fax : 0262 658 99 75

www.akcelik.com.tr

Test protocols

C

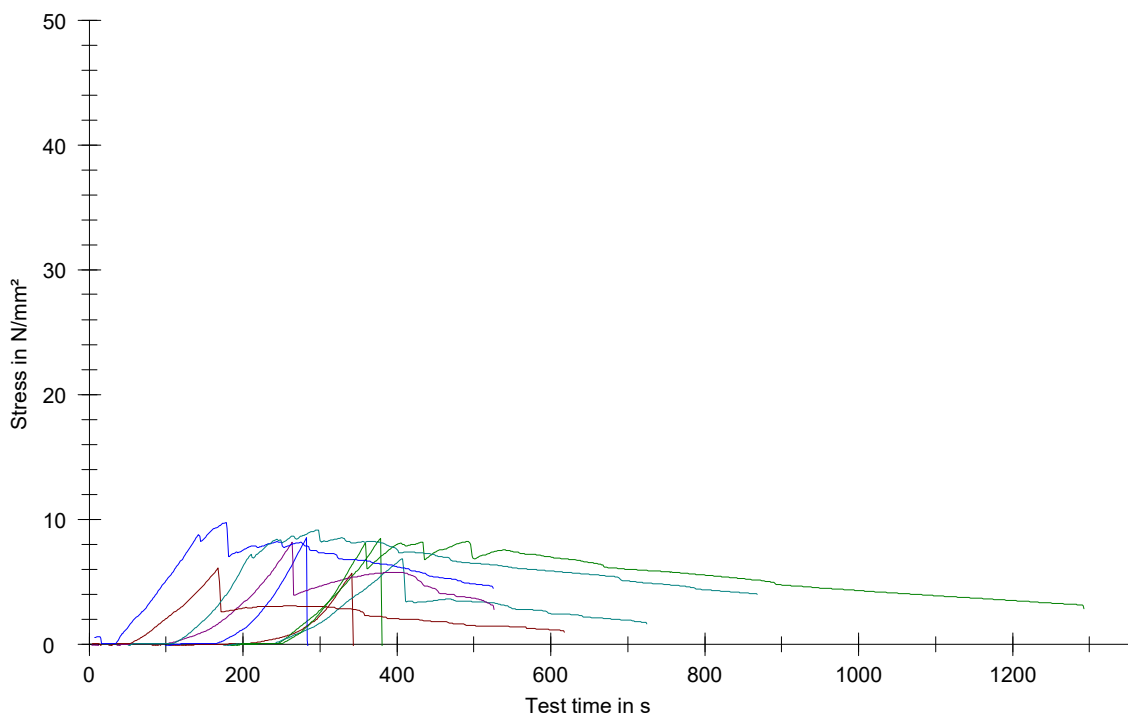
Parameter table:

| | | | |
|-----------------|-------------------------|---------------------------|---------------------|
| Test protocol | : Flexural tensile test | Type strain extensometer: | |
| Tester | : Einar, Shenyi | Machine data | : Controller TT1412 |
| Customer | : | | PistonStroke |
| Test standard | : NS-EN 12390-5:2019 | | LoadCell 250 kN |
| Strength grade: | | | |
| Creation date | : 5 April 2022 | | |
| Age | : 28 T | | |
| Other | : | | |

Results:

| Nr | Date | ID | a mm | b mm | A mm ² | h mm | F _m kN |
|----|------------|-----------------|---------|---------|----------------------|---------|----------------------|
| 1 | 26.04.2022 | 0% specimen 1 | 100,0 | 500,0 | 50000,0 | 100,0 | 8,17 |
| 2 | 26.04.2022 | 0% specimen 2 | 100,0 | 500,0 | 50000,0 | 100,0 | 12,29 |
| 3 | 26.04.2022 | 0% specimen 3 | 100,0 | 500,0 | 50000,0 | 100,0 | 12,35 |
| 4 | 26.04.2022 | 0.5% specimen 1 | 100,0 | 500,0 | 50000,0 | 100,0 | 9,90 |
| 5 | 26.04.2022 | 0.5% specimen 2 | 100,0 | 500,0 | 50000,0 | 100,0 | 11,77 |
| 6 | 26.04.2022 | 0.5% specimen 3 | 100,0 | 500,0 | 50000,0 | 100,0 | 8,83 |
| 7 | 26.04.2022 | 1.0% specimen 1 | 100,0 | 500,0 | 50000,0 | 100,0 | 11,88 |
| 8 | 26.04.2022 | 1.0% specimen 2 | 100,0 | 500,0 | 50000,0 | 100,0 | 14,11 |
| 9 | 26.04.2022 | 1.0% specimen 3 | 100,0 | 500,0 | 50000,0 | 100,0 | 13,25 |

Series graphics:



Statistics:

| Series n = 9 | a mm | b mm | A mm ² | h mm | F _m kN |
|-----------------|---------|---------|----------------------|---------|----------------------|
| \bar{x} | 100,0 | 500,0 | 50000,0 | 100,0 | 11,39 |
| s | 0,0 | 0,0 | 0,0 | 0,0 | 2,00 |
| v | 0,00 | 0,00 | 0,00 | 0,00 | 17,59 |

Parameter table:

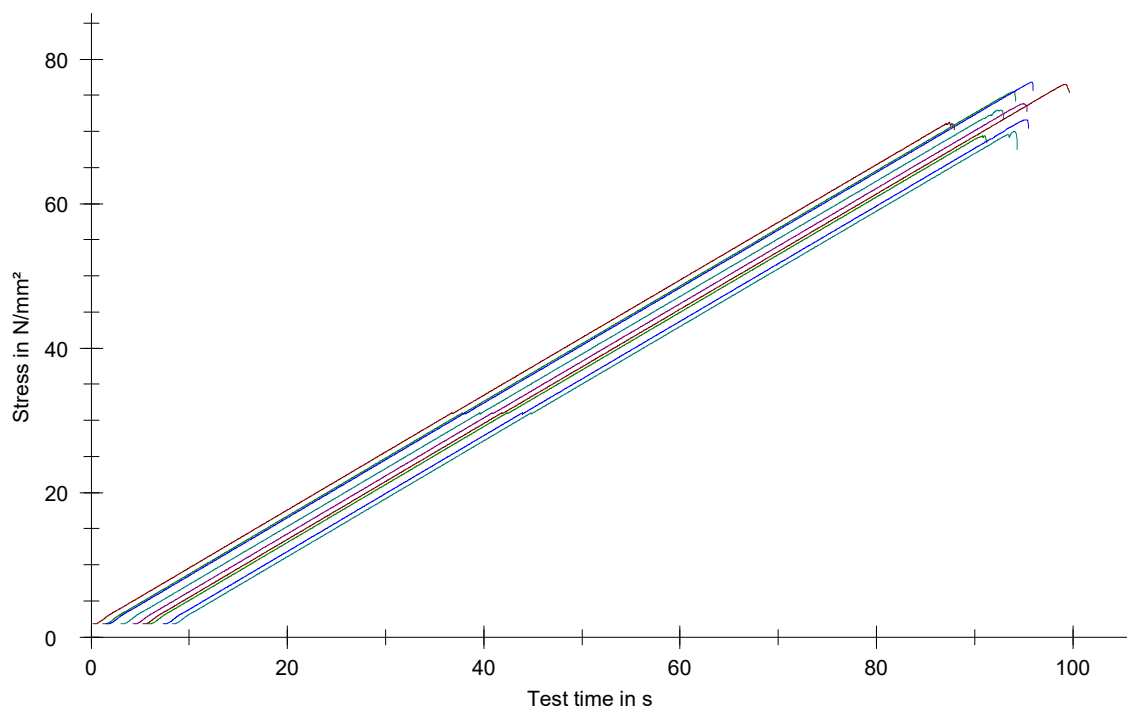
Test protocol : Compression test for cubes
 Tester : Einar Mesloe, Shenyi Shen
 Customer :
 Test standard : NS-EN 12390-3:2019
 Strength grade:
 Creation date : 5 April 2022
 Age : 28 T
 Other :

Type strain extensometer:
 Machine data : Controller TT0322
 PistonStroke
 LoadCell 3 MN

Results:

| Nr | Date | ID | a mm | b mm | A mm ² | h mm | F _m kN | σ _m N/mm ² |
|----|------------|---------------|---------|---------|----------------------|---------|----------------------|-------------------------------------|
| 1 | 26.04.2022 | 0% 1 28days | 100,0 | 100,0 | 10000,0 | 100,0 | 712,86 | 71,29 |
| 2 | 26.04.2022 | 0% 2 28days | 100,0 | 100,0 | 10000,0 | 100,0 | 755,07 | 75,51 |
| 3 | 26.04.2022 | 0% 3 28days | 100,0 | 100,0 | 10000,0 | 100,0 | 768,61 | 76,86 |
| 4 | 26.04.2022 | 0,5% 1 28days | 100,0 | 100,0 | 10000,0 | 100,0 | 729,92 | 72,99 |
| 5 | 26.04.2022 | 0,5% 2 28days | 100,0 | 100,0 | 10000,0 | 100,0 | 738,69 | 73,87 |
| 6 | 26.04.2022 | 0,5% 3 28days | 100,0 | 100,0 | 10000,0 | 100,0 | 765,47 | 76,55 |
| 7 | 26.04.2022 | 1% 1 28days | 100,0 | 100,0 | 10000,0 | 100,0 | 694,25 | 69,42 |
| 8 | 26.04.2022 | 1% 2 28days | 100,0 | 100,0 | 10000,0 | 100,0 | 716,28 | 71,63 |
| 9 | 26.04.2022 | 1% 3 28days | 100,0 | 100,0 | 10000,0 | 100,0 | 699,94 | 69,99 |

Series graphics:



Statistics:

| Series n = 9 | a mm | b mm | A mm ² | h mm | F _m kN | σ _m N/mm ² |
|-----------------|---------|---------|----------------------|---------|----------------------|-------------------------------------|
| \bar{x} | 100,0 | 100,0 | 10000,0 | 100,0 | 731,23 | 73,12 |
| s | 0,0 | 0,0 | 0,0 | 0,0 | 27,62 | 2,76 |
| v | 0,00 | 0,00 | 0,00 | 0,00 | 3,78 | 3,78 |

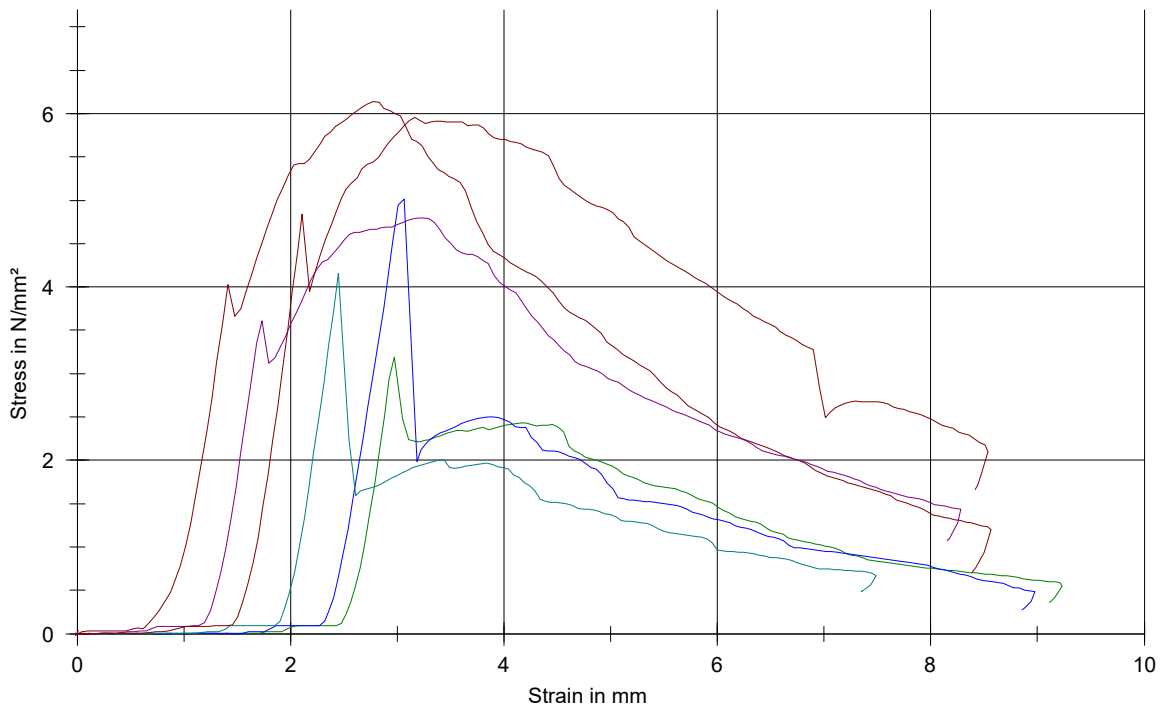
Parameter table:

| | | | |
|-----------------|---------------------|---------------------------|-------------------|
| Test protocol : | | Type strain extensometer: | |
| Tester : | | Machine data : | Controller TT1412 |
| Customer : | | | PistonStroke |
| Test standard : | NS-EN 12390-5- 2019 | | LoadCell 250 kN |
| Strength grade: | B70 | | |
| Creation date : | 05.03.2022 | | |
| Age : | 28 T | | |
| Other : | | | |

Results:

| Nr | ID | a mm | b mm | A mm ² | h mm | F _m kN |
|----|-----------------|---------|---------|----------------------|---------|----------------------|
| 1 | 1% specimen 1 | 150,0 | 550,0 | 90000,0 | 150,0 | 27,62 |
| 2 | 0,5% specimen 1 | 150,0 | 550,0 | 90000,0 | 150,0 | 14,34 |
| 3 | 0,5% specimen 2 | 150,0 | 550,0 | 90000,0 | 150,0 | 22,57 |
| 4 | 0,5% specimen 3 | 150,0 | 550,0 | 90000,0 | 150,0 | 18,71 |
| 5 | 1% specimen 2 | 150,0 | 550,0 | 90000,0 | 150,0 | 21,60 |
| 6 | 1% specimen 3 | 150,0 | 550,0 | 90000,0 | 150,0 | 26,81 |

Series graphics:



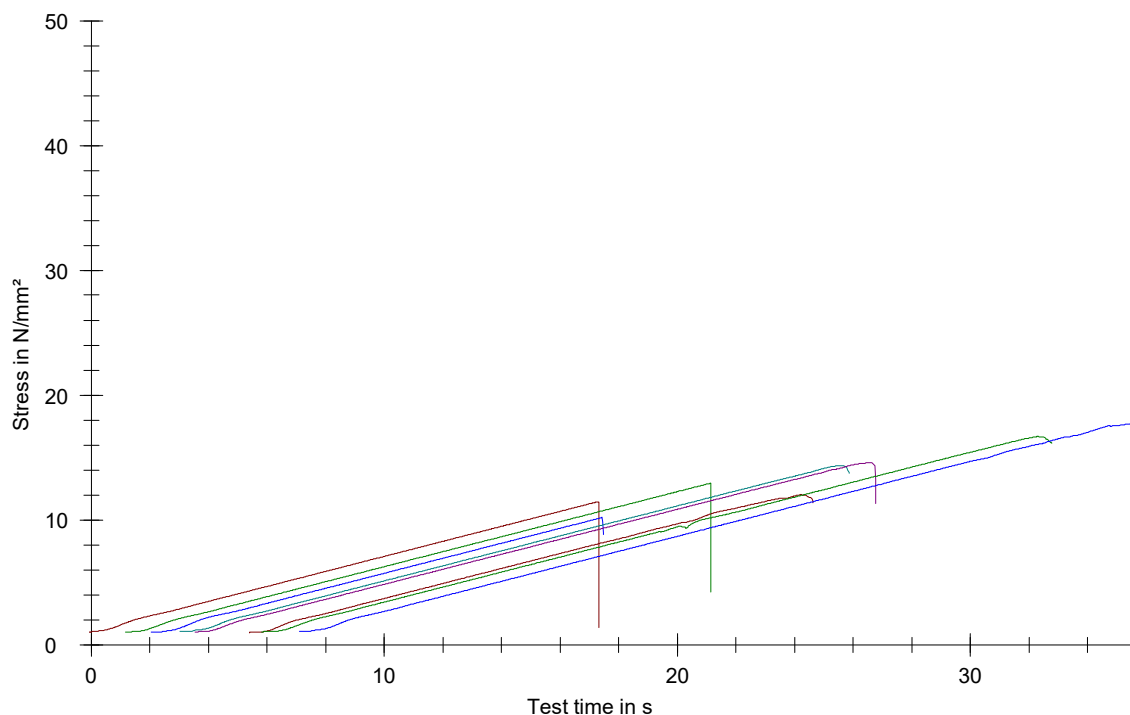
Parameter table:

| | | | |
|-----------------|--------------------------|---------------------------|---------------------|
| Test protocol | : Tensile splitting test | Type strain extensometer: | |
| Tester | : Einar, Shenyi | Machine data | : Controller TT0322 |
| Customer | : | | PistonStroke |
| Test standard | : NS-EN 12390-6:2009 | | LoadCell 3 MN |
| Strength grade: | | | |
| Creation date | : 5 April 2022 | | |
| Age | : 28 T | | |
| Other | : | | |

Results:

| Nr | Date | ID | d mm | A mm ² | h mm | F _m kN | σ _m N/mm ² |
|----|------------|-----------------|---------|----------------------|---------|----------------------|-------------------------------------|
| 1 | 26.04.2022 | 0% cylinder 1 | 150,0 | 17671,5 | 300,0 | 202,25 | 11,44 |
| 2 | 26.04.2022 | 0% cylinder 2 | 150,0 | 17671,5 | 300,0 | 228,60 | 12,94 |
| 3 | 26.04.2022 | 0% cylinder 3 | 150,0 | 17671,5 | 300,0 | 179,99 | 10,19 |
| 4 | 26.04.2022 | 0,5% cylinder 1 | 150,0 | 17671,5 | 300,0 | 253,71 | 14,36 |
| 5 | 26.04.2022 | 0,5% cylinder 2 | 150,0 | 17671,5 | 300,0 | 257,81 | 14,59 |
| 7 | 26.04.2022 | 0,5% cylinder 3 | 150,0 | 17671,5 | 300,0 | 212,26 | 12,01 |
| 8 | 26.04.2022 | 1% cylinder 1 | 150,0 | 17671,5 | 300,0 | 294,62 | 16,67 |
| 10 | 26.04.2022 | 1% cylinder 2 | 150,0 | 17671,5 | 300,0 | 312,87 | 17,71 |

Series graphics:



Statistics:

| Series n = 8 | d mm | A mm ² | h mm | F _m kN | σ _m N/mm ² |
|-----------------|---------|----------------------|---------|----------------------|-------------------------------------|
| \bar{x} | 150,0 | 17671,5 | 300,0 | 242,76 | 13,74 |
| s | 0,0 | 0,0 | 0,0 | 45,77 | 2,59 |
| v | 0,00 | 0,00 | 0,00 | 18,85 | 18,85 |

Accelerometer Data

D

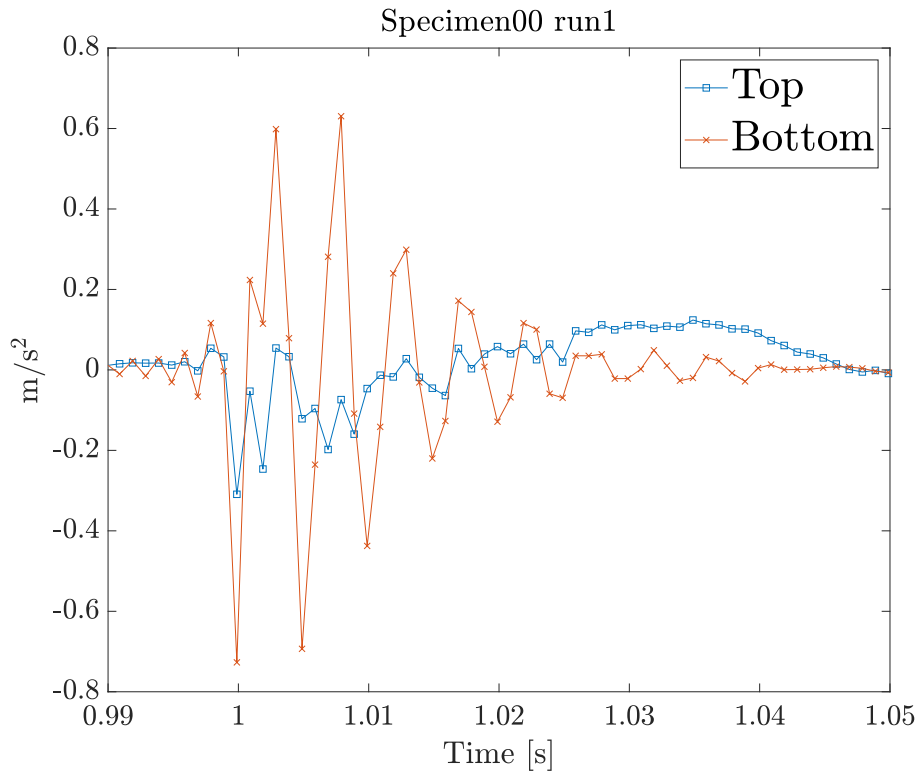


Figure D.1. Specimen00 run1

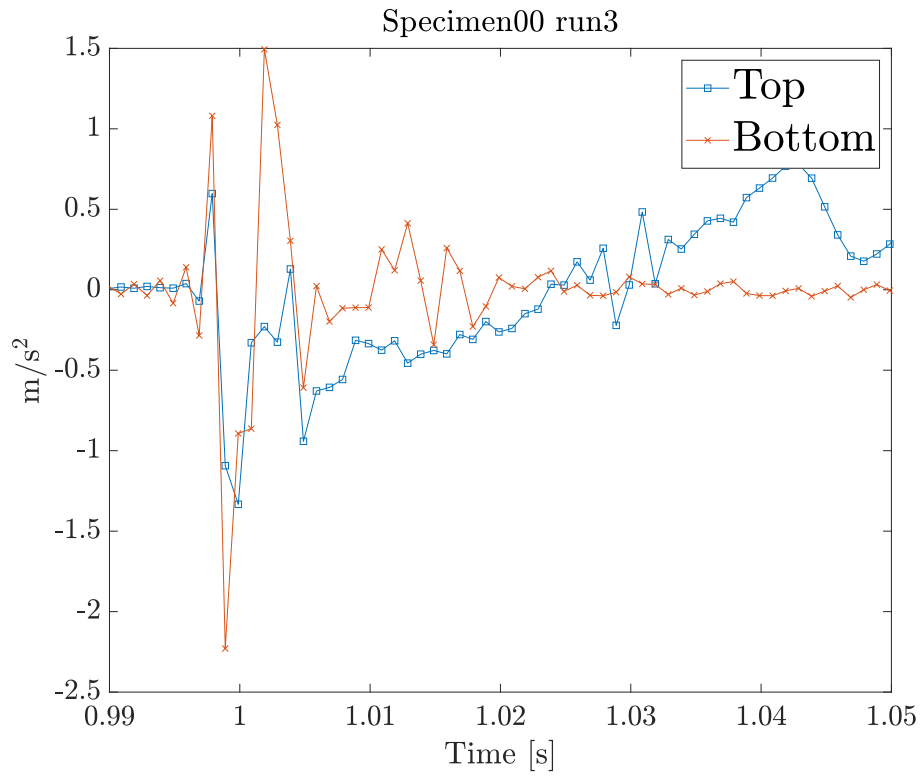


Figure D.2. Specimen00 run3

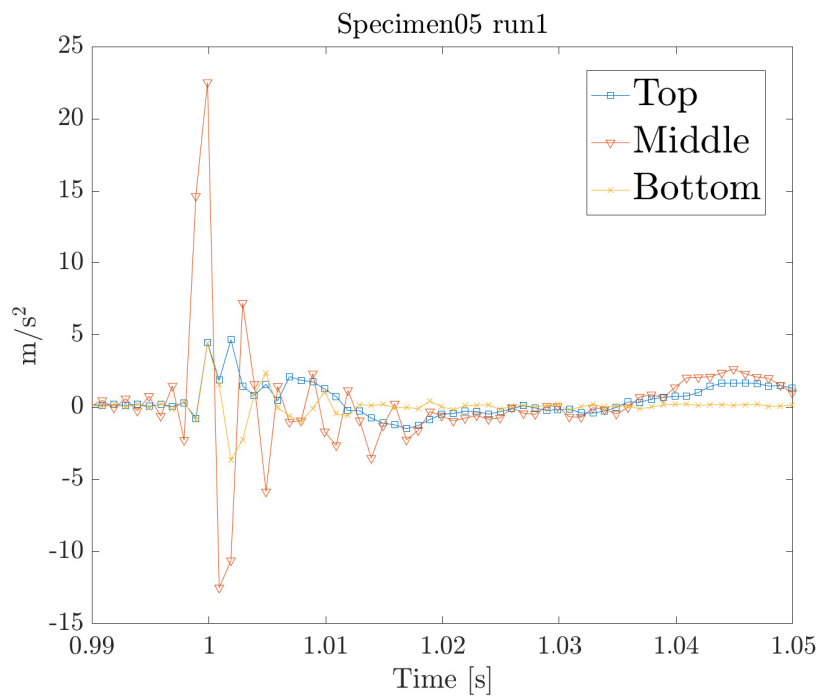


Figure D.3. Specimen05 run1

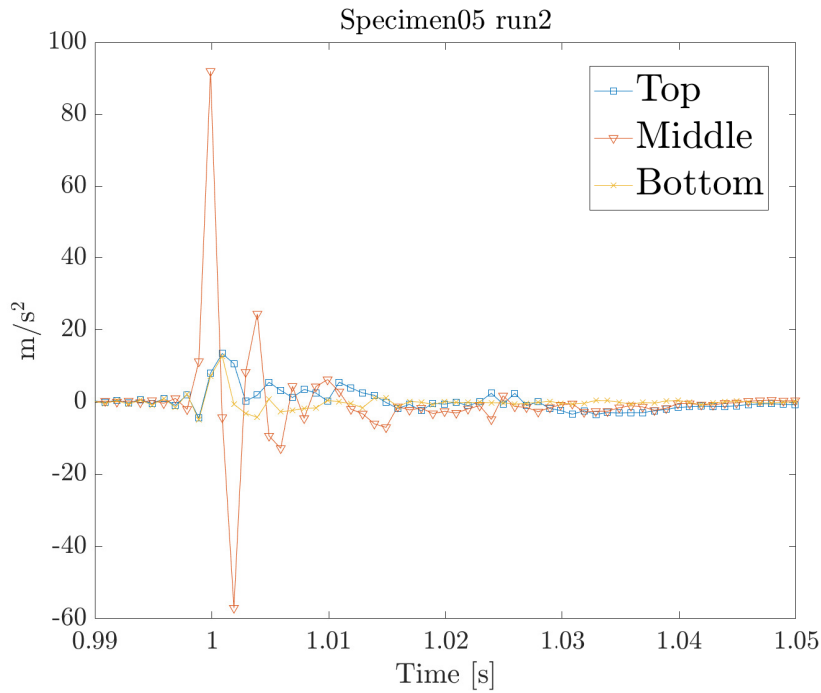


Figure D.4. Specimen05 run2

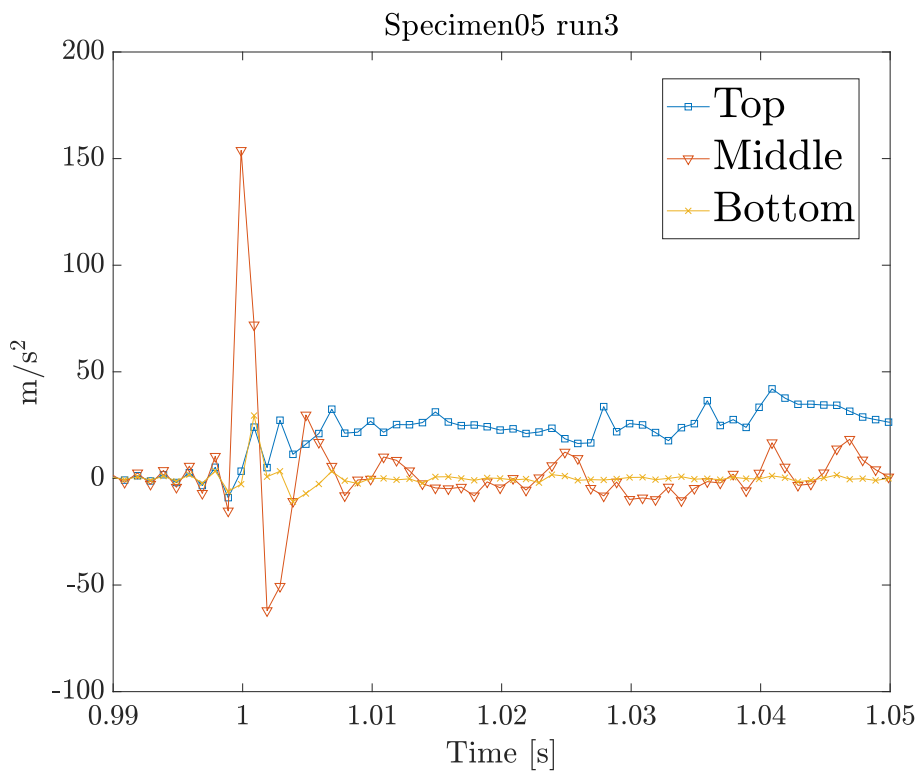


Figure D.5. Specimen05 run3

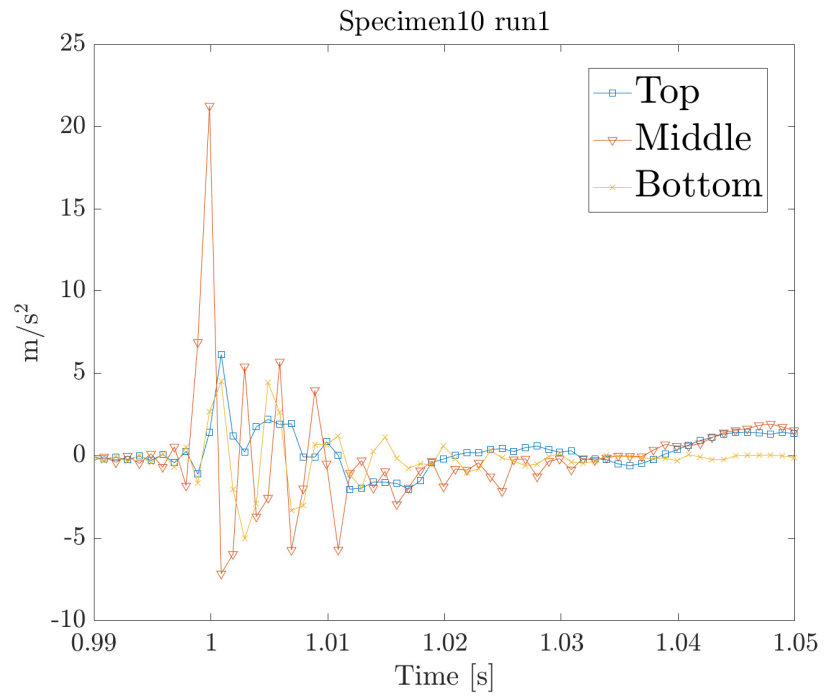


Figure D.6. Specimen10 run1

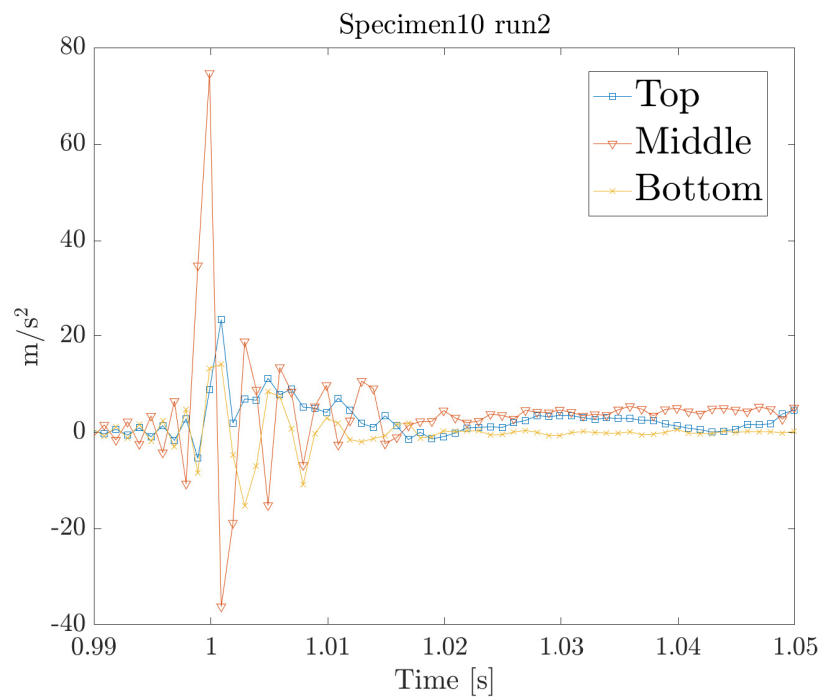


Figure D.7. Specimen10 run2

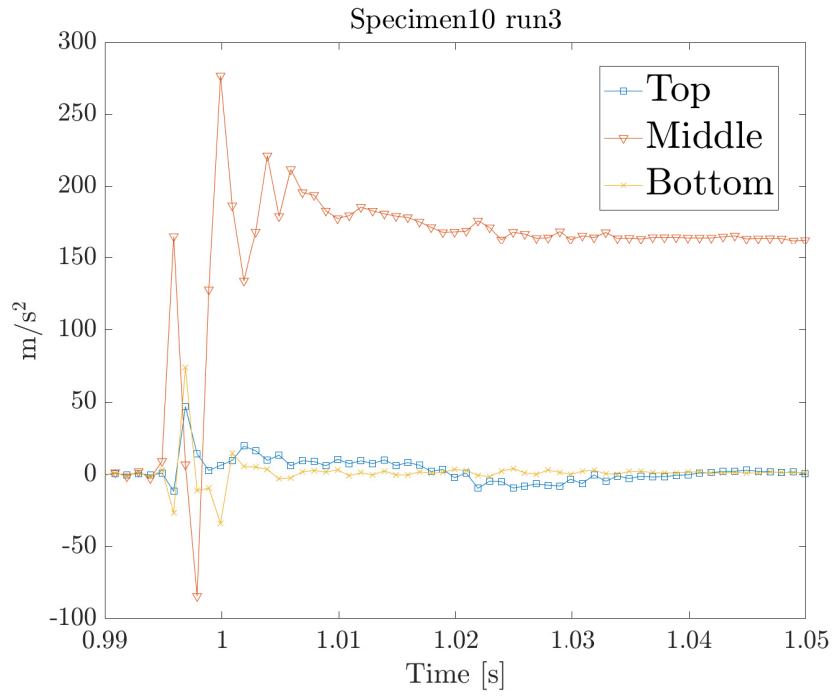


Figure D.8. Specimen10 run3

E.1 Laser Displacement sensors

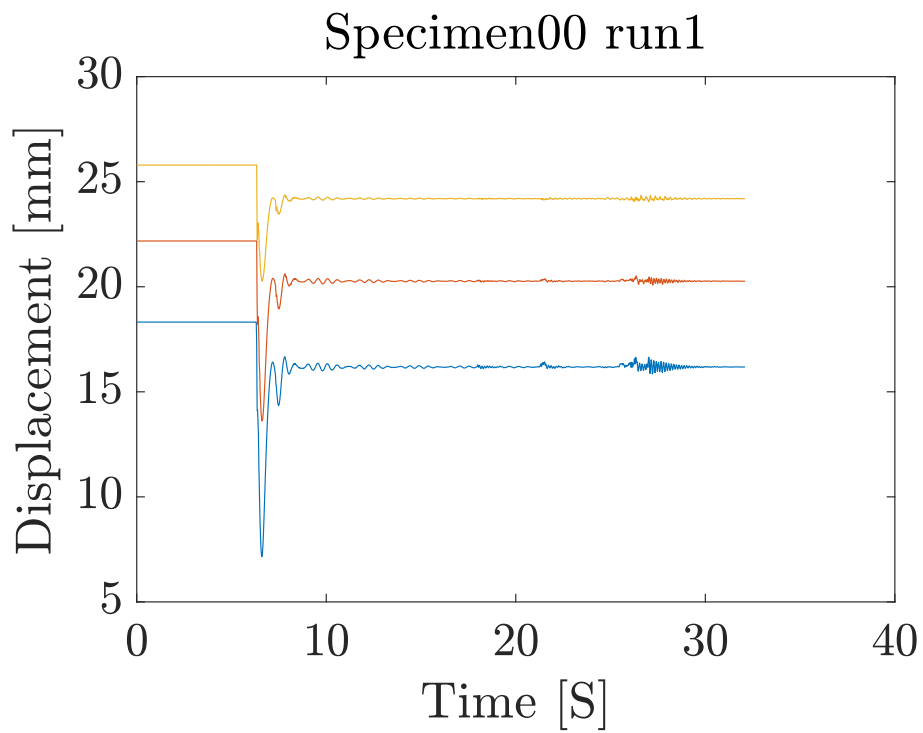


Figure E.1. Raw data Specimen00 run1

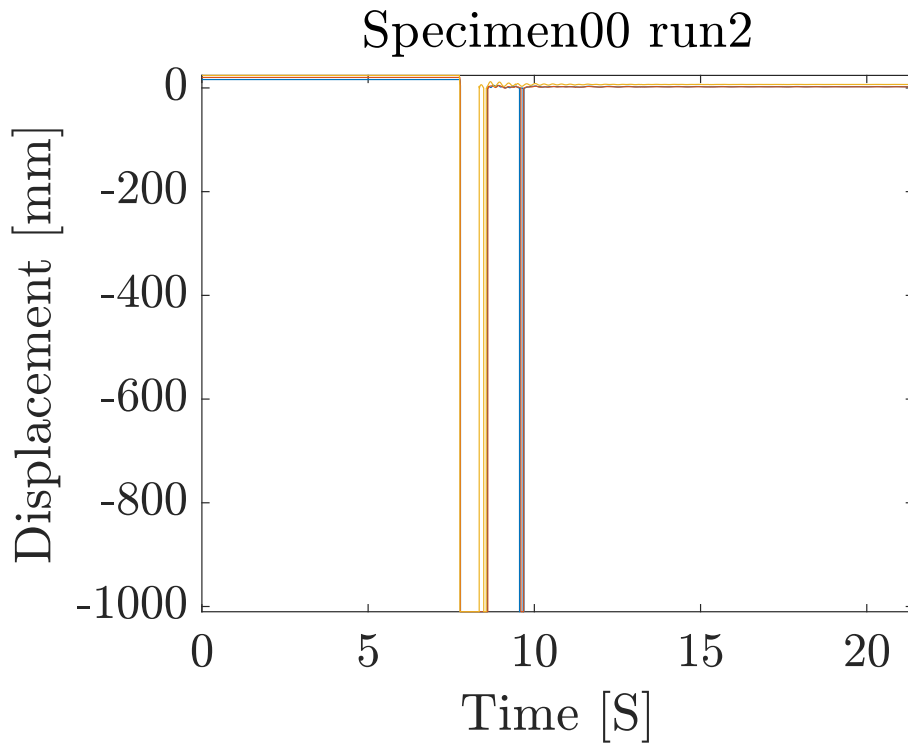


Figure E.2. Raw data Specimen00 run2

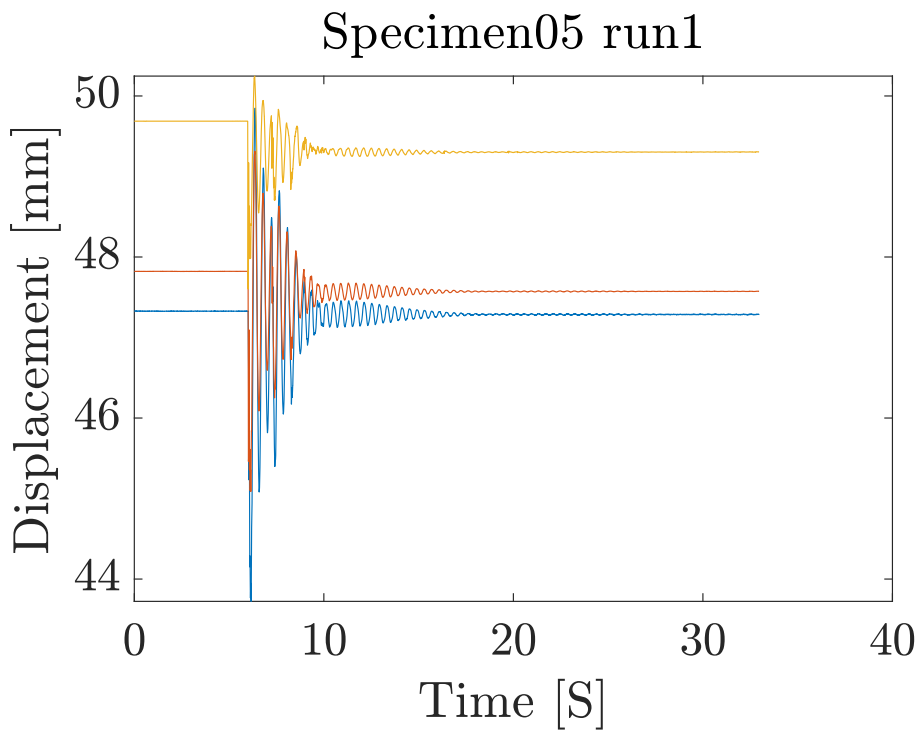


Figure E.3. Raw data Specimen05 run1

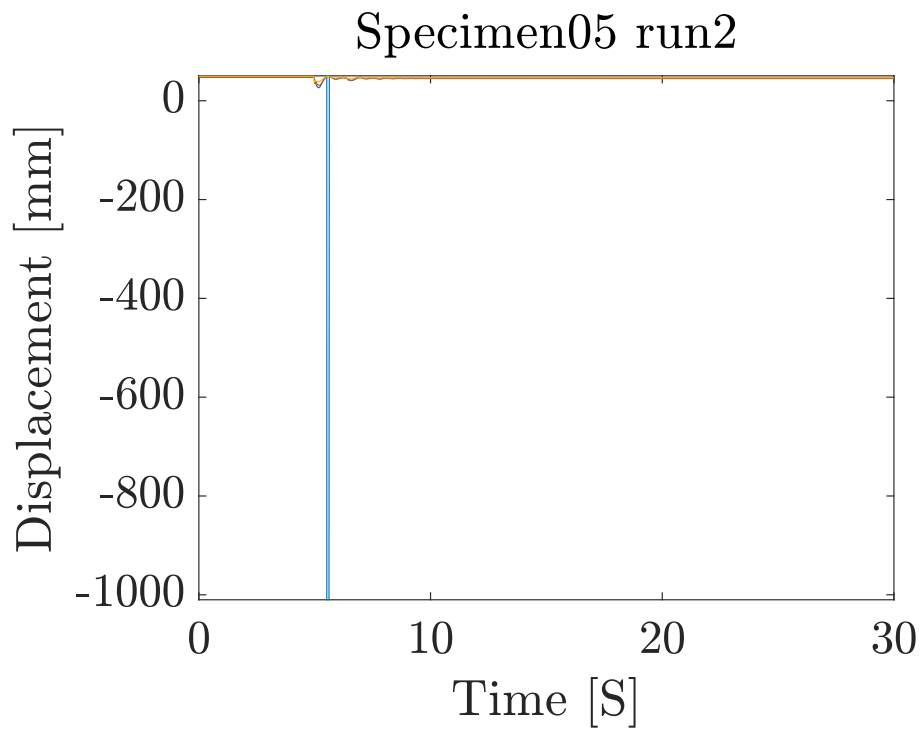


Figure E.4. Raw data Specimen05 run2

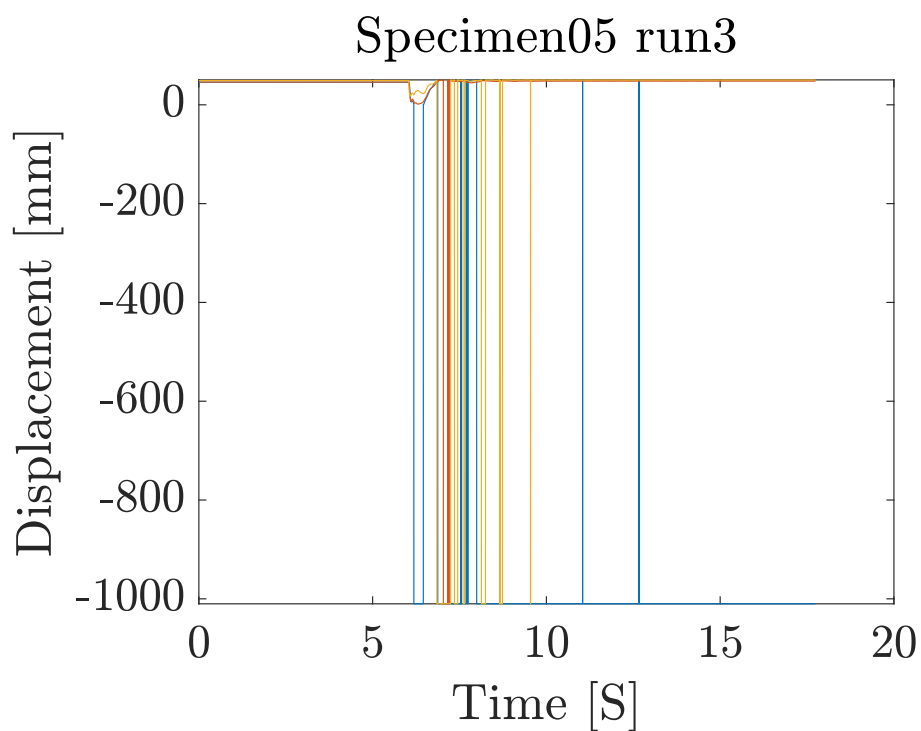


Figure E.5. Raw data Specimen05 run3

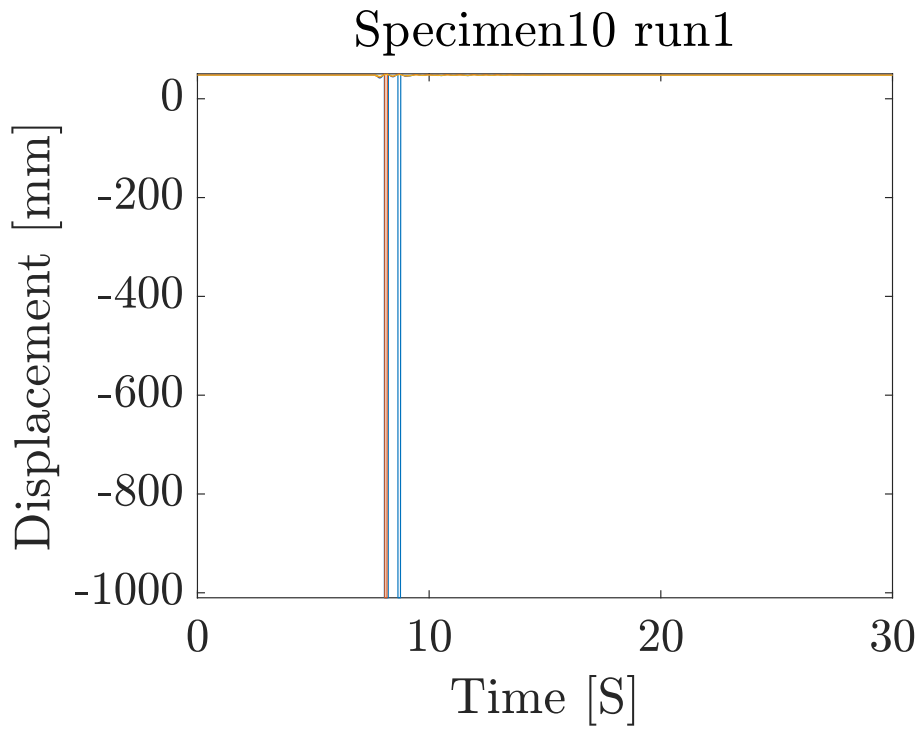


Figure E.6. Raw data Specimen10 run1

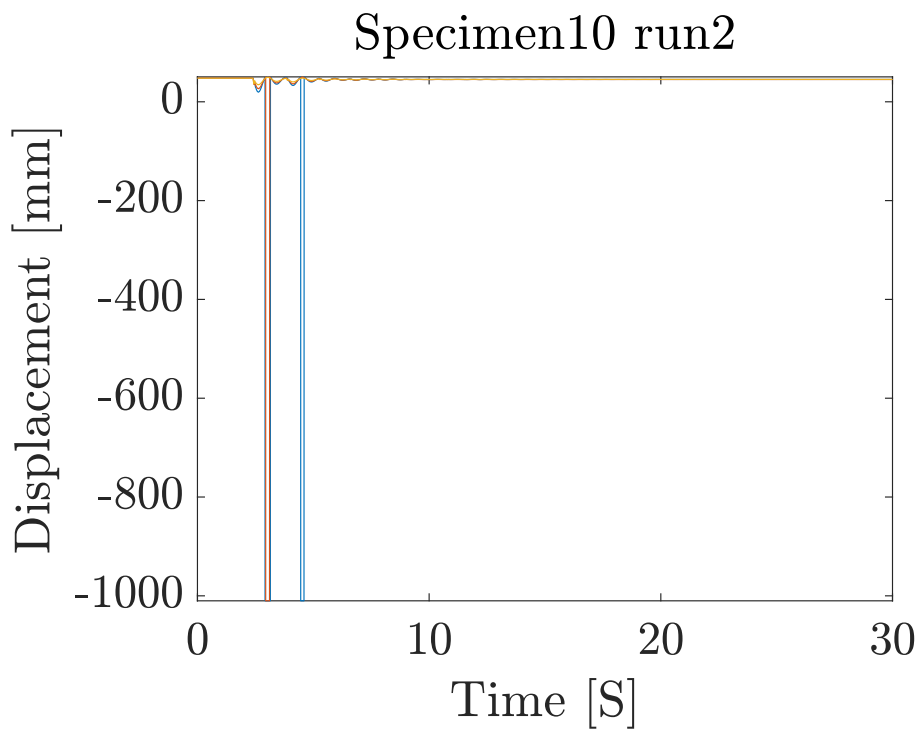


Figure E.7. Raw data Specimen10 run2

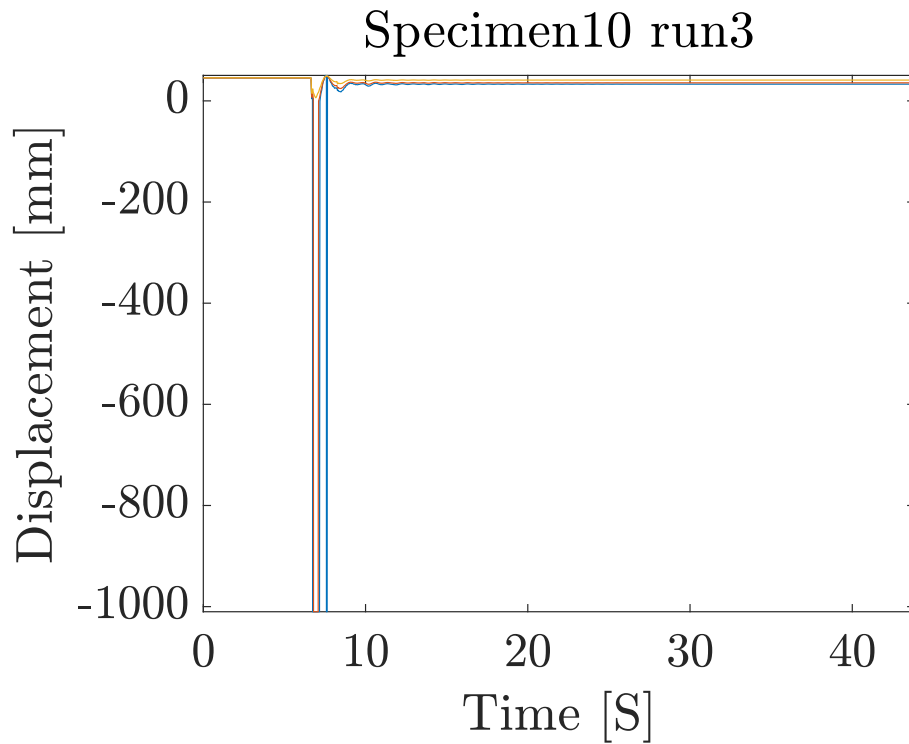


Figure E.8. Raw data Specimen10 run3

E.2 Accelerometer data

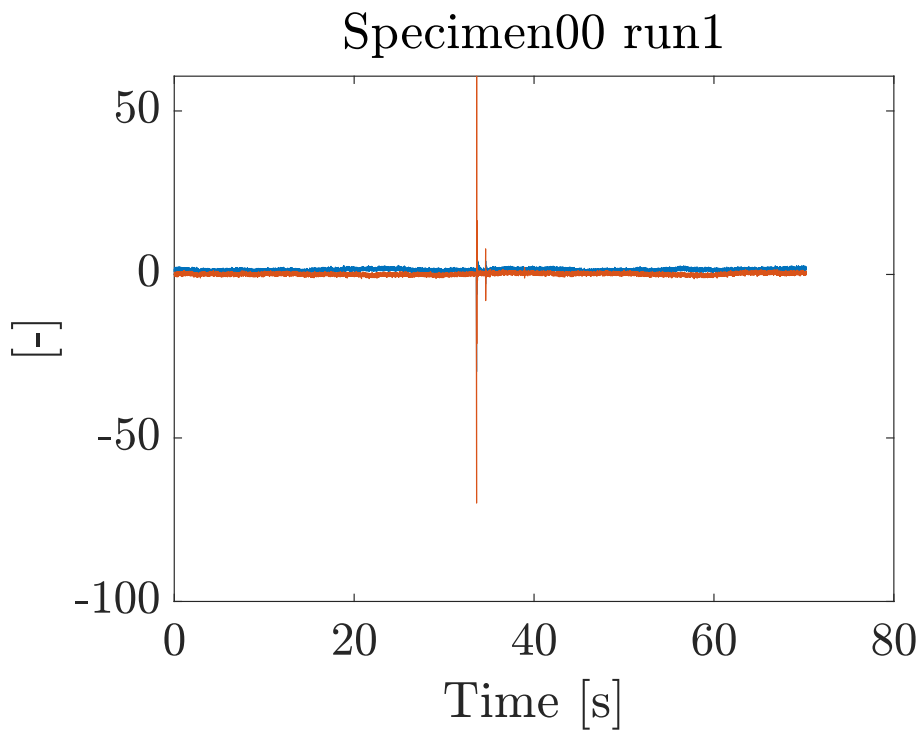


Figure E.9. Raw data Specimen00 run1

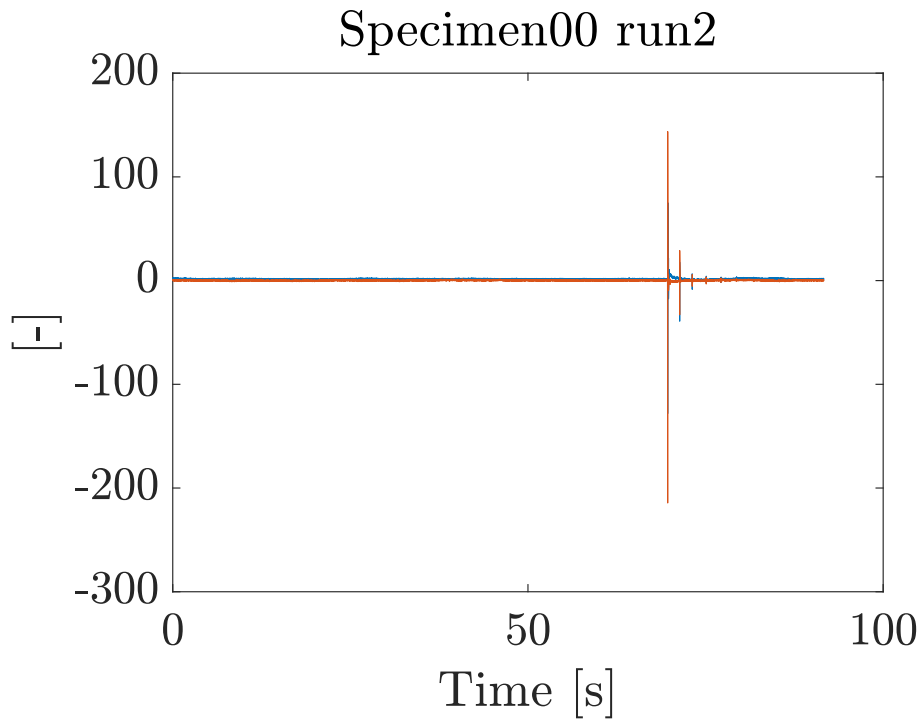


Figure E.10. Raw data Specimen00 run2

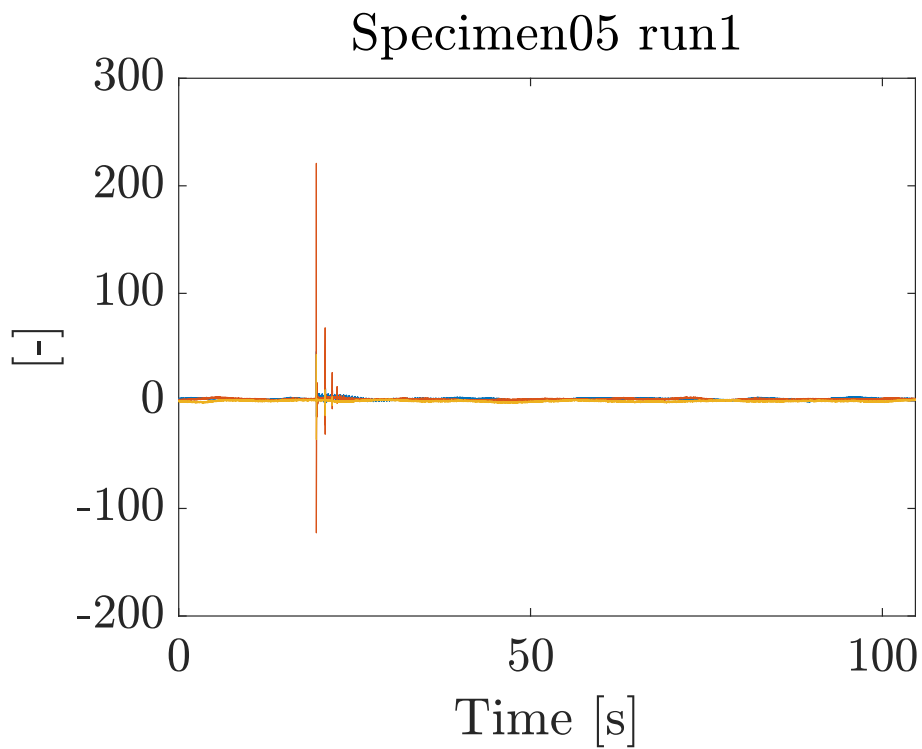


Figure E.11. Raw data Specimen05 run1

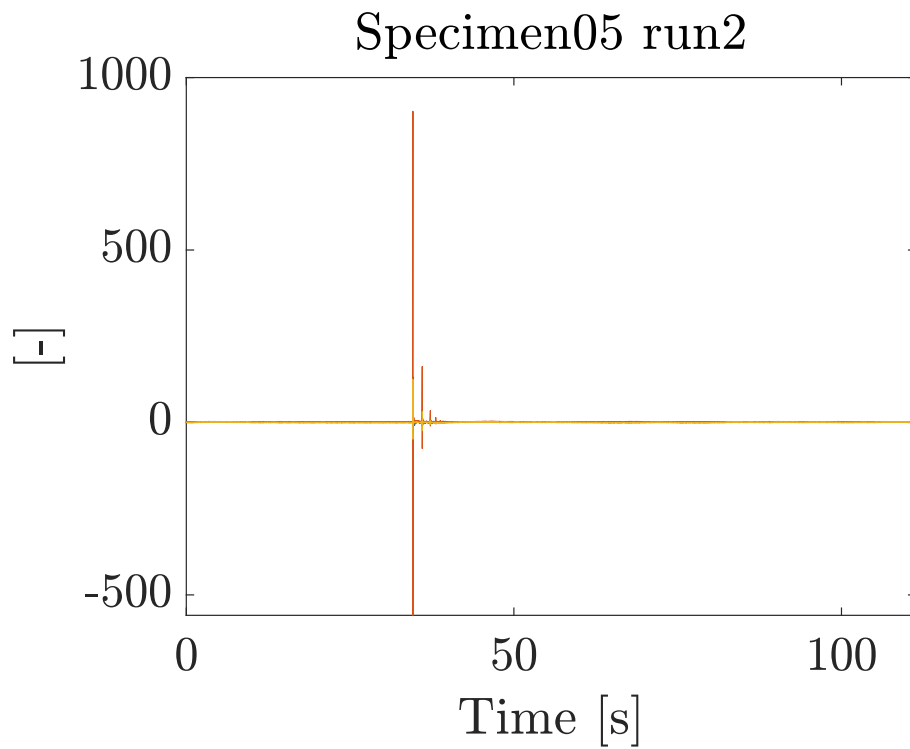


Figure E.12. Raw data Specimen05 run2

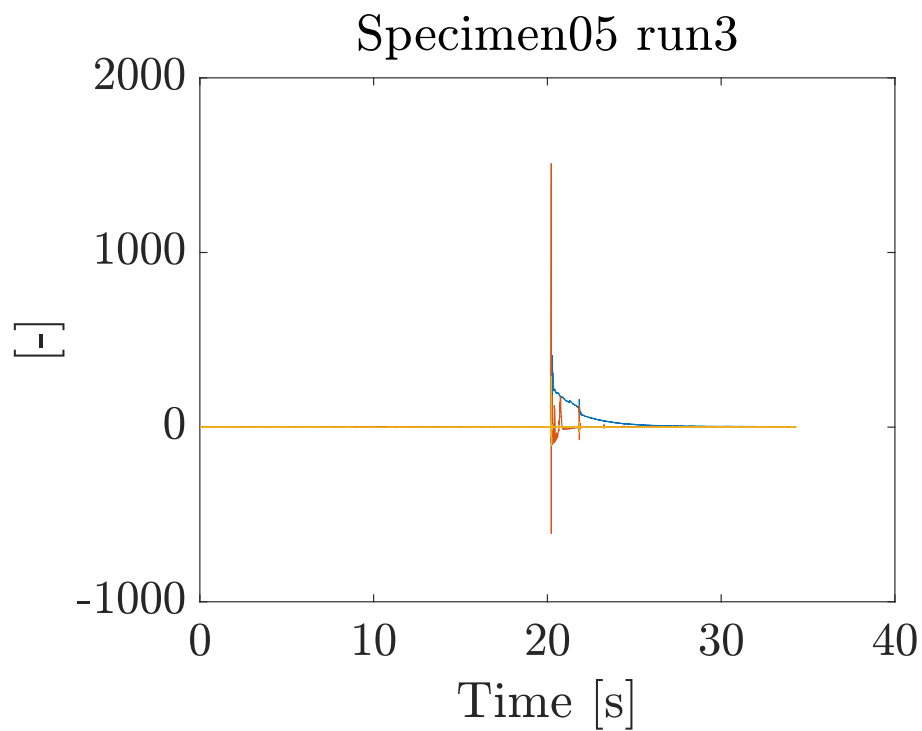


Figure E.13. Raw data Specimen05 run3

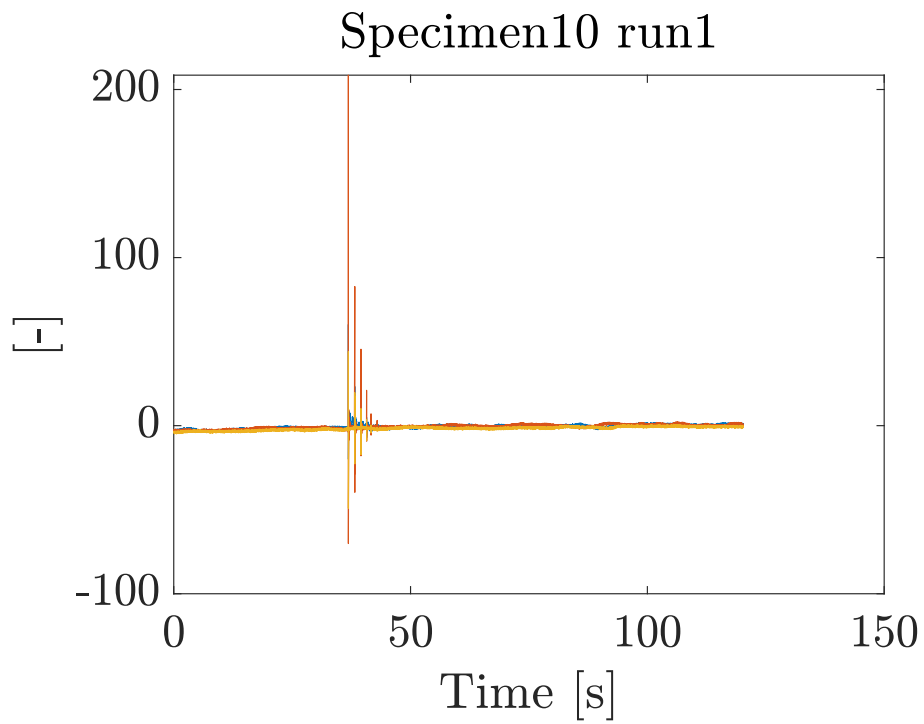


Figure E.14. Raw data Specimen10 run1

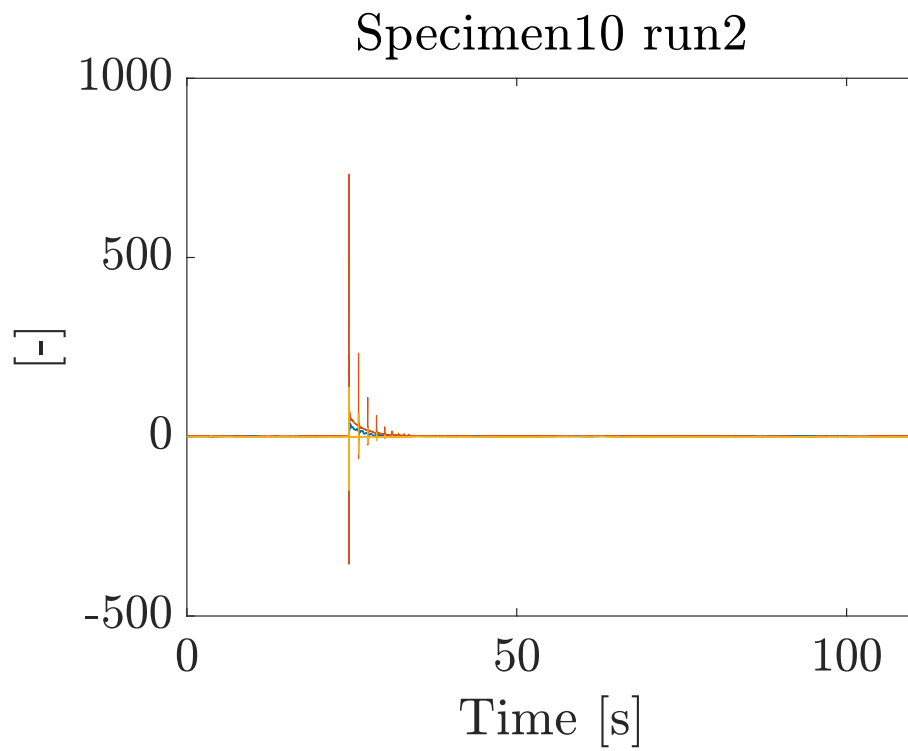


Figure E.15. Raw data Specimen10 run2

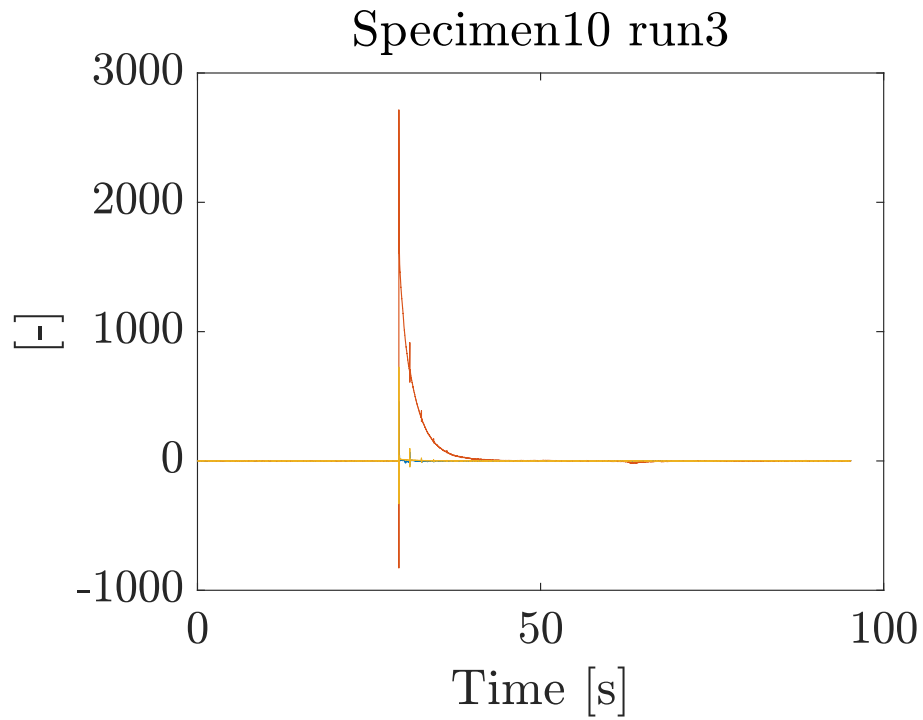


Figure E.16. Raw data Specimen10 run3

E.3 Load-Cell

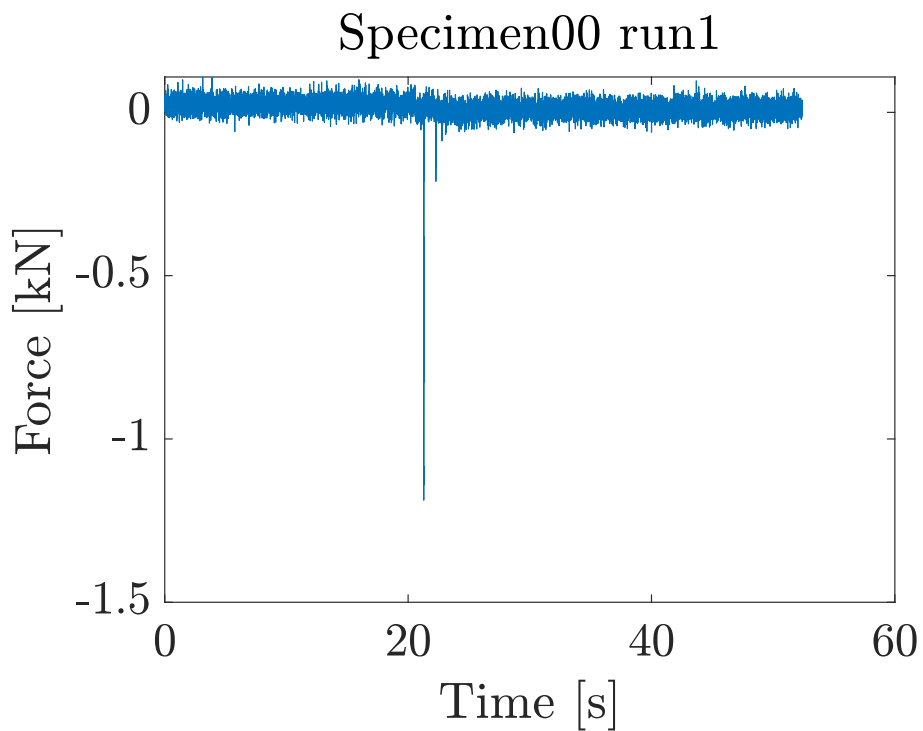


Figure E.17. Raw data Specimen00 run1

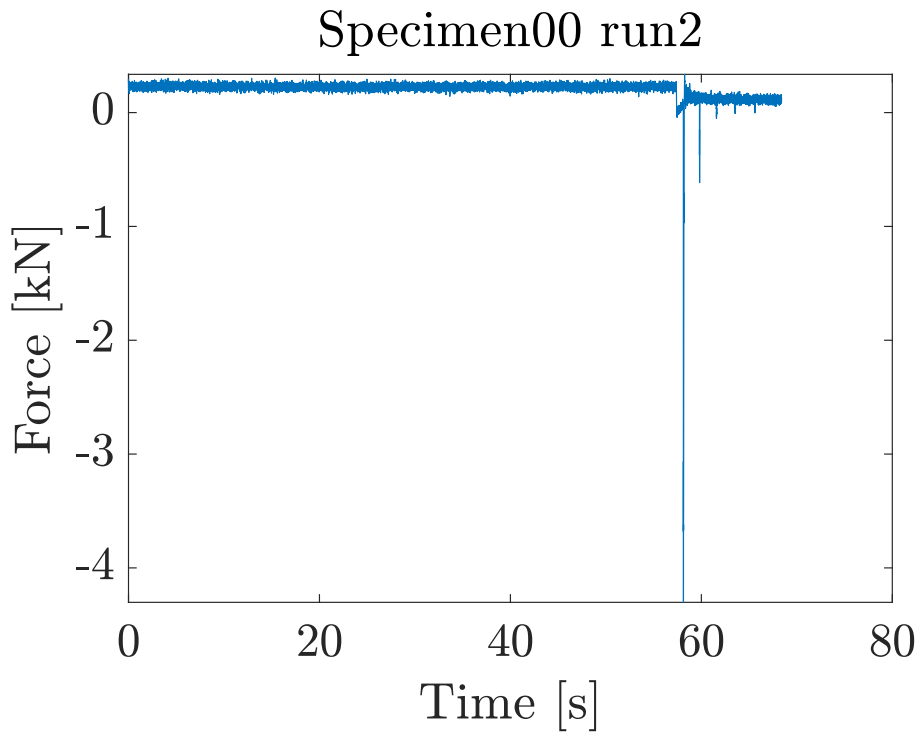


Figure E.18. Raw data Specimen00 run2

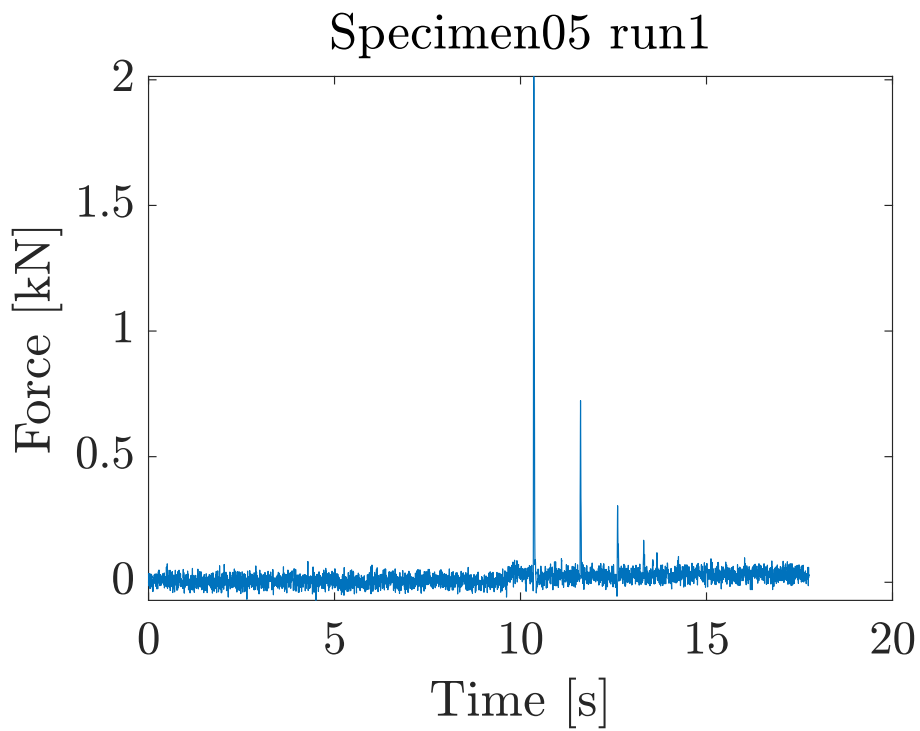


Figure E.19. Raw data Specimen05 run1

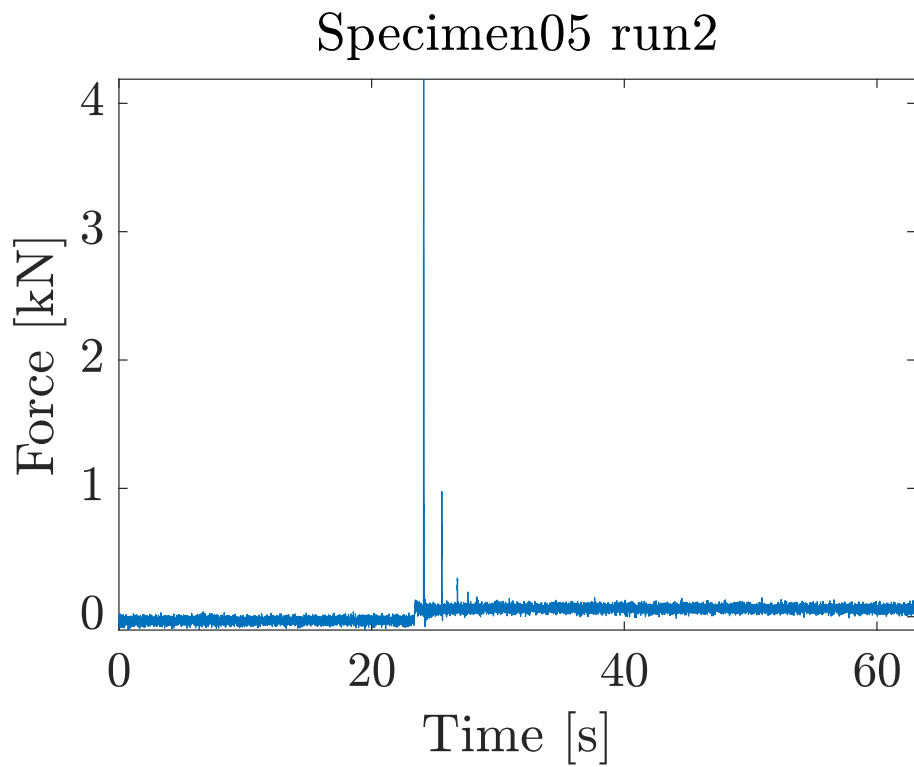


Figure E.20. Raw data Specimen05 run2

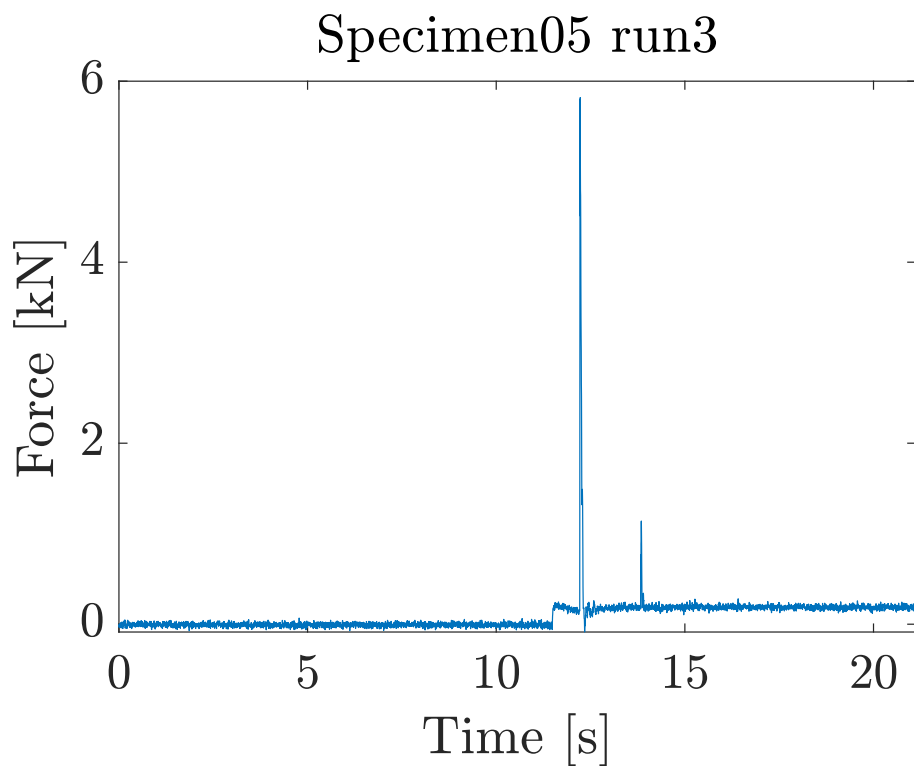


Figure E.21. Raw data Specimen05 run3

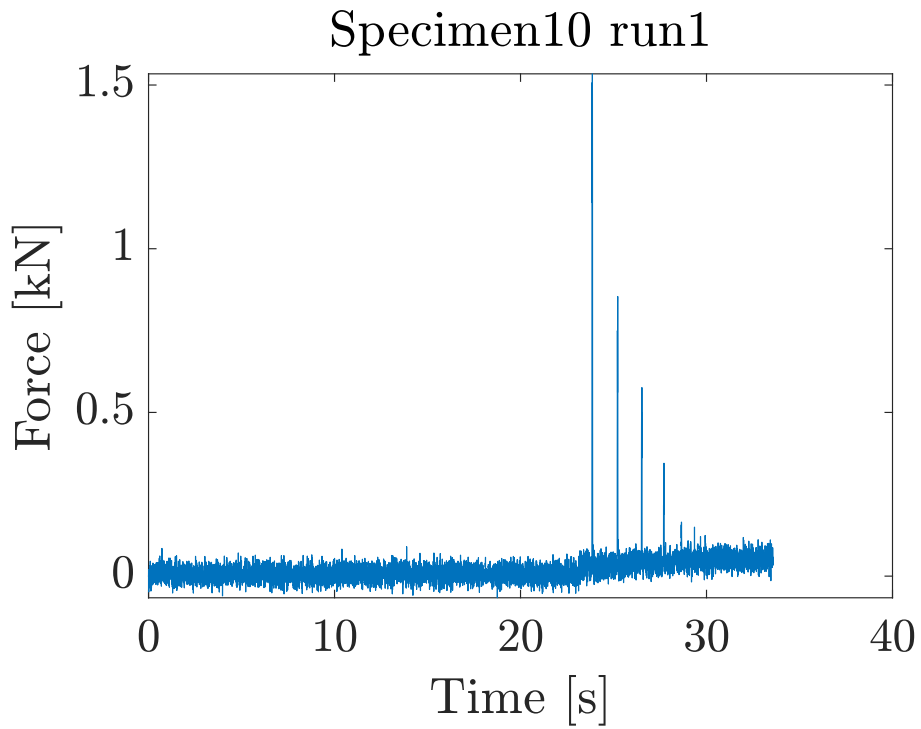


Figure E.22. Raw data Specimen10 run1

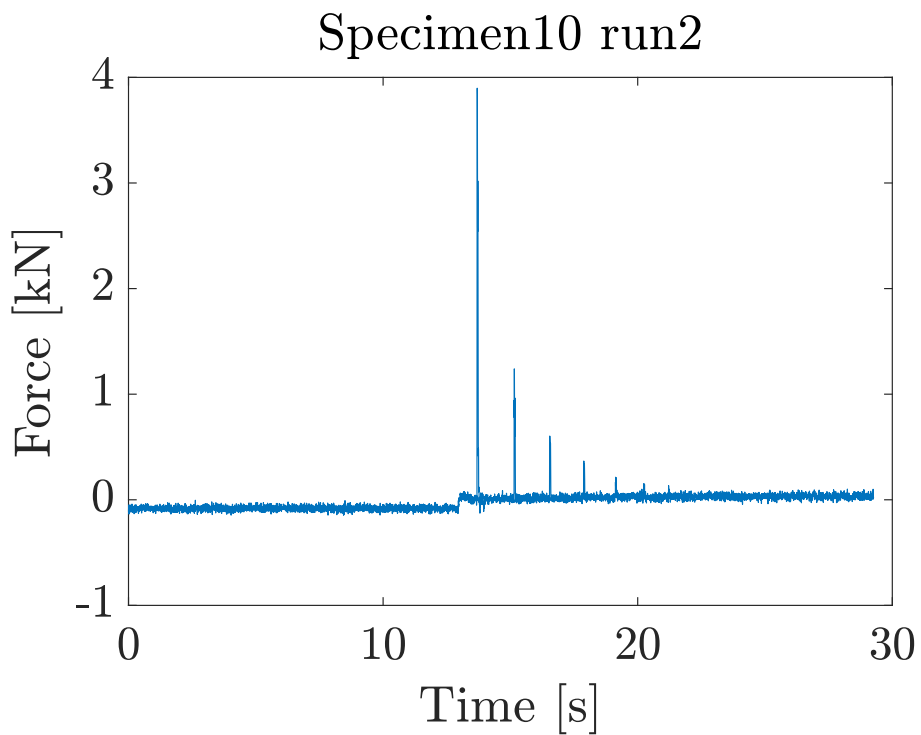


Figure E.23. Raw data Specimen10 run2

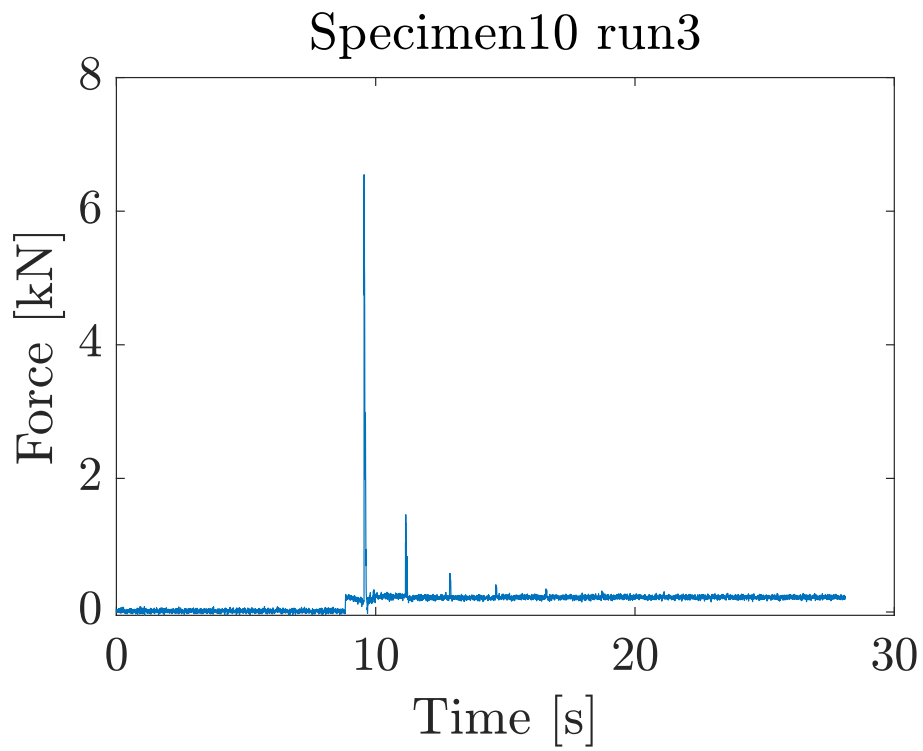


Figure E.24. Raw data Specimen10 run3